An alternative to the Kutta condition for high frequency, separated flows

by

Alexandros Gioulekas

Dipl.Eng., National Technical University of Athens, 1985
S.M., Massachusetts Institute of Technology, 1987

Submitted to the Department of
Aeronautics and Astronautics
in partial fulfillment of the
requirements for the degree of

Doctor of Philosophy

at the

Massachusetts Institute of Technology

May, 1992

Signature of Author _____
May, 1992

Certified by _____
Prof. James E. McCune
Thesis Supervisor

Certified by _____
Prof. Alan Epstein
Thesis Committee Member

Certified by _____
Prof. Mårten T. Landahl
Thesis Committee Member

Certified by _____
Prof. Manuel Martinez-Sanchez
Thesis Committee Member

Accepted by _____
Prof. Harold Y. Wachman
Chairman, Departmental Graduate Committee

An alternative to the Kutta condition for high frequency, separated flows

by

Alexandros Gioulekas

Submitted to the Department of
Aeronautics and Astronautics
in partial fulfillment of the
requirements for the Degree of

Doctor of Philosophy

Abstract

An alternative to the Kutta condition for determining the circulation around a bluff airfoil in unsteady, separated flow is presented. For such flows, there is a need for a practical criterion which would avoid the detailed boundary layer calculations and would predict the time evolution of the airfoil circulation based on the external potential flow only.

This criterion would play for unsteady, separated flows the role that the Kutta condition plays for flows past thin airfoils. It turns out to be a criterion for predicting the location and movement of the "separation points", because they determine the net vorticity flux shed into the wake and thus the rate of change of the airfoil circulation.

The laminar, two-dimensional flow about a bluff airfoil at angle of attack, when the external flow oscillates at a high reduced frequency is considered.

At high frequencies, the vorticity generated as the wall resists the imposed unsteadiness is confined to a thin layer near the blade surface ("Stokes layer") and its contribution to the displacement thickness is proportional to an inverse power of the reduced frequency and thus small. Outside this region, the unsteady part of the boundary layer velocity is approximately the external potential oscillation. Based on this observation and following C.C. Lin, the boundary layer velocity can be divided into two coupled velocity distributions, one predominantly oscillatory ("Stokes velocity") and another predominantly steady ("Prandtl velocity"). The main contributor to the displacement thickness is the latter. Therefore, separation, identified by a dramatic increase in the displacement thickness, can be located by calculating the evolution of the "Prandtl velocity" and finding where the latter bifurcates.

Stratford's ideas, modified to account for unsteadiness in the "Prandtl velocity"

(arising through the coupling of the "Prandtl" to the "Stokes" flow by the no-slip condition on the wall and Reynolds-stress terms in the momentum equation), lead to a criterion for unsteady separation that uses as only inputs parameters of the external flow and avoids a detailed boundary layer calculation.

The airfoil circulation is calculated by an iterative method which calculates how the interaction between the airfoil and its wake affects separation.

An ellipse is adopted as a study case, and results are presented for varying angle of attack, ellipse slenderness, reduced frequency, and strength of unsteadiness. In the limit of a very slender ellipse, the theory recovers the results from the classical unsteady wing theory, which assumes the Kutta condition.

The theory predicts that there exist two limits for the mean value of the circulation. The upper limit is the value of the circulation for which the trailing edge becomes a stagnation point (Γ_{Kutta}). The lower limit is the value of the circulation in steady flow (Γ_{Howarth}).

The pressure-side "separation point" for all practical purposes can be considered fixed, even at small angles of attack. On the other hand, the "separation point" on the suction-side oscillates with amplitude proportional to the strength of the flow unsteadiness, and inversely proportional to the reduced frequency. When the reduced frequency increases or the strength of flow unsteadiness decreases, the trajectory of this "separation point" shrinks and tends toward the position of steady separation. Since the mean location of the suction-side "separation point" controls the mean value of the circulation, and the amplitude of its excursion determines the amplitude of the oscillatory component of the circulation, the above trends explain how the circulation responds to changes in the flow unsteadiness.

Thesis Supervisor: James E. McCune

Title: Professor of Aeronautics and Astronautics

Acknowledgements

I am grateful to Professor McCune for the guidance and the insights that he has offered me during the course of this research. At tough times his encouragement kept me going. I very much appreciate the opportunities he gave me to attend meetings and communicate the results of our research.

I am thankful to Professor Martinez-Sanchez for many interesting and enlightening discussions. His gentle and friendly manner has set an example for my life.

Professor Landahl taught me most of what I know about Fluid Mechanics; I am indebted to him.

I enjoyed working with Professor Epstein as his assistant when he was teaching Jet Engines and Rockets. I appreciate his suggestions and his help with the presentation of this work.

I thank Professor Covert for his strong support, his interest, and his suggestions.

Whenever Professor Marble visited us new ideas sprang; his interest, knowledge, and words of encouragement helped me overcome many obstacles.

My friends have made my stay at MIT fun and fruitful. Knox Millsaps, Petros Voulgaris, Babis Tsaknakis, Stephane Mondoloni, Kevin Huh, Sasi Digavali, Fei Li, Sean Tavares, Norman Lee, Petros Kapasouris, Chris Howell, Dan Gysling, Rodger Biasca, Mark Lewis, Mark Vidov, Harald Weigel, Didier Hazan: thank you very much; I hope that we will always stay in touch.

Πατερα και μητερα: Ευχαριστω για την αγαπη και την ατελειωτη υποστηριξη. Σας οφειλω το ζειν και το ευ ζειν.

Sandra Larsen, you have been a source of comfort and joy all these years; I owe you so much.

This research has been partly supported by the AFOSR under Contract Nr. 90-0035.

To Krista Larsen

Her short life was a hard battle. She fought it with a smile.

Contents

List of Figures

Nomenclature

Symbols	Definition
c	airfoil chord
D	drag
$F \equiv \phi + i\psi$	complex potential
L	lift
M	moment about a specified point
p	pressure
Re	Reynolds number based on the chord
t	time
u	velocity component parallel to the wall
v	velocity component normal to the wall
$w \equiv u - iv$	conjugate velocity
$x_0(t)$	abscissa of the "centre of separation"
$y_0(t)$	ordinate of the "centre of separation"
$x_m(t)$	abscissa of the suction peak
α	angle of attack
Γ	circulation
δ	boundary layer thickness
δ^*	displacement thickness

$\epsilon \equiv \frac{\widehat{U_\infty}}{U_\infty}$	strength of flow unsteadiness
$\lambda^2 \equiv \frac{\omega c}{U_\infty}$	reduced frequency
ν	kinematic viscosity
ρ	density
τ	shear stress
ϕ	potential
ψ	streamfunction
ω	frequency of oscillation
$\Im( )$	imaginary part of a complex number
$\Re( )$	real part of complex numbern

Subscripts	Definition
$()_e$	property of the external flow
$()_b$	property of the "basic flow"; refers to the steady flow created by the mean part of the external velocity
$()_{p,n}$	property of the n-th order component of the "Prandtl flow"
$()_{s,n}$	property of the n-th order component of the "Stokes flow"
$()_w$	conditions at the wall
$()_{in}$	refers to the inner part of the mean "Prandtl" velocity profile
$()_{out}$	refers to the outer part of the mean "Prandtl" velocity profile
$()_f$	property of the mean "Prandtl flow" over a flat plate

Superscripts	Definition
$\overline{()}$	mean value during an oscillation period; except in chapter 5: complex conjugate
$\widetilde{()}$	unsteady part of a periodic function
$\widehat{()}$	amplitude of oscillation
$()^*$	nondimensional function
$\breve{()}$	refers to the airfoil frame of reference

Chapter 1

Introduction

1.1 Survey of previous work and connection to the present work

In flow past streamlined airfoils or cascade blades, use of the Kutta condition as a part of the potential flow calculation provides a means by which airfoil circulation (and hence lift or mean turning) can be determined, thus eliminating the need for complex viscous calculations. For bluff airfoils, however, this approach must be modified (Sears, 1976) so as to include the interaction between the body boundary layers and the wake behind the body.

In the steady flow case, the airfoil circulation is determined by setting the net vorticity flux leaving the airfoil equal to zero. The position of the separation points on both top and bottom surfaces is calculated, taking into account the interference effect of the wakes, and the airfoil circulation is chosen so that the external stream velocities at the points of separation be equal. Howarth (1935) was the first to propose this method for calculating the circulation about a thin elliptic cylinder in steady flow. Moore (1955) used this method to find the circulation at the position of maximum lift (stall position)

about an airfoil oscillating in pitch at low reduced frequency. Having calculated the maximum lift by Howarth's method, Moore took the change in lift, measured from this value, to be proportional to the rate of change in the angle of attack. The quasi-steady motion of the separation points (based on a Kármán-Pohlhausen integral method) gave the net vorticity flux into the wake and consequently the lift hysteresis.

In the unsteady flow case, the rate of change of the airfoil circulation is equal to the net vorticity flux leaving the airfoil. It is then necessary to determine the development of the boundary layers on the airfoil, and in particular the location and the motion of the separation points, because they determine the net vorticity flux into the wakes. The calculation, in addition to the unsteadiness of the incoming flow, must also take into account the interaction between the airfoil and its wake.

The principal goal of this work is to determine how a bluff airfoil interacts with its own wake, by developing a simple method for finding the location and movement of the separation points.

In the case of steady boundary layers, remarkable success has been achieved by Stratford in devising a simplified method for predicting the location of boundary layer separation, for both laminar (Stratford, 1954) and turbulent (Stratford, 1957) boundary layers. This method has originally been developed for cases in which the pressure remains constant for some distance up to the origin of the x-axis, and then rises. Stratford divided the boundary layer into two parts:

- In the outer part of the boundary layer the loss of total head due to viscosity is

small and taken to be the same as in Blasius flow.

- In the inner part of the boundary layer the convection terms are small and can be neglected in the momentum balance.

The two velocity profiles are patched together and the requirement that the velocity and its first and second derivatives match, leads to a relation which describes how the wall stress τ_w changes with x:

$$c_p(x\frac{dc_p}{dx})^2 = 0.0108(1 - \frac{\tau_w}{\tau_f})^2(1 + 2\frac{\tau_w}{\tau_f})$$

where, τ_f is the wall stress of the Blasius flow at the position x. The location of steady separation x, is the location where the wall stress vanishes. By letting $\tau_w = 0$ in the last equation, Stratford found that the separation location x (in laminar flow) is given by:

$$c_p\ (\ x\frac{dc_p}{dx}\ )^2 = 0.0108$$

The presence of a favourable pressure gradient from the leading edge to the suction peak is taken into account by using the "equivalent constant pressure region" (see Kuethe & Chow, p.p. 331-335, also Smith, 1975, p.p. 509-515). Curle & Skan (1957) modified the constant in the above relation to 0.0104 and achieved remarkable accuracy in predicting the location of separation for 7 types of flows. In Rosenhead (1963, p.p. 329-331), the actual separation position for these flows, given either by experiments or by numerical calculations, is compared to the prediction of Stratford's model, and to 5 other approximate methods for locating separation, based either on integrated forms of the boundary layer equations or on division of the boundary layer into inner and outer layers which are then joined together. The comparison shows that Stratford's criterion is the most accurate prediction method.

Stratford's procedure avoids detailed calculation of the boundary layer development by using in the prediction of the separation location key flow properties that control boundary layer behaviour. For that reason it is used effectively in refining airfoil design (Smith, 1975). If the airfoil profile is such that the boundary layer at every position is on the verge of separation, the drag is minimized. This profile can be calculated from Stratford's relation. In Smith's paper it is demonstrated that the Stratford pressure distribution is the path of least drag connecting two given pressure values (even if at the end of this distribution, the pressure has to jump in order to match the second value).

Early in our research on this topic, we decided to apply Stratford's idea to the prediction of steady lift versus incidence on bluff bodies where the Kutta condition cannot be expected to apply. In particular, we applied this procedure to the prediction of the lift on an ellipse at various angles of attack, a problem first discussed by Howarth (1935). We discovered that Stratford's criterion worked very well indeed for such an application and we were able to duplicate Howarth's results right up to the stall of the ellipse. The calculation was done for both turbulent and laminar flows. Thus, this approach, based on Stratford's separation criterion, seems to provide a means of determining airfoil performance with almost the same ease as the Kutta condition, at least in steady flow. The next step was to investigate whether a similar method could be devised for unsteady flow. In particular, we considered an important class of unsteady flows: flows past bodies with external velocity oscillating about a nonzero mean. This situation arises when either the farfield velocity oscillates in magnitude and direction, or the airfoil executes a maneuver which can be decomposed to a combination of a

translatory and a rotational oscillation.

We first consider this general case, analyze the boundary layer (chapter 2), and derive a criterion for unsteady separation (chapters 3, 4). In the applications of chapters 6 and 7 (the airfoil-wake interaction problem) we take the farfield velocity to oscillate in magnitude only; cases, where the direction of the freestream velocity changes, can be treated in a similar manner (see section 8.2).

For oscillating flows we can distinguish between two types of time scales:

- The time scale in which the changes in flow properties which are caused by the imposed unsteadiness become significant, $T_{\text{external}} = \frac{1}{\omega}$.
- The time scales intrinsic to the flow; these are:
  - the convection time scale, $T_{\text{convection}} = \frac{c}{\overline{U}}$, where c is the airfoil chord, and $\overline{U}$ the mean of the freestream velocity,
  - the diffusion time scale, $T_{\text{diffusion}} = \frac{\delta^2}{\nu}$, where δ is the thickness of the vortical layer formed as vorticity simulatanously diffuses away from the airfoil surface and is convected downstream by the mean part of the external velocity,
  - the acoustic time scale, $T_{\text{acoustic}} = \frac{c}{a}$, where a is the speed of sound.

The ratio of the external to the convective time scale determines whether the imposed unsteadiness causes significant changes in the flow properties during the passage of a flow particle by the airfoil:

$$\lambda^2 \equiv \frac{\omega c}{\overline{U}}$$

This parameter is called the reduced frequency, and measures the importance of unsteady effects compared to quasi-steady effects. Examples of periodic flows and the corresponding values of reduced frequency are (Landahl, 1987, course on Unsteady Fluid Mechanics):

- Phugoid motion: $\lambda^2 = 0.001 - 0.1$
- Flutter: $\lambda^2 = 0.1 - 0.3$
- Helicopter rotors undergoing periodic changes in velocity and angle of attack:$\lambda^2 = 0.5 - 1.5$
- Rotor-stator interaction: $\lambda^2 = 3 - 9$. An estimate for the reduced frequency associated with this type of unsteadiness proceeds as follows.

  A stator blade within one period of the shaft rotation, T_{rotation}, cuts through n_{blades} wakes of the upstream rotor. Therefore, the period of the induced unsteadiness is $T = T_{\text{rotation}}/n_{\text{blades}}$, and the frequency of the phenomenon is $\omega = \omega_{\text{rotation}} n_{\text{blades}}$. If the blade spacing is s, and the radius is r, then $2\pi r = n_{\text{blades}} s$. If the rotational speed of the blade is V, we express the reduced frequency as:

$$\begin{aligned} \lambda^2 = \frac{\omega c}{U} &= \frac{\omega_{\text{rotation}} n_{\text{blades}} c}{U} = \frac{\omega_{\text{rotation}} r}{U} \frac{c}{\frac{r}{n_{\text{blades}}}} \\ &= \frac{V}{U} \frac{c}{\frac{2\pi r}{n_{\text{blades}}}} 2\pi = \frac{V}{U} \frac{c}{s} 2\pi \end{aligned}$$

  Since $\frac{V}{U} \approx 1$, and $0.5 < \frac{c}{s} < 1.5$, then $3 < \lambda^2 < 9$. In this range of reduced frequencies both unsteady and quasi-steady effects are important. In the high λ^2 end of this regime, unsteady effects start to dominate. In chapter 2 we analyze

the dual character of the flow (steady-unsteady) for high reduced frequencies and show that the two components can be distinguished from each other.

- Upstream influence of the potential field of the downstream row: $1 < \lambda^2 < 10$ (Greitzer, 1984, pp. 7, 44).

- Inlet distortion: $\lambda^2 < 0.1$.

In this work we consider laminar, incompressible, two-dimensional flows, with external velocity oscillating at high reduced frequency according to the law:

$$U_e(x,t) = \overline{U_e}(x) + \widehat{U_e}(x)e^{i(\omega t+\phi)}$$

In our analysis we consider the general case, where the phase of the external oscillation is a function of the streamwise position, $\phi = \phi(x)$, and the unsteadiness has the form of a travelling wave.

The general unsteady boundary layer equations can be applied to the problem. However, the difficulty for carrying out a general analysis is great, because of the inertia terms in the equation of motion. These terms give rise to periodic variations at higher harmonics of the frequency of the oscillating external stream.

Lighthill (1953) was the first to investigate the problem. He considered the laminar boundary layer in two-dimensional flow past a cylindrical body, when the external velocity oscillates according to the law:

$$U_e(x,t) = U_0(x)(1 + \epsilon e^{i\omega t})$$

He studied both the low and high reduced frequency cases. The solution expanded in powers of ϵ is:

$$u(x,y,t) = u_0(x,y) + \epsilon u_1(x,y)e^{i\omega t}$$

where u_1 is a complex quantity and (as in the rest of this work) only the real part of the complex expressions has physical meaning.

- For low reduced frequency the unsteady part of the velocity is written as the sum of a quasi-steady component in phase with the free stream, and a component which is 90^0 out of phase.

$$u(x,y,t) = u_0(x,y) + \epsilon(u_{q-s}(x,y) + i\omega u_2(x,y))e^{i\omega t}$$

The quasi-steady component $u_{q-s}(x,y)$ is the coefficient of ϵ in the velocity distribution for steady flow with incident stream velocity $U_0(1+\epsilon)$. Lighthill assumes that the second component, u_2, has a Pohlhausen profile and by inegrating the governing equation over the thickness of the boundary layer, finds that it satisfies the equation:

$$\nu \frac{\partial u_2}{\partial y}|_w = \frac{1}{2} U_0 \delta_0^*$$

where δ_0^* is the displacement thickness of the steady flow driven by the mean part of the exernal velocity (in what follows we shall call this flow "basic flow"). Thus, u_2 is independent of ω. In conclusion, the unsteady part of the boundary layer consists of a part depending on the instantaneous stream velocity, and a part depending on the stream acceleration. The skin friction at any instant is:

$$\mu \frac{\partial u_0}{\partial y}|_{y=0} + \epsilon e^{i\omega t}(\mu \frac{\partial u_{q-s}}{\partial y}|_{y=0} + i\omega\mu \frac{\partial u_2}{\partial y}|_{y=0}) = \tau_0 + \epsilon e^{i\omega t}(\frac{3}{2}\tau_0 + i\omega \frac{1}{2}\rho U_0 \delta_0^*) \quad (1.1)$$

- When the external flow oscillates at a high reduced frequency, the only terms retained in the equation governing u_1 are the terms involving ω and the derivative of highest order. This equation is identical to the equation for "shear-waves", boundary layers which oscillate about a zero mean. The solution is

$$u_1 = \epsilon U_0(x)(1 - e^{-y\sqrt{\frac{i\omega}{\nu}}})e^{i\omega t}$$

The skin friction is

$$\mu \frac{\partial u_0}{\partial y}|_{y=0} + \epsilon e^{i\omega t} \mu U_0 \sqrt{\frac{i\omega}{\nu}}$$

Thus, the amplitude of the skin friction oscillations increases with reduced frequency, and its phase leads that of the fluctuations in the external velocity by 45^0. In section 2.5 we show that, when the boundary layer velocity is expanded into powers of $1/\lambda$, Lighthill's result is the lowest order unsteady component of the boundary layer velocity.

Finally, Lighthill joins the high and low frequency approximations at the frequency, for which the phase lead of the skin friction (1.1) rises to its high frequency limit of 45^0. This frequency is

$$\omega_0 = \frac{3\tau_0}{\rho U_0 \delta_0^*}$$

It turns out that for this frequency, the skin friction amplitudes of the two approximations also agree.

In our work we have adopted the analysis due to C. C. Lin (1956) and his student Gibson (1957), which is valid for high reduced frequencies and (unlike Lighthill's linear theory) is not restricted to small amplitudes of oscillation. This analysis is based on

the observation that, for high reduced frequency of the external oscillation, the local acceleration is much larger than the unsteady part of the convection of momentum (this is same idea that underlies Lighthill's analysis of the high frequency oscillation). Then, to a first approximation the fluctuating part of the motion can be treated as in Stokes flow (Stokes's second problem).

The vorticity generated by the flow unsteadiness is confined to a thin layer near the blade surface ("Stokes layer"). In the rest of the boundary layer, the unsteady part of the velocity is equal to that of the external oscillation. In addition to the "Stokes layer", another vortical layer develops as vorticity simultaneously diffuses away from the surface and is convected by the mean part of the external velocity ("Prandtl layer"). Gibson (1957) divides the flow into "Prandtl flow" (driven by the time-mean part of the external flow) and "Stokes flow" (driven by the the oscillating part of the free-stream velocity). The two velocity distributions satisfy a system of coupled equations which add up to the unsteady boundary layer equation. Far from the airfoil, the "Prandtl" and the "Stokes" velocities tend to the time-mean and the oscillating part of the free-stream velocity, respectively.

The "Stokes flow" has a non-vanishing mean component on the airfoil surface, a property created by steady streaming (Schlichting, 1979). This non-vanishing mean velocity on the airfoil surface is cancelled out by the "Prandtl flow". The no-slip condition provides the strongest coupling between the two velocity distributions. Expansion into powers of the small parameter $\frac{1}{\lambda}$ yields the velocity to the desired accuracy.

This approach offers the opportunity to develop a criterion for predicting separa-

tion in the unsteady case. According to the classical generic definition of separation of Landau and Lifshitz (1959), valid for both steady and unsteady flows, separation is the dramatic increase in the normal component of the velocity in the boundary layer, or equivalently the dramatic increase in the displacement thickness. It turns out that the contribution of the "Stokes layer" to the displacement thickness is bounded by $\frac{1}{\sqrt{\text{reduced frequency}}}$, which means that the "Prandtl layer" can be used to identify and locate separation. Whereas the "Stokes velocity" is analytic, the normal "Prandtl velocity" reveals the expected dramatic increase near separation by manifesting singular behaviour in x (compare Sears, 1976).

In a steady boundary layer, reversal of the flow is always associated with separation. In chapter 3 we show that, in high frequency flows, the dominant component of the wall shear originates from the "Stokes flow" and is oscillatory. Therefore, temporary backflow and sign reversal of the wall shear stress in unsteady flow are not associated with separation as experimental findings indicate (Despard 1971, Koromilas 1980, Mezaris 1987).

Proper treatment of the singularity in v_p and in $\frac{\partial u_p}{\partial x}$ leads to two conditions for unsteady separation. According to them, the "separation point" is seen as a point of bifurcation of the "Prandtl velocity" by an observer who moves with a speed equal to the difference between the speed of the separation point and the unsteady part of the free-stream velocity. Such an observer sees the fluid particles being decelerated as they approach the separation point. In order to satisfy continuity, they exchange u-velocity for v-velocity and this causes the dramatic increase in the transverse velocity component at separation.

Moore (1957), Rott(1956), and Sears(1956) proposed as conditions for unsteady separation the simultanous vanishing of the shear and the velocity at a point within the boundary layer and in a frame of reference moving with separation.

$$u = \frac{dx_0}{dt};\ \frac{\partial u}{\partial y}|_{(x_0,y_0)} = 0$$

In chapter 3 we discuss how the separation conditions that we propose relate to the MRS conditions.

Sears and Telionis (1975) demonstrated that these conditions mark the appearance of a singularity in the unsteady boundary layer equations. In chapter 3 we show that the separation conditions which we propose lead to the appearance of singularity in the "Prandtl flow", while the "Stokes flow" remains analytic.

An analogous situation arises in steady flow, where the steady boundary layer equations break down beyond the separation point (identified in that case by the vanishing of the wall shear). The solution cannot be continued beyond the separation point if the pressure gradient beyond separation is taken to be unaltered by separation and equal to that given by the external potential flow. Sychev (1972) removed this singularity by discovering that the local interaction between the boundary layer and the external inviscid flow creates a large local adverse pressure gradient (whose magnitude is $Re^{1/8}$ times the magnitude of the imposed pressure gradient, and acts over a region that includes the separation point and extends over a length $Re^{-3/8}$ times the length over which the imposed pressure gradient acts). This theory is known as "triple deck theory". Sychev (1978) extended this theory to unsteady flows. The method of matched asymptotic expansions that is used in that analysis requires the matching of 6 decks in

the neighbourhood of the moving separation point.

A major advantage to C.C. Lin's analysis of the boundary layer flow is that both the steady and the unsteady components of the "Prandtl velocity" can be expressed in terms of the steady flow driven by the mean part of the free-stream velocity ("basic flow") and certain key unsteady flow parameters. Stratford's ideas, modified to account for unsteadiness in the "Prandtl velocity" (arising through the coupling of the "Prandtl" to the "Stokes" flow by the no-slip condition on the wall and terms that resemble Reynolds stresses in the momentum equation), lead to a relation which describes how the wall stress depends on x and key unsteady flow parameters.

This relation, combined with the two conditions for unsteady separation, yields a criterion for unsteady separation, which uses as only inputs parameters of the external flow and avoids a detailed boundary layer calculation. When the unsteadiness vanishes, Stratford's separation criterion is recovered (see chapter 4).

The motion of the "separation points" on the airfoil determines the net vorticity flux shed into the wake or, equivalently, the rate of change of the circulation around the airfoil (Sears 1976). At the same time, the velocity induced by the wake vorticity changes the external flow and thus the location of separation. The airfoil circulation must be calculated by an iterative procedure which accounts for the wake effects on separation (chapters 5, 7).

An ellipse is adopted as a study case, and results are presented for varying angle of attack, ellipse slenderness, reduced frequency, and strength of unsteadiness.

Van Dommelen and Shen (1977) (see also Van Dommelen, 1981) offered a very illuminating description of the unsteady separation phenomenon from the Lagrangian point of view. A fluid particle is identified by its coordinates ξ, η at $t = 0$. Particle paths are functions of the initial position of the particle and time t: $x = x(\xi, \eta, t), y = y(\xi, \eta, t)$. The authors performed a numerical calculation, where they followed the motion of particles that were situated at the nodes of a rectangular grid (see figure (1.1)). The initial velocity profile was $u_0 = f'(\eta)\sin(\xi)$; $v_0 = -f(\eta)\cos(\xi)$, where $-f(\eta)$ is the profile of the normal velocity in the vortical layer of "stagnation point flow" (the Hiemenz profile). Along the edge of the boundary layer, where $f'(\eta) = 1$, the velocity distribution is the same as the external velocity in flow around a circular cylinder. The motion of the fluid particles is governed by the usteady boundary layer equations cast in the Lagrangian form. The numerical results indicated that x, u, u_ξ, and u_η remain bounded, but y_ξ, y_η, and u_x tend to blow up at appoximately $x_0 = 2$. The shape of the distorted lattice (see figure 1.1) indicates the appearance of a singularity in the normal position y of the fluid particles in the Eulerian frame. As the singular point is approached, x_ξ and x_η tend to zero. The vanishing of $\frac{\partial x}{\partial \xi}|_{x=x_0}$ implies that the position x_0 is reached at the same time by different fluid particles (characterized by different ξ). According to the description of the authors, the paricles run into an imaginary barrier located at x_0 on which they accumulate. Since the flow is incompressible and the x dimension of the fluid particles reduces to zero as they approach x_0, their y dimension blows up, causing the breakaway of the flow.

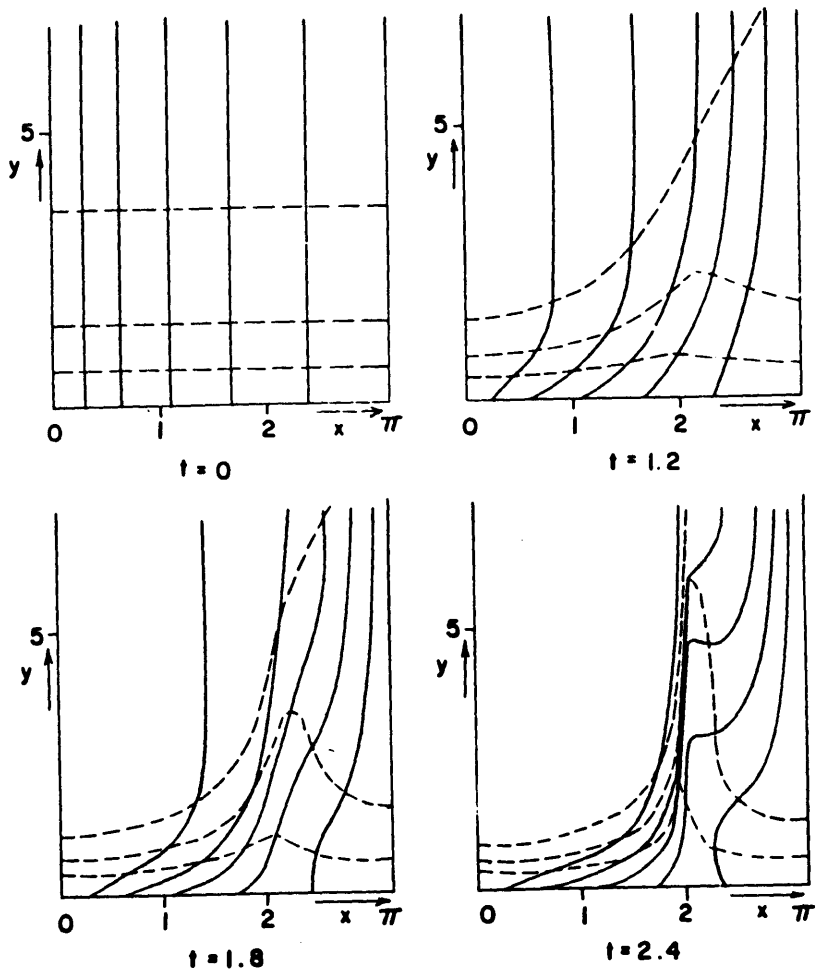

Figure 1.1: The deformation in time of an initially rectangular mesh marking the location of the fluid particles. At $t = 2.4$ the separation location is identifed as a barrier in the flow field against which the fluid paricles pile up being unable to continue their motion downstream.

1.2 Synopsis of the thesis

An alternative to the Kutta condition for determining the circulation around a bluff airfoil in unsteady, separated flow is presented. For such flows, there is a need for a practical criterion which would avoid the detailed boundary layer calculations and would predict the time evolution of the airfoil circulation based on parameters of the external flow only. This criterion would play for unsteady, separated flows the role that the Kutta condition plays for flows past thin airfoils.

This criterion turns out to be a criterion for predicting the location and movement of the "separation points", because they determine the net vorticity flux shed into the wake. Based on this criterion, an iterative method is developed that calculates how the interaction between the airfoil and its wake determines the airfoil circulation.

The laminar, two-dimensional flow about a bluff airfoil at angle of attack, when the external flow oscillates in magnitude but not in direction at a high reduced frequency is considered.

At high frequencies, the vorticity generated as the wall resists the imposed unsteadiness is confined to a thin layer near the blade surface ("Stokes layer") and its contribution to the displacement thickness is proportional to an inverse power of the reduced frequency and thus small. Outside this region, the unsteady part of the boundary layer velocity is approximately the external potential oscillation. Based on this observation and following C.C. Lin, the boundary layer velocity can be divided into two coupled velocity distributions, one predominantly oscillatory ("Stokes velocity") and another

predominantly steady ("Prandtl velocity"). The main contributor to the displacement thickness is the latter. It is the velocity distribution related to the vortical layer which develops as vorticity simultaneously diffuses away from the surface and is convected by the mean part of the external velocity ("Prandtl layer"). Therefore, separation, identified by a dramatic increase in the displacement thickness, can be located by calculating the evolution of the "Prandtl velocity".

The "separation point" is seen as a stagnation point in the "Prandtl velocity" by an observer who moves with a speed equal to the difference between the speed of the separation point and the unsteady part of the free-stream velocity. Stratford's ideas, modified to account for unsteadiness in the "Prandtl velocity" (arising through the coupling of the "Prandtl" to the "Stokes" flow by the no-slip condition on the wall and Reynolds-stress terms in the momentum equation), lead to a criterion for unsteady separation that uses as only inputs parameters of the external flow and avoids a detailed boundary layer calculation. This view of the unsteady separation phenomenon agrees with experimental findings which indicate that the temporary back-flow and the shear stress reversal in the "Stokes flow" are not associated with unsteady separation. In the limit of vanishing unsteadiness, the unsteady separation criterion reduces to Stratford's citerion for steady separation.

The motion of the "separation points" on the airfoil determines the net vorticity flux shed into the wake or, equivalently, the rate of change of the circulation around the airfoil. At the same time, the induction of the developing wake changes the external flow and thus the location of separation. The airfoil circulation is calculated by an iterative method which uses the wake induction effects to locate separation. This closes the loop

of the airfoil-wake interaction problem.

An ellipse is adopted as a study case, and results are presented for varying angle of attack, ellipse slenderness, reduced frequency, and strength of unsteadiness. In the limit of a very slender ellipse, the theory recovers the results from the classical unsteady wing theory, which assumes the Kutta condition.

The theory predicts that there exist two limits for the mean value of the circulation. The upper limit is the value of the circulation for which the trailing edge becomes a stagnation point (Γ_{Kutta}). The lower limit is the value of the circulation in steady flow (Γ_{Howarth}). While the pressure side "separation point" for all practical purposes can be considered fixed, even at small angles of attack, the "separation point" on the suction side oscillates with amplitude proportional to the strength of the flow unsteadiness, and inversely proportional to the reduced frequency. When the reduced frequency increases or the strength of flow unsteadiness decreases, the mean location of this "separation point" tends to the position of steady separation. Since the mean location of the suction-side "separation point" controls the mean value of the circulation, and the amplitude of its excursion determines the amplitude of the unsteady part of the circulation, the above trends explain how the circulation responds to changes in the reduced frequency or in the strength of the unsteadiness.

1.3 Overview

In chapter 2 we discuss how the flow in a boundary layer with a rapidly oscillating external flow can be divided into two velocity distributions, and we determine these velocity distributions by expanding the velocity into powers of the small parameter $1/\lambda^2$ and then by solving for its mean and oscillatory component.

In chapter 3 we explain why one of the two velocity distributions is primarily responsible for separation, and derive the conditions for unsteady separation.

In chapter 4 we derive from the above conditions a practical criterion for predicting unsteady separation by modelling the boundary layer flow.

In chapter 5 we describe how the airfoil interacts with its wake, how the force and moment are calculated, and how the method is implemented on the computer.

In chapter 6 we apply our separation criterion to test cases and compare its predictions to experimental results.

In chapter 7 we make the connection between the separation trajectory predictions and the trends in the aerodynamic forces, when certain unsteady flow parameters are varied.

In chapter 8 we put all the above into perspective, and make suggestions (as well as give a few starting points) for future research.

Chapter 2

Flow in a boundary layer with a rapidly oscillating free-stream velocity

2.1 Assumptions

We consider the laminar, incompressible, two-dimensional flow about a bluff airfoil, at angle of attack (see figure (2.1)). The external flow oscillates about a nonvanishing mean at high reduced frequency ($\lambda^2 = \frac{\omega c}{U} \gg 1$). The amplitude of the oscillation is arbitrary, since the analysis is nonlinear.

The conditions for incompressibility are: $M \ll 1$ and $M\lambda^2 = \frac{\omega c}{a} \ll 2\pi$. The first condition requires that the speed of sound a be lage compared with the speed of the flow. The second condition can be rewritten as: $\frac{c/a}{T} \ll 1$, and requires that the period of the imposed oscillation T be large compared to the time the sound takes to travel over the length of the body. Under these conditions we can neglect that disturbances propagate at finite speed; then changes in the boundary conditions affect instantaneously the whole flow, as if the velocity of sound were infinite.

2.2 The division of the flow-field

We ignore the displacement effect of the thin boundary layer on the external flow. The streamlines follow the airfoil contour up to the locations of separation (one on each side of the airfoil), where they break away from the contour. At these locations, the vorticity which is generated on the surface of the airfoil, leaves the airfoil and is shed into its wake. The wake is bounded by two free streamlines that emanate from the edge of the boundary layer at the separation location on the suction and pressure sides of the airfoil (see figure (2.1)). The velocity induced by the vortical wake is added to the velocity of the oncoming stream to give the external velocity distribution. This external velocity distribution determines the location and motion of the separation points (see chapter 4) which in turn determine the development of the wake. This interaction between the airfoil and its wake is calculated by an iterative procedure, which we present in chapter 5. Taking the external velocity distribution as given by such a calculation, we proceed to analyze the boundary layer flow.

The general unsteady boundary layer equations can be applied to the problem.

$$\frac{\partial u}{\partial t} + (u\frac{\partial}{\partial x} + v\frac{\partial}{\partial y})u - \nu\frac{\partial^2 u}{\partial y^2} = \frac{\partial U}{\partial t} + U\frac{\partial U}{\partial x}$$

$$\frac{\partial u}{\partial x} + \frac{\partial v}{\partial y} = 0$$

$$y = \infty : u = U(x,t); \quad y = 0 : u = v = 0$$

These are derived from the Navier-Stokes equations by neglecting the curvature of the airfoil, the variation of the pressure across the boundary layer, and the streamwise diffusion. The inertia terms in the general equation of motion make an analysis based on that equation extremely hard, because they give rise to periodic variations at higher

harmonics of the frequency of the fluctuating external stream.

But when the reduced frequency of the external oscillation is high, the local acceleration is much larger than the unsteady part of the convection of momentum. Then, to a first approximation the fluctuating part of the motion can be treated as in Stokes's flow (Stokes's second problem). An approximate analysis due to C. C. Lin (1956) and his student Gibson (1957), which is based on the above observation, can be applied. In the following we present Gibson's method of solution. It can be proven (Gibson, 1957, pp. 52-54) that his approach is equivalent to C. C. Lin's method.

First we discuss some physical aspects of the problem that make this method of solution possible. The free-stream velocity, $U(x,t)$, has a mean component, $\overline{U}(x)$, and an oscillating component, $\tilde{U}(x,t)$.

Let us first consider the vortical layer that contains vorticity generated because the no-slip condition on the airfoil surface resists the outer fluid motion at an average speed $\overline{U}$. This vortical layer expands into the outer flow as the vorticity generated on the wall simultaneously diffuses away from the wall and is carried downstream by the external flow. The time required for the vorticity, which is generated on the airfoil surface, to diffuse through a distance δ_p is: diffusion time $= \frac{\delta_p^2}{\nu}$. On the other hand, the time required for the vorticity to be convected through a distance c is: convection time $= \frac{c}{\overline{U}}$, where $\overline{U}$ and c are a reference time-mean speed and a reference length in the direction of the flow.

Let us now consider the ratio:

$$\frac{\text{rate of convection through a distance } c}{\text{rate of diffusion through a distance } \delta_p} = \frac{\frac{\overline{U}}{c}}{\frac{\nu}{\delta_p^2}}$$

In steady flow these rates must balance, otherwise the boundary layer would either shrink or grow fast (as in the case of, say, a body accelerating from rest, or downstream of separation as we shall see later in chapter 3). From this we infer that the boundary layer thickness associated with the mean flow, which we shall call "Prandtl thickness", is on the order of:

$$\delta_p = \sqrt{\frac{\nu c}{\overline{U}}} = \frac{c}{\sqrt{Re_c}}$$

Let us now turn to the unsteady part of the flow, and consider the change of the external velocity from $\overline{U} - \hat{U}$ to $\overline{U} + \hat{U}$, which occurs in time on the order of $\frac{1}{\omega}$. The time required for viscosity to counter this increase in velocity is the diffusion time $\frac{\delta_s^2}{\nu}$. By equating these time scales we find the thickness of a secondary layer ("Stokes layer") within which, the oscillation is affected by viscous forces:

$$\delta_s = \sqrt{\frac{\nu}{\omega}}$$

The ratio of the "Prandtl thickness" to the "Stokes thickness" is equal to the square root of the reduced freqency:

$$\frac{\delta_p}{\delta_s} = \sqrt{\frac{c\omega}{\overline{U}}} = \lambda$$

When the reduced frequency is high, the outer part of the boundary layer reacts to the external oscillation in an inviscid fashion, because viscosity has insufficient time to counter the change with time in the free-stream velocity.

When the reduced frequency is low, the vorticity which is generated as the wall resists the imposed unsteadiness, is convected away and does not accumulate to form

a secondary layer of vorticity. Indeed, the rate of diffusion of this additional vorticity which is approximately equal to the rate at which it is formed, $\frac{1}{\omega}$, is much smaller than the convection rate, $\frac{c}{U}$. In this case, the "Stokes layer" does not exist and the method of "splitting the solution" fails, as we explain in Appendix A.

We now concentrate on the high frequency case. The boundary layer for most of its thickness (from its outer edge $y = \delta_p$ to the edge of the secondary layer of vorticity generated by the flow unsteadiness $y = \delta_s$) responds to the external oscillation in an inviscid fashion. The presence of the solid boundary changes the unsteady component of the velocity from its potential value only within the secondary layer of vorticity. The situation is the same as in Stokes's second problem. If this velocity field is subtracted from the boundary layer velocity what remains is a velocity field of predominantly steady charater, which at the edge of the boundary layer tends to the mean value of the external veocity.

This motivates the division of the boundary layer velocity (u, v) into two components: the "Stokes velocity" (u_s, v_s), corresponding to the fluctuating component $\tilde{U}(x,t)$, and the "Prandtl velocity" (u_p, v_p), associated with the mean component $\overline{U}(x)$, of the external velocity, respectively:

$$y = \infty : u_p = \overline{U}(x), u_s = \tilde{U}(x,t)$$

At the wall, the two components together satisfy the no-slip condition

$$y = 0 : u_p + u_s = 0, v_p = v_s = 0$$

In order to find how the momentum equation should be divided, let us examine the flow in the region of thickness $\delta_p - \delta_s$ that lies between the edges of the two layers. In this

region, the "Stokes flow " has attained its free-stream value:

$$u_s = \tilde{U}(x,t),\ v_s = V_s = -y\frac{\partial \tilde{U}}{\partial x}(x,t) + W_s(x,t)$$

W_s represents the difference between the actual value of the normal external velocity, V_s, and the potential value, $-y\frac{\partial \tilde{U}}{\partial x}(x,t)$, caused by the displacement of the free-stream by the oscillation layer.

If we now express the velocity in this region as the sum of the "Prandtl velocity" and the above value of the "Stokes velocity":

$$u = u_p + \tilde{U},\ v = v_p + V_s$$

and substitute it in the general momentum equation we get:

$$\frac{\partial u_p}{\partial t} + \frac{\partial \tilde{U}}{\partial t} - \nu\frac{\partial^2 u_p}{\partial y^2} + (u_p\frac{\partial}{\partial x} + v_p\frac{\partial}{\partial y})(u_p + \tilde{U}) + (\tilde{U}\frac{\partial}{\partial x} + V_s\frac{\partial}{\partial y})u_p + \tilde{U}\frac{\partial \tilde{U}}{\partial x}$$
$$= \frac{\partial \tilde{U}}{\partial t} + \overline{U}\frac{\partial \overline{U}}{\partial x} + \frac{\partial \overline{U}\tilde{U}}{\partial x} + \tilde{U}\frac{\partial \tilde{U}}{\partial x}$$

After some cancelations, the momentum equation for the "Prandtl flow" reads:

$$\frac{\partial u_p}{\partial t} - \nu\frac{\partial^2 u_p}{\partial y^2} + (u_p\frac{\partial}{\partial x} + v_p\frac{\partial}{\partial y})u_p + (u_p\frac{\partial}{\partial x} + v_p\frac{\partial}{\partial y})\tilde{U} + (\tilde{U}\frac{\partial}{\partial x} + V_s\frac{\partial}{\partial y})u_p$$
$$= \overline{U}\frac{\partial \overline{U}}{\partial x} + \frac{\partial \overline{U}\tilde{U}}{\partial x}$$

This equation is identically satisfied by the free-stream value of $u_p = \overline{U}(x)$. If we subtract it from the general momentum equation, we obtain the equation for the "Stokes flow":

$$\frac{\partial u_s}{\partial t} - \nu\frac{\partial^2 u_s}{\partial y^2} + (u_s\frac{\partial}{\partial x} + v_s\frac{\partial}{\partial y})u_s + [(u_s - \tilde{U})\frac{\partial}{\partial x} + (v_s - V_s)\frac{\partial}{\partial y}]u_p$$
$$+(u_p\frac{\partial}{\partial x} + v_p\frac{\partial}{\partial y})(u_s - \tilde{U}) = \frac{\partial \tilde{U}}{\partial t} + \tilde{U}\frac{\partial \tilde{U}}{\partial x}$$

This equation is identically satisfied by the free-stream value of $u_s = \tilde{U}(x,t)$.

In summary, the system of equations and boundary conditions for the "Prandtl flow" is:

$$\begin{aligned}
&\frac{\partial u_p}{\partial t} - \nu\frac{\partial^2 u_p}{\partial y^2} + (u_p\frac{\partial}{\partial x} + v_p\frac{\partial}{\partial y})u_p + (u_p\frac{\partial}{\partial x} + v_p\frac{\partial}{\partial y})\tilde{U} + (\tilde{U}\frac{\partial}{\partial x} + V_s\frac{\partial}{\partial y})u_p \\
&= \overline{U}\frac{\partial \overline{U}}{\partial x} + \frac{\partial \overline{U}\tilde{U}}{\partial x} \\
&\frac{\partial u_p}{\partial x} + \frac{\partial v_p}{\partial y} = 0 \\
&y = \infty : u_p = \overline{U}(x); \;\; y = 0 : u_p + u_s = 0, v_p = 0
\end{aligned} \tag{2.1}$$

The effect of the "Stokes" on the "Prandtl flow" is described by the terms involving the external velocity $(\tilde{U}, V_s)$, and by the coupling boundary condition at the wall.

The corresponding system for the "Stokes" flow is:

$$\begin{aligned}
&\frac{\partial u_s}{\partial t} - \nu\frac{\partial^2 u_s}{\partial y^2} + (u_s\frac{\partial}{\partial x} + v_s\frac{\partial}{\partial y})u_s + [(u_s - \tilde{U})\frac{\partial}{\partial x} + (v_s - V_s)\frac{\partial}{\partial y}]u_p \\
&+(u_p\frac{\partial}{\partial x} + v_p\frac{\partial}{\partial y})(u_s - \tilde{U}) = \frac{\partial \tilde{U}}{\partial t} + \tilde{U}\frac{\partial \tilde{U}}{\partial x} \\
&\frac{\partial u_s}{\partial x} + \frac{\partial v_s}{\partial y} = 0 \\
&y = \infty : u_s = \tilde{U}(x,t); \;\; y = 0 : u_s + u_p = 0, v_s = 0
\end{aligned} \tag{2.2}$$

For most of the boundary layer thickness the "Stokes flow" is a potential oscillation, because, at distances from the wall larger than δ_s (the distance at which the vorticity produced on the wall diffuses within time $\frac{1}{\omega}$), the unsteady flow does not realize that there exists a solid boundary imposing the no-slip condition. It is in the thin region $0 < y < \delta_s$ that the "Stokes flow" becomes vortical. Since $\delta_s \ll \delta_p$, we can simplify the momentum equation governing the "Stokes flow" in the above region by substituting u_p and v_p with their Taylor series expansion about the point $(x,0)$.

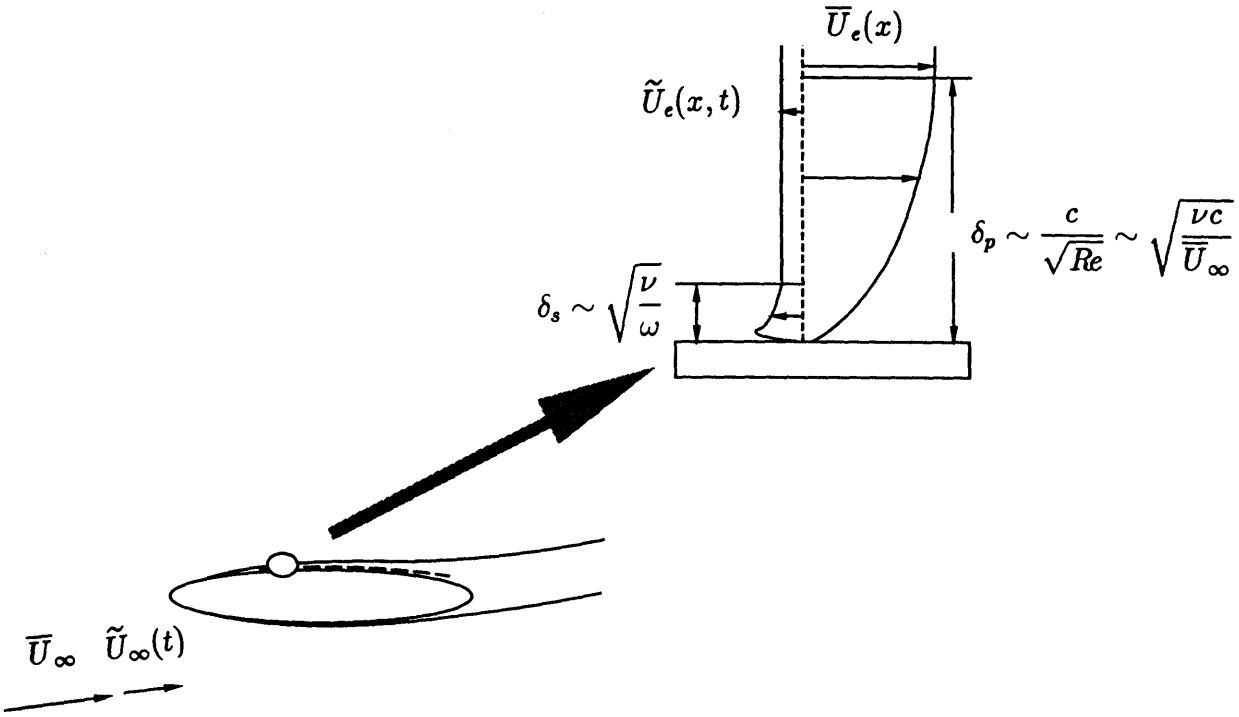

Figure 2.1: The boundary layer structure when the external flow oscillates at high reduced frequency

2.3 The non-dimensional form of the equations

We introduce the following dimensionless variables and dimensionless functions:

$$x^* = \frac{x}{c},\ y_p^* = \frac{y}{\delta_p},\ y_s^* = \frac{y}{\delta_s},\ t^* = \omega t$$

$$u_p^*(x^*, y_p^*, t^*) = \frac{u_p}{U_{\text{ref}}},\ v_p^*(x^*, y_p^*, t^*) = \frac{c}{U_{\text{ref}}\delta_p} v_p = \sqrt{Re}\frac{v_p}{U_{\text{ref}}},$$

$$u_s^*(x^*, y_s^*, t^*) = \frac{u_s}{U_{\text{ref}}},\ v_s^*(x^*, y_s^*, t^*) = \frac{c}{U_{\text{ref}}\delta_s} v_s,$$

$$U^*(x^*, t) = \frac{U(x,t)}{U_{\text{ref}}},\ \overline{U}^*(x^*) = \frac{\overline{U}(x)}{U_{\text{ref}}},\ \widetilde{U}^*(x^*, t^*) = \frac{\widetilde{U}(x,t)}{U_{\text{ref}}},$$

$$V_s(x,y,t) = \frac{U_{\text{ref}}\delta_s}{c} V_s^* = \frac{U_{\text{ref}}\delta_s}{c}[-y_s^*\frac{\partial \widetilde{U}^*}{\partial x^*} + W_s^*(x^*, t^*)] = \frac{U_{\text{ref}}\delta_p}{c}[-y_p^*\frac{\partial \widetilde{U}^*}{\partial x^*} + \frac{1}{\lambda} W_s^*(x^*, t^*)]$$

where:

c is the chord of the airfoil,

U_{ref} is a reference velocity, say the mean farfield velocity $\overline{U_\infty}$,

Re is the Reynolds number based on the airfoil chord,

$\delta_p = \frac{c}{\sqrt{Re}}$ is the "Prandtl thickness",

$\delta_s = \sqrt{\frac{\nu}{\omega}}$ is the "Stokes thickness",

and $\lambda = \frac{\delta_p}{\delta_s} = \sqrt{\frac{\omega c}{U_{\text{ref}}}}$ is the square root of the reduced frequency.

The non-dimensional form of the system (2.1) is:

$$U_{\text{ref}}\omega\frac{\partial u_p^*}{\partial t^*} - \underbrace{\frac{\nu U_{\text{ref}} Re}{c^2}}_{\frac{U_{\text{ref}}^2}{c}}\frac{\partial^2 u_p^*}{\partial y_p^{*2}} + \frac{U_{\text{ref}}^2}{c}(u_p^*\frac{\partial}{\partial x^*} + v_p^*\frac{\partial}{\partial y_p^*})u_p^* + \frac{U_{\text{ref}}^2}{c}(u_p^*\frac{\partial}{\partial x^*} + v_p^*\frac{\partial}{\partial y_p^*})\tilde{U}^*$$

$$+(\frac{U_{\text{ref}}^2}{c}\tilde{U}^*\frac{\partial}{\partial x^*} + \underbrace{\frac{U_{\text{ref}}\delta_p}{c}[-y_p^*\frac{\partial \tilde{U}^*}{\partial x^*} + \frac{1}{\lambda}W_s^*]}_{V_s}\frac{\partial}{\partial y_p^*})u_p^* = \frac{U_{\text{ref}}^2}{c}\overline{U}^*\frac{\partial \overline{U}^*}{\partial x^*} + \frac{U_{\text{ref}}^2}{c}\frac{\partial \overline{U}^*\tilde{U}^*}{\partial x^*}$$

$$\frac{\partial u_p^*}{\partial x^*} + \frac{\partial v_p^*}{\partial y_p^*} = 0$$

$$y_p^* = \infty : u_p^* = \overline{U}^*(x);\ \ y_p = 0 : u_p^* + u_s^* = 0, v_p^* = 0$$

After dividing by $U_{\text{ref}}\omega$ and omitting the asterisks, we rewrite the above system as:

$$\frac{\partial u_p}{\partial t} + \frac{1}{\lambda^2}\{-\frac{\partial^2 u_p}{\partial y_p^2} + (u_p\frac{\partial}{\partial x} + v_p\frac{\partial}{\partial y_p})u_p + (u_p\frac{\partial}{\partial x} + v_p\frac{\partial}{\partial y_p})\tilde{U}$$

$$+[\tilde{U}\frac{\partial}{\partial x} + (-y_p\frac{\partial \tilde{U}}{\partial x} + \frac{1}{\lambda}W_s)\frac{\partial}{\partial y_p}]u_p\} = \frac{1}{\lambda^2}(\overline{U}\frac{d\overline{U}}{dx} + \frac{\partial \overline{U}\tilde{U}}{\partial x})$$

$$\frac{\partial u_p}{\partial x} + \frac{\partial v_p}{\partial y_p} = 0$$

$$y_p = \infty : u_p = \overline{U}(x);\ \ y_p = 0 : u_p + u_s = 0, v_p = 0 \qquad (2.3)$$

We write the "Stokes" system (2.2) in non-dimensional form as follows:

$$U_{\text{ref}}\omega\frac{\partial u_s^*}{\partial t^*} - \nu\frac{U_{\text{ref}}}{\delta_s^2}\frac{\partial^2 u_s^*}{\partial y_s^{*2}} + \frac{U_{\text{ref}}^2}{c}(u_s^*\frac{\partial}{\partial x^*} + v_s^*\frac{\partial}{\partial y_s^*})u_s^*$$

$$+\frac{U_{\text{ref}}^2}{c}[(u_s^* - \tilde{U}^*)\frac{\partial}{\partial x^*} + (v_s^* - V_s^*)\frac{\partial}{\partial y_s^*}]u_p^* + (\frac{U_{\text{ref}}^2}{c}u_p^*\frac{\partial}{\partial x^*} + \frac{U_{\text{ref}}\delta_p}{c}v_p^*\frac{1}{\delta_s}\frac{\partial}{\partial y_s^*}U_{\text{ref}})(u_s^* - \tilde{U}^*)$$

$$= U_{\text{ref}}\omega\frac{\partial \tilde{U}^*}{\partial t^*} + \frac{U_{\text{ref}}^2}{c}\tilde{U}^*\frac{\partial \tilde{U}^*}{\partial x^*}$$

$$\frac{\partial u_s^*}{\partial x^*} + \frac{\partial v_s^*}{\partial y_s^*} = 0$$

$$y_s^* = \infty : u_s^* = \tilde{U}^*(x,t); y_s^* = 0 : u_s^* + u_p^* = 0, v_s^* = 0$$

Dividing by $U_{\text{ref}}\omega$ and omitting the asterisks leads to:

$$\frac{\partial u_s}{\partial t} - \frac{\partial^2 u_s}{\partial y_s^2} + \frac{1}{\lambda^2}\{(u_s\frac{\partial}{\partial x} + v_s\frac{\partial}{\partial y_s})u_s +$$
$$+ [(u_s - \tilde{U})\frac{\partial}{\partial x} + (v_s - V_s)\frac{\partial}{\partial y_s}]u_p +$$
$$+(u_p\frac{\partial}{\partial x} + \lambda v_p\frac{\partial}{\partial y_s})(u_s - \tilde{U})\} = \frac{\partial \tilde{U}}{\partial t} + \frac{1}{\lambda^2}\tilde{U}\frac{\partial \tilde{U}}{\partial x}$$
$$\frac{\partial u_s}{\partial x} + \frac{\partial v_s}{\partial y_s} = 0$$
$$y_s = \infty : u_s = \tilde{U}(x,t); \quad y_s = 0 : u_s + u_p = 0, v_s = 0 \tag{2.4}$$

Since $\frac{\delta_s}{\delta_p} = \sqrt{\frac{U}{\omega c}} = \frac{1}{\lambda} \ll 1$, u_p and v_p are replaced in (2.4) by their Taylor series expansions, about the point $(x, y_p = 0)$:

$$u_p = \sum_{n=0}^{\infty} \frac{y_p^n}{n!}\frac{\partial^n u_p}{\partial y_p^n}(x,0) = \sum_{n=0}^{\infty} \frac{1}{\lambda^n}\frac{y_s^n}{n!}\frac{\partial^n u_p}{\partial y_p^n}(x,0)$$

$$v_p = \sum_{n=0}^{\infty} \frac{y_p^n}{n!}\frac{\partial^n v_p}{\partial y_p^n}(x,0) = \sum_{n=0}^{\infty} \frac{1}{\lambda^n}\frac{y_s^n}{n!}\frac{\partial^n v_p}{\partial y_p^n}(x,0)$$

The boundary condition at the wall requires that $v_p(x,0) = 0$, while $u_p(x,0) \neq 0$ is allowed by the coupling condition. Of course, for the outer values of y_p the "Stokes flow" is simply the potential oscillation $(\tilde{U}, V_s)$.

In Appendix B we describe how these substitutions lead to the following final form of (2.4):

$$
\begin{aligned}
&\frac{\partial u_s}{\partial t} - \frac{\partial \tilde{U}}{\partial t} - \frac{\partial^2 u_s}{\partial y_s^2} + \frac{1}{\lambda^2}\{ -(\tilde{U} + u_p(x,0))\frac{\partial(\tilde{U} + u_p(x,0))}{\partial x} \\
&+ [\,(u_s + u_p(x,0))\frac{\partial}{\partial x} + (v_s + y_s\frac{\partial v_p}{\partial y_p}(x,0))\frac{\partial}{\partial y_s}\,]\,(u_s + u_p(x,0))\,\} \\
&+ \sum_{n=1}^{\infty}\frac{1}{\lambda^{n+2}}\{\,[\,(\frac{y_s^n}{n!}\frac{\partial^n u_p}{\partial y_p^n}(x,0)\frac{\partial}{\partial x} + \frac{y_s^{n+1}}{(n+1)!}\frac{\partial^{n+1} v_p}{\partial y_p^{n+1}}(x,0)\frac{\partial}{\partial y_s}\,]\,(u_s - \tilde{U}) \\
&+ [(u_s - \tilde{U})\frac{\partial}{\partial x} + (v_s - V_s)\frac{\partial}{\partial y_s}\,]\,\frac{y_s^n}{n!}\frac{\partial^n u_p}{\partial y_p^n}(x,0)\,\} = 0 \\
&\frac{\partial u_s}{\partial x} + \frac{\partial v_s}{\partial y_s} = 0 \\
&y_s = \infty : u_s = \tilde{U}(x,t);\;\; y_s = 0 : u_s + u_p = 0, v_s = 0
\end{aligned}
\tag{2.5}
$$

By examining the systems (2.3), and (2.5) we see that the "Stokes" and "Prandtl" layers interact in the following ways:

- They together satisfy the no-slip condition at the airfoil surface. This effect is on the order of $\frac{1}{\lambda^2}$.
- The potential oscillation, $(\tilde{U}(x,t),\ -y\frac{\partial \tilde{U}}{\partial x}(x,t))$, and a smaller additional cross-flow $W_s(x,t)$ emanating from the "Stokes" layer, transfer momentum within the "Prandtl" layer (the situation is analogous to the creation of Reynolds stress in turbulent flows and the generation of viscosity due to the Brownian motion of molecules; velocity fluctuations in a background of shear flow create a stress; a gradient of this stress accelerates the fluid). These effects have magnitudes on the order of $\frac{1}{\lambda^2}$, and $\frac{1}{\lambda^3}$, respectively (see the third and the fourth term on the left-hand side of the momentum equation (2.3)).
- The "Prandtl flow" near the wall convects momentum in the "Stokes layer". The

magnitude of this effect is on the order of $\frac{1}{\lambda^3}$ (see the last term on the left-hand side of the momentum equation of (2.5)).

The terms:

$$\frac{1}{\lambda^2}\{-(\tilde{U}+u_p(x,0))\frac{\partial(\tilde{U}+u_p(x,0))}{\partial x} + [(u_s+u_p(x,0))\frac{\partial}{\partial x}+(v_s+y_s\frac{\partial v_p}{\partial y_p}(x,0))\frac{\partial}{\partial y_s}](u_s+u_p(x,0))\}$$

also involve the "Prandtl" velocity, so we anticipate results that we derive in section 2.4, and show that the terms involving $u_p(x,0)$ and $v_p(x,0)$ are of order higher than $\frac{1}{\lambda^3}$.

In that section we prove that the zero-th order solution to the the "Stokes equations" is decoupled from the zero-th order solution to the "Prandtl equations". The former is the "shear-wave" flow, a flow oscillating about a zero mean that is driven by the unsteady part of the pressure gradient. The latter is the steady boundary layer flow corresponding to the mean part of the external velocity and consquently has the properties $u_{p,0}(x,0)=0$, and $\frac{\partial u_{p,0}}{\partial x}(x,0)=0$.

Thus, on the wall: $u_p(x,0)=\frac{1}{\lambda^2}u_{p,2}+O(\frac{1}{\lambda^3})$ and $\frac{\partial v_p}{\partial y_p}(x,0)=-\frac{\partial u_p}{\partial x}(x,0)=-\frac{1}{\lambda^2}\frac{\partial u_{p,2}}{\partial x}(x,0)+O(\frac{1}{\lambda^3})$, and the contribution of these terms to the momentum equation (notice that they are multiplied by $\frac{1}{\lambda^2}$) is on the order of $O(\frac{1}{\lambda^4})$.

In figure 2.2 we sketch the two velocity distributions at two different times t and $t+T/2$: the "Stokes" velocity in the outer part of the boundary layer oscillates about a vanishing mean. Inside the secondary layer of vorticity, the steady streaming (see section 2.6) creates a steady "Stokes flow" ($\overline{u}_{s,2}$) that does not vanish on the wall. The analysis in section 2.6 reveals that on the wall, in addition to $\overline{u}_{s,2}$, the "Stokes flow" has a

nonvanishing unsteady component of the same order ($\tilde{u}_{s,2}$). This unsteady component, through the no-slip condition, generates an unsteady component of the same order in the "Prandtl flow". Far form the wall, the steady character of the "Prandtl flow" prevails.

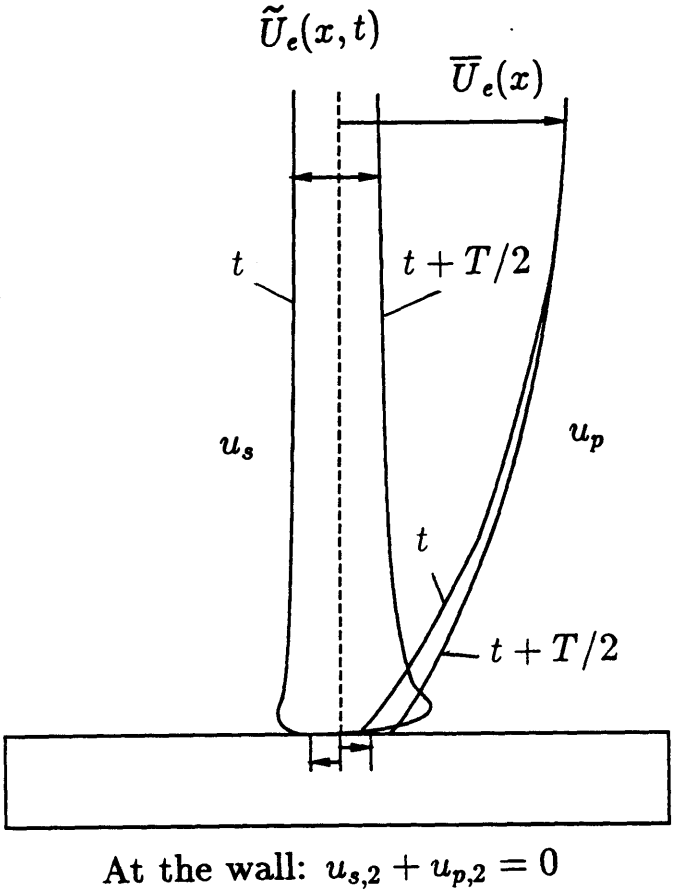

Figure 2.2: A sketch of the two components of the boundary layer velocity at times t and t+T/2. The "Stokes" velocity distribution at the outer part of the boundary layer is purely oscillatory, but as it approaches the boundary its mean value is no longer zero (due to steady streaming). The boundary condition at the wall creates a unsteady component in the "Prandtl" velocity distribution which vanishes away from the wall.

2.4 The solution

We obtain the solution to the systems of equations (2.3) $\equiv (S_p)$ and (2.5) $\equiv (S_s)$ by expanding u_p and u_s into powers of $\frac{1}{\lambda}$:

$$u_p = \sum_{n=0}^{\infty} \frac{1}{\lambda^n} u_{p,n}, \quad u_s = \sum_{n=0}^{\infty} \frac{1}{\lambda^n} u_{s,n}$$

At each level of approximation, we express the two velocity distributions in terms of their mean and fluctuating part: $u_{p,n} = \overline{u}_{p,n} + \widetilde{u}_{p,n}$, $u_{s,n} = \overline{u}_{s,n} + \widetilde{u}_{s,n}$, . We find the equations for the mean flow by taking the time-average of the above systems: $(\overline{S}_{p,n}), (\overline{S}_{s,n})$. Then, we subtract those systems from the original systems and derive the equations that govern the fluctuating part of the flow: $(\widetilde{S}_{p,n}), (\widetilde{S}_{s,n})$,. The equations for the oscillating part of the flow must be solved before the equations for the mean part of the flow (note for example, that the equation for $\overline{u}_{p,2}$ involves $\widetilde{u}_{p,2}$).

Since the first power of the small parameter $\frac{1}{\lambda}$ does not appear in equations (2.3) and (2.5), $u_{p,1} = v_{p,1} = u_{s,1} = v_{s,1} = 0$.

For this reason we have omitted the systems : $(\widetilde{S}_{p,1}), (\overline{S}_{p,1}), (\widetilde{S}_{s,1}), (\overline{S}_{s,1})$ in the procedure of successive approximations.

We carry out the calculation of the flow field in the following steps:

$$O(1): \quad \frac{\partial \widetilde{u}_{p,0}}{\partial t} = 0 \tag{2.6}$$

$$O(1): \quad (\overline{u}_{p,0}\frac{\partial}{\partial x} + \overline{v}_{p,0}\frac{\partial}{\partial y_p})\overline{u}_{p,0} - \frac{\partial^2 \overline{u}_{p,0}}{\partial y_p^2} = \overline{U}\frac{d\overline{U}}{dx} \tag{2.7}$$

$$O(\frac{1}{\lambda^2}): \quad \frac{\partial \widetilde{u}_{p,2}}{\partial t} = -u_{p,0}\frac{\partial \widetilde{U}}{\partial x} - \widetilde{U}\frac{\partial u_{p,0}}{\partial x} + y_p\frac{\partial \widetilde{U}}{\partial x}\frac{\partial u_{p,0}}{\partial y_p} + \frac{\partial}{\partial x}(\widetilde{U}\overline{U}) \tag{2.8}$$

$$O(\frac{1}{\lambda^2}): \quad -\frac{\partial^2 \overline{u}_{p,2}}{\partial y_p^2} + (\overline{u}_{p,2}\frac{\partial}{\partial x} + \overline{v}_{p,2}\frac{\partial}{\partial y_p})u_{p,0} + (u_{p,0}\frac{\partial}{\partial x} + v_{p,0}\frac{\partial}{\partial y_p})\overline{u}_{p,2}$$
$$= -\tilde{u}_{p,2}\frac{\partial \tilde{U}}{\partial x} - \tilde{U}\frac{\partial \tilde{u}_{p,2}}{\partial x} + y_p\frac{\partial \tilde{U}}{\partial x}\frac{\partial \tilde{u}_{p,2}}{\partial y_p} \tag{2.9}$$

$$O(1): \quad \frac{\partial^2 \overline{u}_{s,0}}{\partial y_s^2} = 0 \tag{2.10}$$

$$O(1): \quad \frac{\partial \tilde{u}_{s,0}}{\partial t} - \frac{\partial^2 \tilde{u}_{s,0}}{\partial y_s^2} - \frac{\partial \tilde{U}}{\partial t} = 0 \tag{2.11}$$

$$O(\frac{1}{\lambda^2}): \quad \frac{\partial \tilde{u}_{s,2}}{\partial t} - \frac{\partial^2 \tilde{u}_{s,2}}{\partial y_s^2} = \tilde{U}\frac{\partial \tilde{U}}{\partial x} - (\tilde{u}_{s,0}\frac{\partial}{\partial x} + \tilde{v}_{s,0}\frac{\partial}{\partial y_s})\tilde{u}_{s,0}$$
$$- [\,(\tilde{u}_{s,0} - \tilde{U})\frac{\partial}{\partial x} + (\tilde{v}_{s,0} - V_s)\frac{\partial}{\partial y_s}\,]\, u_{p,0}(x,0) - u_{p,0}(x,0)\frac{\partial}{\partial x}(\tilde{u}_{s,0} - \tilde{U}) \tag{2.12}$$

$$O(\frac{1}{\lambda^2}): \quad -\frac{\partial^2 \overline{u}_{s,2}}{\partial y_s^2} = \overline{(\tilde{U} + u_{p,0}(x,0))\frac{\partial(\tilde{U} + u_{p,0}(x,0))}{\partial x}}$$
$$-[\,(\tilde{u}_{s,0} + u_{p,0}(x,0))\frac{\partial}{\partial x} + (\tilde{v}_{s,0} + y_s\frac{\partial v_{p,0}}{\partial y_p}(x,0))\frac{\partial}{\partial y_s}\,]\,(\tilde{u}_{s,0} + u_{p,0}(x,0)) \tag{2.13}$$

The calculations of the following section result in a further simplification of the second order "Stokes" equations because the terms $u_{p,0}(x,0)$ and $\frac{\partial u_{p,0}}{\partial x}(x,0)$ are found to be equal to zero.

2.5 Zero-th order approximation

We first consider the unsteady part of the "Prandtl velocity"

$$\frac{\partial \tilde{u}_{p,0}}{\partial t} = 0$$

$$y_p = \infty : \tilde{u}_{p,0} = 0$$

The solution is identically zero:

$$\tilde{u}_{p,0} \equiv 0$$

Next we solve the equation for the unsteady part of the "Stokes flow"

$$\frac{\partial \tilde{u}_{s,0}}{\partial t} - \frac{\partial^2 \tilde{u}_{s,0}}{\partial y_s^2} - \frac{\partial \tilde{U}}{\partial t} = 0$$

$$y_s = \infty, \tilde{u}_{s,0} = \tilde{U}; \;\; y_s = 0, \tilde{u}_{s,0} = 0, \tilde{v}_{s,0} = 0$$

This is the "Stokes's second problem" with solution:

$$\tilde{u}_{s,0} = \Re\{ \; (1 - e^{-y_s\sqrt{i}})\tilde{U} \; \} = \hat{U}\cos(t) - \hat{U}e^{-y_s/\sqrt{2}}\cos(t - \frac{y_s}{\sqrt{2}})$$

$$\tilde{v}_{s,0} = \Re\{(-y_s + \frac{1 - e^{-y_s\sqrt{i}}}{\sqrt{i}})\tilde{U}'\}$$

where $\hat{U}$ is the amplitude of $\tilde{U}$. This is the unsteady part of the boundary layer velocity in Lighthill's linear theory (1953, see introduction).

The steady part of the "Stokes velocity" is given by:

$$\frac{\partial^2 \overline{u}_{s,0}}{\partial y_s^2} = 0$$

$$y_s = \infty : \overline{u}_{s,0} = 0; \;\; y_s = 0 : \overline{u}_{s,0} = 0$$

The solution is identically zero:

$$\overline{u}_{s,0} \equiv 0$$

The steady component of the "Prandtl velocity" is given by:

$$(\overline{u}_{p,0}\frac{\partial}{\partial x} + \overline{v}_{p,0}\frac{\partial}{\partial y_p})\overline{u}_{p,0} - \frac{\partial^2 \overline{u}_{p,0}}{\partial y_p^2} - \overline{U}\frac{d\overline{U}}{dx} = 0$$

$$y_p = \infty : \overline{u}_{p,0} = \overline{U}; \;\; y_p = 0 : \overline{u}_{p,0} = 0, \overline{v}_{p,0} = 0$$

We call the solution to $(\overline{S}_{p,0})$ the "basic flow" $(u_b, v_b) \equiv (u_{p,0}, v_{p,0})$. It is the velocity distribution which corresponds to the steady free-stream velocity $\overline{U}(x)$. In the following section,we use the "basic flow" as the building block to construct the full "Prandtl flow".

In conclusion, the zero-th order components of the two velocity distributions are uncoupled; the "Stokes" velocity is purely oscillatory and the "Prandtl" velocity is steady.

2.6 Second order approximation

The unsteady pressure gradient is composed of three terms:

$$\frac{\partial \tilde{p}}{\partial x} = -\lambda^2 \frac{\partial \tilde{U}}{\partial t} - \frac{\partial \overline{U}\tilde{U}}{\partial x} - \tilde{U}\frac{\partial \tilde{U}}{\partial x} \tag{2.14}$$

The first term, which is the dominant term, drives the zero-th order component of the "Stokes velocity", as we saw in the last section. The second and third term, drive the unsteady "Prandtl" and the second order unsteady "Stokes" flow, respectively.

The unsteady "Prandtl flow" $(\tilde{u}_{p,2}, \tilde{v}_{p,2})$ is the solution to the equation (2.8):

$$O(\frac{1}{\lambda^2}): \quad \frac{\partial \tilde{u}_{p,2}}{\partial t} = -u_{p,0}\frac{\partial \tilde{U}}{\partial x} - \tilde{U}\frac{\partial u_b}{\partial x} + y_p \frac{\partial \tilde{U}}{\partial x}\frac{\partial u_b}{\partial y_p} + \frac{\partial}{\partial x}(\overline{U}\tilde{U})$$

According to this equation, the flow is driven by the second component of the unsteady pressure gradient in equation (2.14), and by the purely oscillatory part of the gradient of the Reynolds stress created by the potential oscillation $(\tilde{U}, -y_p\frac{\partial \tilde{U}}{\partial x})$ in the background of the shear of the "basic flow".

The above equation can be rewritten as:

$$\frac{\partial \tilde{u}_{p,2}}{\partial t} = \frac{\partial}{\partial x}[\tilde{U}(\overline{U} - u_b)] + y_p \frac{\partial u_b}{\partial y_p}\frac{\partial \tilde{U}}{\partial x}$$

$$y_p = \infty : \tilde{u}_{p,2} = 0; \quad y_p = 0 : \tilde{u}_{p,2} + \tilde{u}_{s,2} = 0, \tilde{v}_{p,2} = 0$$

The solution is:

$$\tilde{u}_{p,2} = \Re\{ \frac{1}{i}\{\frac{\partial}{\partial x}[\tilde{U}(\overline{U} - u_b)] + y_p \frac{\partial u_b}{\partial y_p}\frac{\partial \tilde{U}}{\partial x}\} \} \tag{2.15}$$

This unsteady "Prandtl velocity" does not reduce to zero at the wall because there are no viscous terms in the momentum equation (2.8). The resultant slip velocity, $\tilde{u}_{p,2}(x,0) = \Re\{ \frac{1}{i}\frac{\partial}{\partial x}(\tilde{U}\overline{U}) \}$, is balanced by the unsteady "Stokes flow" when the coupling boundary condition at the wall is applied.

In the "Stokes" layer, the combination of the remaining component of the unsteady pressure gradient in equation (2.14), and of the gradient of the Reynolds stress created by the shear-wave oscillations, gives rise to $(\tilde{u}_{s,2}, \tilde{v}_{s,2})$, which by viscous diffusion adjusts to the wall boundary condition. The result of the previous section $u_{p,0}(x,0) = \frac{\partial u_{p,0}}{\partial x}(x,0) = 0$ simplifies equation (2.12) to

$$\frac{\partial \tilde{u}_{s,2}}{\partial t} - \frac{\partial^2 \tilde{u}_{s,2}}{\partial y_s^2} = -\tilde{u}_{s,0}\frac{\partial \tilde{u}_{s,0}}{\partial x} - \tilde{v}_{s,0}\frac{\partial \tilde{u}_{s,0}}{\partial y_s} + \tilde{U}\frac{\partial \tilde{U}}{\partial x}$$

$$y_s = \infty : \tilde{u}_{s,2} = 0; \quad y_s = 0 : \tilde{u}_{s,2} = -\Re\{ \frac{e^{it}}{i}\frac{\partial}{\partial x}(\hat{U}\overline{U}) \}, \tilde{v}_{s,2} = 0$$

By substituting in the above the calculated values of $\tilde{u}_{s,0}, \tilde{v}_{s,0}$ we obtain:

$$\begin{aligned} \frac{\partial \tilde{u}_{s,2}}{\partial t} - \frac{\partial^2 \tilde{u}_{s,2}}{\partial y_s^2} &= -(1 - e^{-y_s\sqrt{i}})^2 \hat{U}\hat{U}' e^{2it} \\ &\quad -(-y_s + \frac{1 - e^{-y_s\sqrt{i}}}{\sqrt{i}})\sqrt{i}\hat{U}\hat{U}' e^{2it} + \hat{U}\hat{U}' e^{2it} \\ &= e^{-y_s\sqrt{i}}(1 + y_s\sqrt{i})\hat{U}\hat{U}' e^{2it} \end{aligned}$$

$$y_s = \infty : \tilde{u}_{s,2} = 0; \qquad y_s = 0 : \tilde{u}_{s,2} = -\frac{e^{it}}{i}\frac{d}{dx}(\hat{U}\overline{U})$$

The solution is:

$$\tilde{u}_{s,2} = f e^{2it} - \frac{e^{it - y_s\sqrt{i}}}{i}\frac{d}{dx}(\overline{U}\hat{U})$$

where the function f satisfies:

$$2f - \frac{d^2 f}{d(y_s\sqrt{i})^2} = \frac{e^{-y_s\sqrt{i}}(1+y_s\sqrt{i})}{i}$$

$$y_s = \infty : f = 0; \quad y_s = 0 : f = 0$$

Let $\varsigma \equiv y_s\sqrt{i}$. A particular solution has the form: $f_p = (A + B\varsigma)e^{-\varsigma}$. Substitution in the last equation yields: $(A+2B)e^{-\varsigma} + B\varsigma e^{-\varsigma} = \frac{e^{-\varsigma}(1+\varsigma)}{i}$, thus: $f_p = i(1-\varsigma)e^{-\varsigma}$.

The general solution is: $f_g = Ce^{-y_s\sqrt{2i}} + i(1 - y_s\sqrt{i})e^{-y_s\sqrt{i}}$. Since $f(0) = 0$, $C = -i$.

In summary,

$$\tilde{u}_{s,2} = \Re\{\, [-ie^{-y_s\sqrt{2i}} + i(1 - y_s\sqrt{i})e^{-y_s\sqrt{i}}]\hat{U}\frac{d\hat{U}}{dx}e^{2it} - \frac{e^{it-y_s\sqrt{i}}}{i}\frac{d}{dx}(\overline{U}\hat{U})\,\}$$

The steady component of the "Stokes flow" is driven by the mean pressure gradient of the external oscillation ($\overline{\tilde{U}\frac{\partial\tilde{U}}{\partial x}}$), and by the gradient of the Reynolds stress created by the shear-wave oscillations of the "Stokes flow":

$$-\frac{\partial^2\overline{u}_{s,2}}{\partial y_s^2} = \overline{-\tilde{u}_{s,0}\frac{\partial\tilde{u}_{s,0}}{\partial x} - \tilde{v}_{s,0}\frac{\partial\tilde{u}_{s,0}}{\partial y_s} + \tilde{U}\frac{\partial\tilde{U}}{\partial x}}$$

If we use asterisks to denote the complex conjugates, the right-hand-side of the above expression is written in complex notation as follows:

$$
\begin{aligned}
&\overline{-\tilde{u}_{s,0}\frac{\partial \tilde{u}_{s,0}}{\partial x} - \tilde{v}_{s,0}\frac{\partial \tilde{u}_{s,0}}{\partial y_s} + \tilde{U}\frac{\partial \tilde{U}}{\partial x}} \\
&= -\frac{1}{2}\tilde{u}_{s,0}\frac{\partial \tilde{u}^*_{s,0}}{\partial x} - \frac{1}{4}\tilde{v}^*_{s,0}\frac{\partial \tilde{u}_{s,0}}{\partial y_s} - \frac{1}{4}\tilde{v}_{s,0}\frac{\partial \tilde{u}^*_{s,0}}{\partial y_s} + \frac{1}{2}\tilde{U}^*\frac{\partial \tilde{U}}{\partial x} \\
&= -\frac{1}{2}(1 - e^{-y_s\sqrt{i}})\hat{U}(1 - e^{-y_s\sqrt{i}^*})\hat{U}' \\
&\quad - \frac{1}{4}[-y_s + (\frac{1 - e^{-y_s\sqrt{i}}}{\sqrt{i}})^*]\hat{U}'(\sqrt{i}e^{-y_s\sqrt{i}})\hat{U} \\
&\quad - \frac{1}{4}(-y_s + \frac{1 - e^{-y_s\sqrt{i}}}{\sqrt{i}})\hat{U}'(\sqrt{i}e^{-y_s\sqrt{i}})^*\hat{U} + \frac{1}{2}\hat{U}\hat{U}' \\
&= \hat{U}\hat{U}'\,[\,\frac{2-i}{4}e^{-y_s\sqrt{i}} + \frac{2+i}{4}e^{-y_s\sqrt{i}^*} - \frac{e^{-y_s\sqrt{2}}}{2} \\
&\quad + \frac{1}{4}y_s\sqrt{i}^*e^{-y_s\sqrt{i}} + \frac{1}{4}y_s\sqrt{i}e^{-y_s\sqrt{i}^*}\,]
\end{aligned}
$$

By performing the double integration from ∞ to y_s we get:

$$
\begin{aligned}
\overline{u}_{s,2} &= -\hat{U}\hat{U}'\,[\,\frac{-1-2i}{4}e^{-y_s\sqrt{i}} + \frac{-1+2i}{4}e^{-y_s\sqrt{i}^*} - \frac{e^{-y_s\sqrt{2}}}{4} \\
&\quad + \frac{1-i}{4\sqrt{2}}y_s e^{-y_s\sqrt{i}} - \frac{e^{-y_s\sqrt{i}}}{2} + \frac{1+i}{4\sqrt{2}}y_s e^{-y_s\sqrt{i}^*} - \frac{e^{-y_s\sqrt{i}^*}}{2}\,]
\end{aligned}
$$

If we let $n \equiv \frac{y_s}{\sqrt{2}}$, then the real part of the expression for $\overline{u}_{s,2}$ is:

$$
\begin{aligned}
\overline{u}_{s,2} &= -\hat{U}\hat{U}'\,[\,-\frac{1}{4}e^{-n}(2\cos(n) - 4\sin(n)) - \frac{e^{-2n}}{4} \\
&\quad + \frac{n}{4}e^{-n}(2\cos(n) - 2\sin(n)) + e^{-n}\sin(n)\,] \\
&= \hat{U}\hat{U}'\,[\,\frac{1}{2}e^{-n}\cos(n) + \frac{e^{-2n}}{4} - \frac{n}{2}e^{-n}(\cos(n) - \sin(n)) + 2e^{-n}\sin(n)\,]
\end{aligned}
$$

On the wall there is a non-vanishing u-component, which is responsible for generating the steady Prandtl flow of order $\frac{1}{\lambda^2}$.

$$
\overline{u}_{s,2}(x,0) = \frac{3}{4\lambda^2}\hat{U}\frac{d\hat{U}}{dx} = \frac{3}{2\lambda^2}\overline{\tilde{U}\frac{d\tilde{U}}{dx}}
$$

The steady "Stokes flow" is related to the steady streaming (Schlichting, 1979). Schlichting considered the case of flow over a cylindrical body with an imposed free stream velocity oscillating about a zero mean. Then, the Reynolds stresses associated with the periodic flow create a mean flow at the edge of the Stokes layer (steady streaming) equal to $-\overline{u}_{s,2}(x,0)$. Inside the "Stokes layer" his solution is equal to $\overline{u}_{s,2}(x,y_s) - \overline{u}_{s,2}(x,0)$. The reason that the steady streaming appears either in the far field (as in Schlichting, where $\overline{U} = 0$), or on the body surface (as in our case, where $\overline{U} \neq 0$), is that only one of the two boundary conditions can be satisfied: the velocity can vanish either on the body surface or at infinity, respectively. The presence of a mean flow in our case allows a nonzero "Stokes velocity" on the wall, which is counterbalanced by an opposite "Prandtl velocity", so that the no-slip condition on the body is satisfied when the flow is viewed as a whole.

The second order mean part of the "Prandtl flow" is given by:

$$-\frac{\partial^2 \overline{u}_{p,2}}{\partial y_p^2} + (\overline{u}_{p,2}\frac{\partial}{\partial x} + \overline{v}_{p,2}\frac{\partial}{\partial y_p})u_b + (u_b\frac{\partial}{\partial x} + v_b\frac{\partial}{\partial y_p})\overline{u}_{p,2}$$
$$= \overline{-\tilde{u}_{p,2}\frac{\partial \tilde{U}}{\partial x} - \tilde{U}\frac{\partial \tilde{u}_{p,2}}{\partial x} + y_p\frac{\partial \tilde{U}}{\partial x}\frac{\partial \tilde{u}_{p,2}}{\partial y_p}}$$
$$y_p = \infty : \overline{u}_{p,2} = 0; \quad y_p = 0 : \overline{u}_{p,2} = -\frac{3}{4}\hat{U}\frac{d\hat{U}}{dx}, \tilde{v}_{p,2} = 0$$

The second and third term of the momentum equation indicate that this flow is generated by the force which is created as the "basic flow" transfers momentum vertically from the wall towards the external flow. The right-hand-side of the above equation can be written as:

$$\overline{-\tilde{u}_{p,2}\frac{\partial \tilde{U}}{\partial x} - \tilde{U}\frac{\partial \tilde{u}_{p,2}}{\partial x} + y_p\frac{\partial \tilde{U}}{\partial x}\frac{\partial \tilde{u}_{p,2}}{\partial y_p}} = -\frac{\partial}{\partial x}\overline{(\tilde{u}_{p,2}\tilde{U})} + y_p\overline{\frac{\partial \tilde{U}}{\partial x}\frac{\partial \tilde{u}_{p,2}}{\partial y_p}}$$

According to (2.15) the unsteady "Prandtl velocity" lags the external fluctuating velocity by $\frac{\pi}{2}$. This means that

$$\overline{\widetilde{U}\widetilde{u}_{p,2}} = 0$$

If we assumed the phase angle of $\widetilde{U}$ to be constant with x , then

$$\overline{\frac{\partial \widetilde{U}}{\partial x}\frac{\partial \widetilde{u}_{p,2}}{\partial y_p}} = 0$$

In general, the presence of the wake (or possibly usteady motion of the airfoil for example rotation) introduces a phase shift in $\widetilde{U}$ with respect to $\widetilde{U}_{-\infty}$, which depends on streamwise location:

$$U(x,t) = \overline{U}(x) + \hat{U}(x)e^{i(t+\phi(x))}$$

Since we are interested in a region which spans 1-5 % of the airfoil chord (this is typically the chordwise breadth of the separation point trajectory), we expect the phase angle to be approximately constant in this range, and equal to the phase angle at, say, the time-average location of the separation point $\phi(x) \approx \phi(\overline{x_0(t)}) \equiv \phi_0$. Thus, in calculating the unsteady second order component of the Prandtl velocity we may assume that the phase angle of the external velocity is constant, $\widetilde{U}(x,t) = \hat{U}(x)e^{i(t+\phi_0)}$. We note that this simplifying assumption is made only here; everywhere else we allow the phase angle of $\widetilde{U}$ to vary with x.

The above system becomes:

$$\frac{\partial u_b \overline{u}_{p,2}}{\partial x} + v_b\frac{\partial \overline{u}_{p,2}}{\partial y_p} + \overline{v}_{p,2}\frac{\partial u_b}{\partial y_p} - \frac{\partial^2 \overline{u}_{p,2}}{\partial y_p^2} = 0$$

$$y_p = \infty : \overline{u}_{p,2} = 0; \;\; y_p = 0 : \overline{u}_{p,2} = -\frac{3}{4}\hat{U}\frac{d\hat{U}}{dx}, \; \widetilde{v}_{p,2} = 0$$

Its solution has the form:

$$\overline{u}_{p,2} = \frac{\partial}{\partial y_p}(h(x)u_b), \;\; \overline{v}_{p,2} = -\frac{\partial}{\partial x}(h(x)u_b)$$

It obviously satisfies the continuity equation, the boundary condition at infinity, and the boundary condition for $\overline{v}_{p,2}$ at the wall.

Substitution into the above equation yields:

$$\frac{dh}{dx}u_b\frac{\partial u_b}{\partial y_p} + h\frac{\partial u_b}{\partial x}\frac{\partial u_b}{\partial y_p} + hu_b\frac{\partial^2 u_b}{\partial x \partial y_p} + v_b h\frac{\partial^2 u_b}{\partial y_p^2} - \frac{\partial}{\partial x}(hu_b)\frac{\partial u_b}{\partial y_p} - h\frac{\partial^3 u_b}{\partial y_p^3}$$
$$= h\frac{\partial}{\partial y_p}\left(u_b\frac{\partial u_b}{\partial x} + v_b\frac{\partial u_b}{\partial y_p} - \frac{\partial^2 u_b}{\partial y_p^2}\right) - h\frac{\partial u_b}{\partial y_p}\frac{\partial u_b}{\partial x} - h\frac{\partial v_b}{\partial y_p}\frac{\partial u_b}{\partial y_p} = 0$$

where the momentum and the continuity equations of the "basic flow" have been used.

The boundary condition at the wall is satisfied by the following choice of $h(x)$:

$$h(x) = \frac{\overline{u}_{p,2}(x,0)}{\frac{\partial u_b}{\partial y_p}(x,0)} = \frac{\overline{u}_{p,2}(x,0)}{\tau_b(x,0)} = \frac{-\frac{3}{4}\widehat{U}\frac{d\widehat{U}}{dx}}{\tau_b(x,0)}$$

The presence of $(\overline{u}_{p,2}, \overline{v}_{p,2})$ can be interpreted as a vertical displacement of the "basic flow" by the vertical distance $\frac{h(x)}{\lambda^2}$, because

$$\overline{u}_p = u_b + \frac{\overline{u}_{p,2}}{\lambda^2} = u_b + \frac{h(x)}{\lambda^2}\frac{\partial u_b}{\partial y_p} = u_b(x, y_p + \frac{h(x)}{\lambda^2})$$

In the case of an adverse pressure gradient, $h(x) > 0$, and the boundary condition on the wall effectively "clips" a portion of height $h(x)/\lambda^2$ from the "basic" velocity profile. Thus the flow has a smaller mean displacement thickness (is more energetic) than the "basic flow" (see figure (2.3)). For that reason, as we shall see in the examples of chapter 6, the mean location of unsteady separation is displaced downstream of the steady separation location.

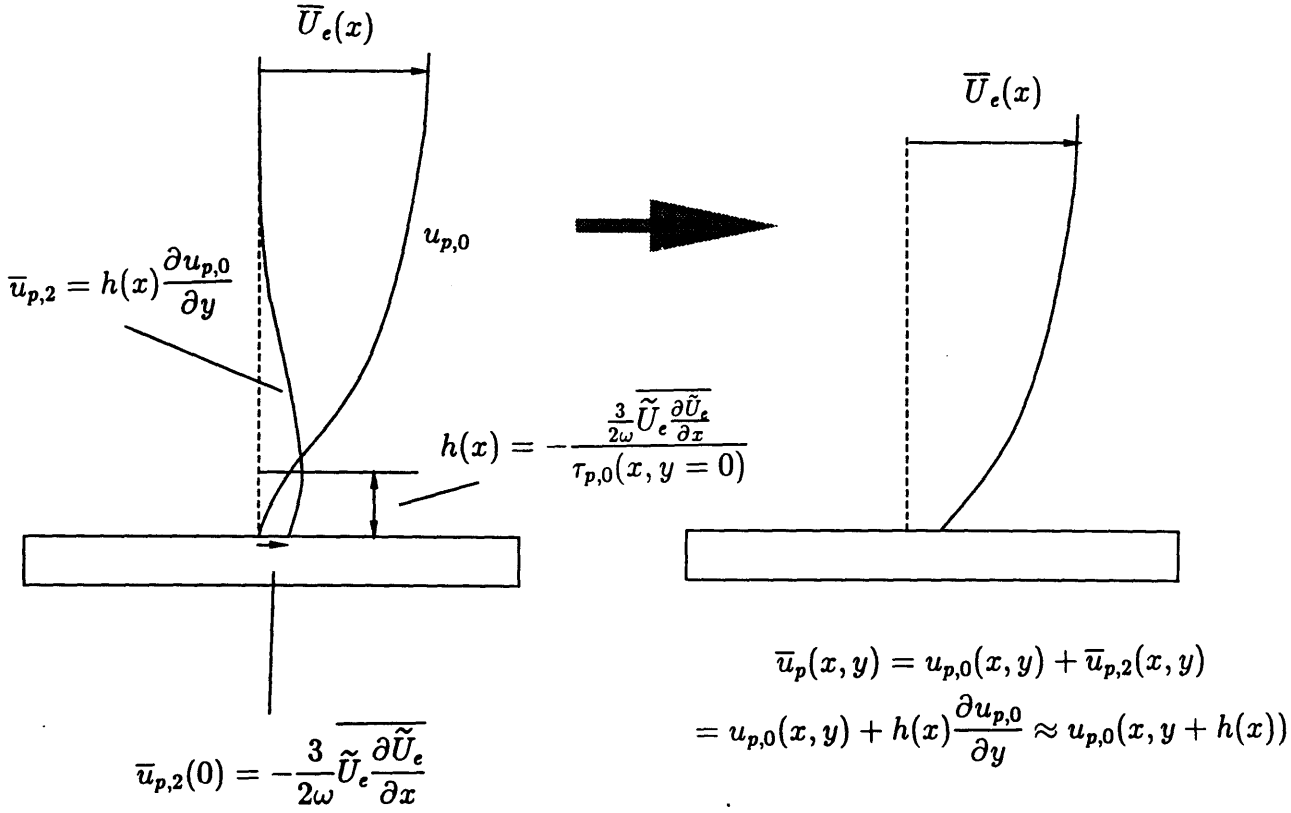

Figure 2.3: The addition of the second-order correction $\overline{u}_{p,2}$ to the "basic flow" is equivalent to a vertical displacement of the "basic flow". In an adverse pressure gradient, the mean flow becomes more energetic.

Chapter 3

Unsteady separation

3.1 Conditions for unsteady separation

Based on the analysis of the last chapter, we can express the wall-stress (in non-dimensional variables) as the sum of the following components:

$$\tau_{p,0,w} = \frac{\partial u_b}{\partial y_p}$$

$$\overline{\tau}_{p,2,w} = \frac{1}{\lambda^2}\frac{\partial \overline{u}_{p,2}}{\partial y_p} = \frac{h}{\lambda^2}\frac{\partial u_b}{\partial y_p} = -\frac{3}{4\lambda^2}\hat{U}\hat{U}'$$

$$\tilde{\tau}_{p,2,w} = \frac{1}{\lambda^2}\frac{\partial \tilde{u}_{p,2}}{\partial y_p} = \frac{\tilde{U}}{\lambda^2 i}(\frac{\partial u_b}{\partial y_p} + y_p\frac{\partial^2 u_b}{\partial y_p^2})$$

$$\tau_{s,0,w} = \frac{\partial u_{s,0}}{\partial y_p} = \lambda\frac{\partial u_{s,0}}{\partial y_s} = \lambda\sqrt{i}\tilde{U}$$

$$\overline{\tau}_{s,2,w} = \frac{1}{\lambda^2}\frac{\partial \overline{u}_{s,2}}{\partial y_p} = \frac{1}{\lambda}\frac{\partial \overline{u}_{s,2}}{\partial y_s} = \frac{1}{\lambda 2\sqrt{2}}\hat{U}\hat{U}'$$

$$\tilde{\tau}_{s,2,w} = \frac{1}{\lambda}\{[\frac{1+i}{2} + \sqrt{2}(1+i)]\tilde{U}\tilde{U}' + \frac{1-i}{\sqrt{2}}\frac{\partial}{\partial x}(\overline{U}\tilde{U})\}$$

$$\tau_w = \tau_{p,w} + \tau_{s,w}$$

$$= \underbrace{\frac{\partial u_b}{\partial y}|_w + O(\frac{1}{\lambda^2})}_{\tau_{p,w}} + \underbrace{\lambda\sqrt{i}\tilde{U} + \frac{1}{\lambda}\{[\frac{1+i}{2} + \sqrt{2}(1+i)]\tilde{U}\tilde{U}' + \frac{1-i}{\sqrt{2}}\frac{\partial}{\partial x}(\overline{U}\tilde{U})\} + \frac{1}{\lambda 2\sqrt{2}}\hat{U}\hat{U}' + O(\frac{1}{\lambda^2})}_{\tau_{s,w}}$$

The mass flux defect is :

$$\Delta\dot{m} = \rho\int_0^\infty (U-u)dy = \rho\overline{U}\,\overline{\delta}^* + \rho\frac{\tilde{U}}{\lambda\sqrt{i}} + O(\frac{1}{\lambda^2})$$

where $\overline{\delta}^*$ is the displacement thickness of the mean flow.

The "Stokes flow" contributes to τ_w a term on the order of $O(\lambda)$, whereas to $\Delta\dot{m}$ a term on the order of $O(\frac{1}{\lambda})$.

According to the classical generic definition of separation of Landau and Lifshitz (1959), valid for both steady and unsteady flows, separation is the sharp increase in the normal component of the velocity in the boundary layer, or equivalently the sharp increase in the displacement thickness δ^* and consequently in $\Delta\dot{m}$. Since the contribution of the "Stokes flow" to the displacement thickness is bounded by $\frac{1}{\lambda}$, we must focus on the "Prandtl" component of the flow in our effort to derive the conditions for unsteady separation.

Furthermore, if we examine the momentum equations that govern the behaviour of the first three components of the "Stokes flow", we see that they all are diffusion equations and thus they do not exhibit singular behaviour. On the other hand, the equations for $u_{p,0}$ and $\overline{u}_{p,2}$ are nonlinear equations similar to the boundary layer equation, which is known to be singular.

In a steady boundary layer, reversal of the flow is always associated with separation. As we have shown in the first paragraph of the present chapter, in high frequency flows the dominant component of the wall shear originates from the "Stokes flow" and is oscillatory. Therefore, temporary back-flow and sign reversal of the wall shear stress in unsteady flow are not associated with separation, as experimental findings indicate (Despard 1971, Koromilas 1980, Mezaris 1987).

The equation for the "Prandtl" component of the velocity is in non-dimensional form:

$$\frac{\partial u_p^*}{\partial t^*} + \frac{1}{\lambda^2}\,[\,-\frac{\partial^2 u_p^*}{\partial y_p^{*2}} + (u_p^*\frac{\partial}{\partial x^*} + v_p^*\frac{\partial}{\partial y_p^*})u_p^* + (u_p^*\frac{\partial}{\partial x^*} + v_p^*\frac{\partial}{\partial y_p^*})\tilde{U}^* +$$

$$+(\tilde{U}^*\frac{\partial}{\partial x^*} + \frac{1}{\lambda}V_s^*\frac{\partial}{\partial y_p^*})u_p^* - \overline{U}^*\frac{d\overline{U}^*}{dx^*} - \frac{\partial \overline{U}^*\tilde{U}^*}{\partial x^*}\,] = 0$$

$$\frac{\partial u_p^*}{\partial x^*} + \frac{\partial v_p^*}{\partial y_p^*} = 0$$

$$y_p^* = \infty : u_p^* = \overline{U}^*(x^*);\;\; y_p^* = 0 : u_p^* + u_s^* = 0, v_p^* = 0 \qquad (3.1)$$

Far upstream of the point of separation:

$$\frac{v_p}{u_p} \sim \frac{1}{\sqrt{Re}}$$

At separation, the flow breaks away from the wall. This means that the normal velocity component becomes of the same order as the tagential velocity component,

$$\frac{v_p}{u_p} \sim 1$$

and the ratio of the dimensionless velocity components becomes:

$$\frac{v_p^*}{u_p^*} = \frac{v_p\sqrt{Re}}{u_p} \sim \sqrt{Re}$$

Let us examine how the derivatives of the velocity components change in magnitude at separation.

Far upstream:	At separation:
$\frac{\partial u_p^*}{\partial y_p^*} \sim \sqrt{Re}$	$\frac{\partial u_p^*}{\partial y_p^*} \sim \sqrt{Re}$
$\frac{\partial v_p^*}{\partial y_p^*} \sim 1$	$\frac{\partial v_p^*}{\partial y_p^*} \sim \sqrt{Re}$, because v_p^* increases by a factor of $\sqrt{Re}$
$\frac{\partial u_p^*}{\partial x^*} \sim 1$	$\frac{\partial u_p^*}{\partial x^*} \sim \frac{\partial v_p^*}{\partial y_p^*} \sim \sqrt{Re}$, because of continuity

Since the magnitude of u_p^* does not change at separation, we conclude from the last asymptotic relation that:

$$\frac{\partial}{\partial x^*} \sim \sqrt{Re} \tag{3.2}$$

Finally,

Far upstream:	At separation:
$\frac{\partial v_p^*}{\partial x^*} \sim \frac{1}{\sqrt{Re}}$	$\frac{\partial v_p^*}{\partial x^*} \sim \sqrt{Re}$, because both v_p^* and $\frac{\partial}{\partial x^*}$ increase by a factor of $\sqrt{Re}$

According to (3.2), changes in the x-direction become very pronounced near separation (Shen, 1968); this means that the boundary layer equations fail, second x-derivatives become important, and the equations that govern the flow are elliptic. Then there is upstream influence, and in order to continue the solution beyond the separation point one must find how the boundary layer flow, which is ejected into the external flow, alters the imposed pressure gradient in the neighbourhood of separation. For steady flows, the triple deck theory (Sychev, 1972) successfully explains this local interaction, which extends over a region (surrounding the separation point) of length $Re^{-3/8}$ times the length over which the imposed pressure gradient acts, and creates a large local adverse pressure gradient (of magnitude $Re^{1/8}$ times the magnitude of the imposed pressure gradient). An analogous comprehensive theory for unsteady separation does not exist (for a first attempt see Sychev, 1978). But for all practical purposes, since the length of the interaction region is expected to scale with an inverse power of the Reynolds number, we can locate separation by finding the point $(x_0(t), y_0(t))$ where the boundary layer equations become singular (as we shall prove in this chapter, the singularity appears in

the "Prandtl component" of the flow). The separation point in unsteady flow lies inside the boundary layer whereas in steady flow lies on the wall and is the point where the shear stress vanishes (Goldstein, 1948, found the form of singular behaviour that the solution to the steady boundary equation exhibits at the vanishing point of the skin friction).

If $x^* = x^*(u_p^*, v_p^*, t^*)$, $y_p^* = y_p^*(u_p^*, v_p^*, t^*)$, $t^* = t^*$, are considered to be the independent variables, then:

$$\frac{\partial x^*}{\partial u_p^*} = J\left(\frac{\partial v_p^*}{\partial y_p^*}\frac{\partial t^*}{\partial t^*} - \frac{\partial v_p^*}{\partial t^*}\frac{\partial t^*}{\partial y_p^*}\right) = \frac{\frac{\partial v_p^*}{\partial y_p^*}}{\frac{\partial u_p^*}{\partial x^*}\frac{\partial v_p^*}{\partial y_p^*} - \frac{\partial u_p^*}{\partial y_p^*}\frac{\partial v_p^*}{\partial x^*}}$$

Near separation the magnitude of this expression is:

$$\frac{\partial x^*}{\partial u_p^*} \sim \frac{\sqrt{Re}}{\sqrt{Re}\sqrt{Re-1}\sqrt{Re}} = \frac{1}{\sqrt{Re}}, \text{ as } x \to x_0(t).$$

We drop the asterisks. In the rest of this section, all symbols represent dimensionless quantities.

Let the x-component of the "Prandtl velocity" at the station of separation be $u_p(x_0(t), y_p, t) \equiv u_0(y_p, t)$.

Near the "separation point" the differences $u_p - u_0$ and $x_0(t) - x$ are small, and $x_0(t) - x$ can be expanded in powers of $u_p - u_0$.

Since $\frac{\partial x}{\partial u_p} \sim \frac{1}{\sqrt{Re}}$ as $u_p \to u_0$, the first term in this expansion is $c\frac{u_p - u_0}{\sqrt{Re}}$, where c is a constant coefficient of O(1).

The expression for $u_p - u_0$, if the first two terms in the Taylor expansion are retained,

is:

$$(x - x_0(t)) = -\frac{u_p - u_0}{\sqrt{Re}} + f(y_p, t)(u_p - u_0)^2$$

The negative sign on the first term of the right-hand-side indicates that the streamwise velocity component decreases as x increases.

$$u_p - u_0 = \frac{-\frac{1}{\sqrt{Re/c}} + \sqrt{\frac{1}{Re/c} + 4f(x_0(t) - x)}}{2f} = -\frac{1}{2f\sqrt{Re}} + \frac{1}{\sqrt{f}}\sqrt{\frac{1}{4fRe} + (x_0(t) - x)} \Rightarrow$$

$$u_p - u_0 = -\epsilon_1(y_p, t) + a(y_p, t)\sqrt{\epsilon_2(y_p, t) + (x_0(t) - x)}$$

where: $a(y,t) = \frac{1}{\sqrt{f(y,t)}}$, $\epsilon_1 = \frac{1}{2f(y,t)\sqrt{Re/c}}$, $\epsilon_2 = \frac{1}{4f(y,t)Re/c}$.

Thus,

$$u_p(x, y_p, t) = u_0(y_p, t) + a(y_p, t)\sqrt{x_0(t) - x + O(\frac{1}{Re})}$$

From continuity:

$$\frac{\partial v_p}{\partial y_p} = -\frac{\partial u_p}{\partial x} = \frac{a(y_p, t)}{2\sqrt{x_0(t) - x + O(\frac{1}{Re})}}$$

therefore,

$$v_p(y_p, t) = \frac{b(y_p, t)}{\sqrt{x_0(t) - x + O(\frac{1}{Re})}}$$

where: $b(y_p, t) = \frac{1}{2}\int_{y_0(t)}^{y} a(y, t)dy$.

The dominant terms in (3.1) are those on the order of $\frac{1}{\sqrt{x_0(t)-x+O(\frac{1}{Re})}}$.

The terms in (3.1) that contribute to the dominant balance at separation are:

$$\lambda^2\frac{\partial u_p}{\partial t} = \lambda^2(\frac{\partial u_0}{\partial t} + \frac{a(y_p, t)}{2\sqrt{x_0(t) - x + O(\frac{1}{Re})}}\frac{dx_0}{dt} + \frac{\partial a}{\partial t}\sqrt{x_0(t) - x + O(\frac{1}{Re})})$$

$$u_p\frac{\partial u_p}{\partial x} = -u_p\frac{\partial v_p}{\partial y_p} = -[u_0 + a(y_p, t)\sqrt{x_0(t) - x + O(\frac{1}{Re})}]\frac{\frac{\partial b}{\partial y_p}}{\sqrt{x_0(t) - x + O(\frac{1}{Re})}}$$

$$v_p \frac{\partial u_p}{\partial y_p} = \frac{b(y_p,t)}{\sqrt{x_0(t) - x + O(\frac{1}{Re})}} [\frac{\partial u_0}{\partial y_p} + \frac{\partial a}{\partial y_p} \sqrt{x_0(t) - x + O(\frac{1}{Re})}]$$

$$\tilde{U} \frac{\partial u_p}{\partial x} = -\tilde{U} \frac{\partial v_p}{\partial y_p} = -\tilde{U} \frac{\frac{\partial b}{\partial y_p}}{\sqrt{x_0(t) - x + O(\frac{1}{Re})}}$$

After multiplying by $\sqrt{x_0(t) - x + O(\frac{1}{Re})}$ and using the fact that: $\frac{a}{2} = \frac{\partial b}{\partial y_p}$ we get:

$$\lambda^2 \frac{a}{2} \frac{dx_0}{dt} - u_0 \frac{\partial b}{\partial y_p} + b \frac{\partial u_0}{\partial y_p} - \tilde{U} \frac{\partial b}{\partial y_p} = 0 \Rightarrow$$

$$\frac{\partial b}{\partial y_p}(u_0 + \tilde{U} - \lambda^2 \frac{dx_0}{dt}) = b \frac{\partial u_0}{\partial y_p} \tag{3.3}$$

From (3.3) it follows that

$$b(y_p,t) = C(t)[u_0(y_p,t) + \tilde{U} - \lambda^2 \frac{dx_0}{dt}]$$

The expressions for the velocity components, valid as $x \to x_0(t)$, become:

$$u_p(x,y_p,t) = u_0(y_p,t) + 2C(t) \frac{\partial u_0}{\partial y_p}(y_p,t) \sqrt{x_0(t) - x + O(\frac{1}{Re})} \tag{3.4}$$

$$v_p(x,y_p,t) = \frac{C(t)[u_0(y_p,t) + \tilde{U} - \lambda^2 \frac{dx_0}{dt}]}{\sqrt{x_0(t) - x + O(\frac{1}{Re})}} \tag{3.5}$$

Since, as we have seen in chapter 2, $\frac{\partial u_0(0,t)}{\partial x} = -\frac{3}{2} \frac{\partial}{\partial x}(\overline{\tilde{U} \frac{d\tilde{U}}{dx}}) - i \frac{\partial^2}{\partial x^2}(\tilde{U}\overline{U})$ is finite, it is reasonable to expect $\frac{\partial u_0(y,t)}{\partial x}$ to be finite in a region which extends from the wall to the "separation point" $(0 < y < y_0(t))$. Using (3.4),

$$\frac{\partial u_p}{\partial x} = \frac{-C(t) \frac{\partial u_0}{\partial y_p}}{\sqrt{x_0(t) - x + O(\frac{1}{Re})}}$$

This expression is finite at $(x_0(t), y_0(t))$ when

$$\frac{\partial u_0}{\partial y_p} = 0 \tag{3.6}$$

At $x = x_0(t)$ for $y \gg y_0$, $v_p \sim \sqrt{Re}\, u_p$. On the other hand, v_p must satisfy the boundary condition at the wall, $v_p = 0$ for $y_p = 0$. Thus, there must exist a connecting region,

which extends from the "separation point" to the wall, where $v_p \sim u_p \sim 1$. According to (3.5), $v_p(x_0(t), y_0(t))$ is finite if

$$u_0(y_0, t) + \tilde{U}_0 - \lambda^2 \frac{dx_0}{dt} = 0 \tag{3.7}$$

Now we turn our attention to the equation for the "Stokes flow", and investigate whether it imposes any additional conditions on the flow at separation.

$$\begin{aligned}
&\frac{\partial u_s}{\partial t} - \frac{\partial \tilde{U}}{\partial t} - \frac{\partial^2 u_s}{\partial y_s^2} + \frac{1}{\lambda^2}(u_s \frac{\partial}{\partial x} + v_s \frac{\partial}{\partial y_s}) u_s + \\
&+ \frac{1}{\lambda^2}[(u_s - \tilde{U}) \frac{\partial}{\partial x} + (v_s - V_s) \frac{\partial}{\partial y_s}] u_p + \\
&+ \frac{1}{\lambda^2}(u_p \frac{\partial}{\partial x} + \lambda v_p \frac{\partial}{\partial y_s})(u_s - \tilde{U}) - \frac{1}{\lambda^2} \tilde{U} \frac{\partial \tilde{U}}{\partial x} = 0 \\
&\frac{\partial u_s}{\partial x} + \frac{\partial v_s}{\partial y_s} = 0 \\
&y_s = \infty : u_s = \tilde{U}(x, t); \quad y_s = 0 : u_s + u_p = 0, v_s = 0
\end{aligned}$$

In the momentum equation, the leading terms are those on the order of $\frac{1}{\sqrt{x_0(t) - x + O(\frac{1}{Re})}}$:

$$\begin{aligned}
(u_s - \tilde{U}) \frac{\partial u_p}{\partial x} &= (u_s - \tilde{U})(-\frac{\partial v_p}{\partial y_p}) = -(u_s - \tilde{U}) \frac{\frac{\partial b}{\partial y_p}}{\sqrt{x_0(t) - x + O(\frac{1}{Re})}} \\
\lambda v_p \frac{\partial (u_s - \tilde{U})}{\partial y_s} &= \lambda v_p \frac{\partial (u_s - \tilde{U})}{\lambda \partial y_p} = \frac{b(y_p, t)}{\sqrt{x_0(t) - x + O(\frac{1}{Re})}} \frac{\partial u_s}{\partial y_p}
\end{aligned} \tag{3.8}$$

After multiplying (3.1) by $\sqrt{x_0(t) - x + O(\frac{1}{Re})}$ we find that the "Stokes flow" must satisfy the following equation at separation:

$$-(u_s - \tilde{U}) \frac{\partial b}{\partial y_p} = b \frac{\partial (u_s - \tilde{U})}{\partial y_p}$$

This equation is identically satisfied at $(x_0(t), y_0(t)))$ because:

$$\begin{aligned}
b(y_0, t) &= C(t)[u_0(y_0, t) + \tilde{U} - \lambda^2 \frac{dx_0}{dt}] = 0 \\
\frac{\partial b}{\partial y_p}|_{y_p = y_0} &= C(t) \frac{\partial u_0}{\partial y_p}|_{y_p = y_0} = 0
\end{aligned}$$

according to (3.7) and (3.6) and no additional condition is imposed by the "Stokes flow".

Thus, there are two conditions for unsteady separation (see figure(3.1)):

$$\frac{\partial u_0}{\partial y_p} = 0$$

$$u_0(y_0, t) + \tilde{U}_0 - \lambda^2 \frac{dx_0}{dt} = 0$$

This is the nondimensional form of the separation conditions. According to these, an observer moving with a speed equal to the difference between the speed of the separation point and the oscillating part of the free-stream velocity, sees a stagnation point within the "Prandtl" velocity field (see figure (3.2)). Such an observer sees the fluid particles being decelerated as they approach the separation point. In order to satisfy continuity, they exchange u-velocity for v-velocity and this causes the dramatic increase in the transverse velocity component at separation. At that location, fluid particles originating from the wake penetrate the boundary layer and deflect it away from the wall, thus invalidating the boundary layer approximation.

Moore (1957), Rott (1956), and Sears (1956) proposed as conditions for unsteady separation the simultanous vanishing of the shear and the velocity at a point within the boundary layer and in a frame of reference moving with separation. In dimensional form these conditions are:

$$\frac{\partial u}{\partial y}|_{(x_0, y_0)} = 0$$

$$u = \frac{dx_0}{dt}$$

If we compare the MRS conditions to the separation conditions that we propose for the high frequency case, we notice that the latter are obtained form the former by

replacing the boundary layer velocity $u = u_p + u_s$ by the sum $u_p + \tilde{U}_e$. This is because in the "Prandtl velocity" (the only component of the boundary layer velocity developing singularity) the "Stokes flow" is modelled by:

- the wall boundary condition
- the potential oscillation $(\tilde{U}_e, \tilde{V}_s)$ in the momentum equation

This modelling, on which we based the solution of the boundary layer equations, introduces $u_p + \tilde{U}_e$ instead of $u_p + u_s$ in the separation conditions.

As the reduced frequency increases, the separation point lies above the edge of the "Stokes layer" ($y_{sep} > \delta_s$) and the two conditions are identical. According to the results of chapter 6 this happens for all but the smallest value of the reduced frequency that we have considered; for the smallest reduced frequency approximately half of the separation trajectory lies within the "Stokes layer" (see figure 6.9).

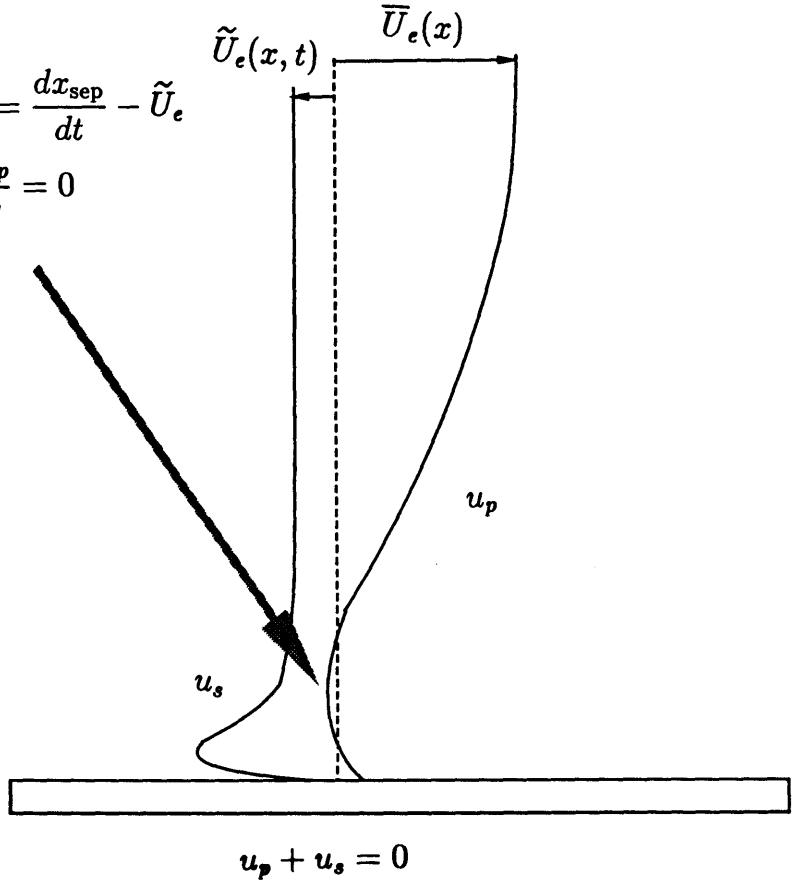

Figure 3.1: The "Prandtl" and "Stokes" velocity profiles at the instantaneous separation location. The separation point is the point where the shear of the "Prandtl velocity" vanishes. The speed at which the separation point moves is the sum of the local "Prandtl velocity" and the unsteady part of the external velocity.

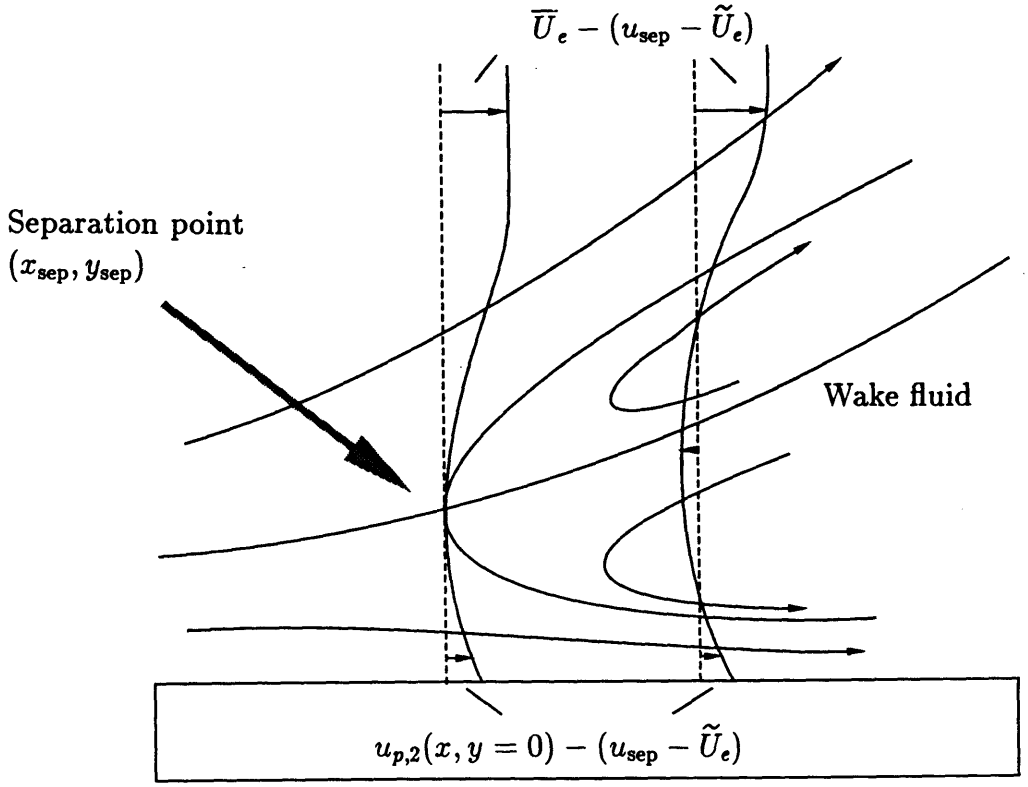

Figure 3.2: The "Prandtl" velocity field at separation, as appears to an observer moving with speed $\frac{dx_0}{dt} - \widetilde{U}$. The separation point is a stagnation point, created as wake fluid penetrates the boundary layer and deflects it away from the wall.

Chapter 4

A criterion for predicting unsteady separation

4.1 Derivation of the criterion

We have shown in Chapter 3 that if the unsteady part of the free-stream velocity oscillates at a high reduced frequency, the occurence of unsteady separation can be identified by focussing attention on the behaviour of the "Prandtl" part of the flow as the overall boundary layer develops along the blade surface. Furthermore, we have seen in chapter 2 that the first two components of the "Prandtl" velocity distribution, $u_{p,0}$ and $u_{p,2} = \overline{u}_{p,2} + \widetilde{u}_{p,2}$, can be constructed by using the "basic velocity" (i.e. the velocity distribution generated by the steady part of the external velocity; in fact $u_{p,0} \equiv u_b$) and the unsteady part of the free-stream velocity.

If we can find how the "basic velocity" changes along the blade contour, then we will be able to construct the whole "Prandtl velocity" using the former as the building block, and to locate the separation point by solving the two conditions (3.6) and (3.7), for $x_0(t)$ and $y_0(t)$. It is obvious that in order to calculate the development of the "basic flow", we must concentrate on the steady part of the "Prandtl flow". In the momentum balance we must consider the steady "Prandtl layer" as a whole: $\overline{u}_p = u_b + h(x)\frac{du_b}{dy}$ (the last term describes how the steady streaming affects the mean "Prandtl velocity"; as

we recall from chapter 2: $h(x) = -\frac{3\mu}{4\omega}\hat{U}\hat{U}'/\tau_{b,w})$.

In order to find how the mean "Prandtl velocity" profile (and consequently u_b) changes with streamwise location under the influence of the adverse pressure gradient, we use a variation of the ideas which led Stratford (1954) to his steady separation criterion, and derive a new relation which describes how the wall stress τ_w changes with x. The wall stress $\tau_w(x)$ determines the "basic velocity" profile $u_b(x, y)$ uniquely. Then, as we mentioned in the above paragraph, we use $u_b(x, y)$ and parameters of the external flow (steady and unsteady) to construct the whole "Prandtl velocity" $u_p(x, y, t)$, and use the latter in the separation conditions to locate unsteady separation.

Stratford in deriving his steady separation criterion divided the boundary layer into two parts:

- In the outer part of the boundary layer the loss of total head due to viscosity is small and taken to be the same as in Blasius flow.
- In the inner part of the boundary layer the convection terms are small and can be neglected in the momentum balance.

Then he patched the two velocity profiles together and required that the velocity and its first and second derivatives match. This led to a relation which describes how the wall stress τ_w changes with x:

$$c_p(x\frac{dc_p}{dx})^2 = 0.0108(1 - \frac{\tau_w}{\tau_f})^2(1 + 2\frac{\tau_w}{\tau_f})$$

where, τ_f is the wall stress of the Blasius flow, which is used in the modelling of the outer part of the boundary layer (more details on this are given in the following pages).

The location of steady separation x, is the location where the wall stress vanishes. By letting $\tau_w = 0$ in the last equation, Stratford obtained the steady separation criterion:

$$c_p \left(x\frac{dc_p}{dx} \right)^2 = 0.0108$$

In the unsteady case, by modelling the development of the mean "Prandtl velocity", as we have outlined above, we obtain an equation (4.14) which in functional form and in nondimensional variables is:

$$F(x^*, \frac{\tau_w}{\tau_f}, c_p, \frac{dc_p}{dx^*}, \frac{\overline{\widetilde{U}^*\widetilde{U}^{*\prime}}}{\lambda^2}) = 0$$

where, the velocities are nondimensionalized by the velocity at the suction peak U_m, and $c_p \equiv 1 - (\overline{U}^*)^2$.

The instantenous location of separation is found be combining this alegbraic equation with the two separation conditions:

$$\frac{\partial u_p^*}{\partial y^*} = 0$$

$$u_p^* + \widetilde{U}^* - \lambda^2 \frac{dx_0^*}{dt^*} = 0$$

where, $u_p^* = u_b^* + \frac{h(x)}{\lambda^2}\frac{\partial u_b^*}{\partial y^*} + \Re\{ \frac{1}{\lambda^2 i}\{\frac{\partial}{\partial x^*}[\widetilde{U}^*(\overline{U}^* - u_b^*)] + y^*\frac{\partial u_b^*}{\partial y^*}\frac{\partial \widetilde{U}^*}{\partial x^*}\} \}$.

We consider an unsteady flow with free-steam velocity $U(x,t) = \overline{U}(x) + \widetilde{U}(x,t) = \overline{U}(x) + \widehat{U}(x)\cos(\omega t + \phi(x))$, which has the properties: $\overline{U}' = \widetilde{U}' = 0$ from $x = 0$ to $x = x_m$, and $\overline{U}', \widehat{U}' < 0$ downstream of $x = x_m$. The presence of a favourable pressure gradient from the leading edge to the suction peak at $x = x_m$ is taken into account by using the "equivalent constant pressure region" (see Kuethe & Chow, p.p. 331-335). In what follows we shall use the convention that u_{out}, u_{in} stand for $\overline{u}_{p,out}$, $\overline{u}_{p,in}$ and that y and y^* represent y_p and y_p^* respectively.

In the outer part of the boundary layer the flow is nearly inviscid, and Bernoulli's equation yields:

$$(p + \frac{1}{2}\rho u_{out}^2)_{x_m,\psi} = (p + \frac{1}{2}\rho u_{out}^2)_{x,\psi} + \Delta H \tag{4.1}$$

where $\delta H = \int_{x_m}^{x} \frac{\partial \tau}{\partial y}(x,\psi)ds$ represents a (small) loss of total head along a streamline due to viscosity. The term $\frac{\partial \tau}{\partial y}$ does not change very rapidly along a streamline in the outer part of the boundary layer. In analogy with the assumption made by Stratford for steady flow, we assume that the loss of total head along a streamline in the outer part of the boundary layer is independent of the pressure rise, and is the same as for the corresponding streamline in the case of flow over a flat plate u_f, where the pressure remains constant.

$$(p + \frac{1}{2}\rho u_{out}^2)_{x_m,\psi} = (p + \frac{1}{2}\rho u_f^2)_{x,\psi} + \Delta H = p_m + \frac{1}{2}\rho(u_f^2)_{x,\psi} + \Delta H \tag{4.2}$$

u_f has two components: the "basic velocity" is the "Blasius velocity"; the second order component, which is generated by the flow unsteadiness, is $h\frac{\partial u_{Blasius}}{\partial y}$.

$$u_f = u_{Blasius} + h\frac{\partial u_{Blasius}}{\partial y} \tag{4.3}$$

Subtracting (4.2) from (4.1) we get:

$$(p + \frac{1}{2}\rho u_{out}^2)_{x,\psi} = p_m + \frac{1}{2}\rho(u_f^2)_{x,\psi} \tag{4.4}$$

By differentiating this result with respect to ψ we get:

$$(\, u_{out}\frac{\partial u_{out}}{\partial \psi}\,)_{x,\psi} = (\, u_f\frac{\partial u_f}{\partial \psi}\,)_{x,\psi},$$

or

$$(\, \frac{\partial u_{out}}{\partial y}\,)_{x,\psi} = (\, \frac{\partial u_f}{\partial y}\,)_{x,\psi} \tag{4.5}$$

If we differentiate once more with respect to ψ, we get:

$$\left(\frac{1}{u_{out}} \frac{\partial^2 u_{out}}{\partial y^2} \right)_{x,\psi} = \left(\frac{1}{u_f} \frac{\partial^2 u_f}{\partial y^2} \right)_{x,\psi} \tag{4.6}$$

Equations (4.4), (4.5), and (4.6) relate the properties of the "outer profile" to those of u_f. We assume that the "inner layer" extends over only a small part of the total boundary layer thickness; then, at the junction y_j, $u_{Blasius}$ and thus u_f (see equation (4.4)) are linear. Indeed, in our calculations $y_j^* = y_j \sqrt{\frac{U_m}{\nu c}}$ lies in the range $1 < y_j^* < 3$. If we examine the form of the Blasius profile (see for example Kuethe & Chow, 1986, p. 324, where the abscissa η relates to y^* by $y^* = 2\eta$) we see that in the range of interest (from $\eta = 0$ to $0.5 < \eta_j < 1.5$) the Blasius profile is almost linear: $\frac{\partial u_{Blasius}}{\partial y} = \frac{\tau_f}{\mu}$, where, $\tau_f = 0.33206 \frac{\mu \overline{U}_m}{x} \sqrt{Re_x}$ is the Blasius skin friction

This greatly simplifies the analysis, because at the location y_j, where the "outer profile" is joined to the "inner profile", u_f is also linear according to (4.3) (the second term on the right hand side does not depend on y). Then: $\frac{\partial u_f}{\partial y} = \frac{\tau_f}{\mu}$ according to (4.3). This relation rewritten as:

$$\frac{\partial u_f}{\partial y} = \frac{\partial u_f}{\partial \psi} \frac{\partial \psi}{\partial y} = \frac{1}{2} \frac{\partial u_f^2}{\partial \psi} = \frac{\tau_f}{\mu}$$

with the boundary condition at the wall:

$$u_f(x, \Psi = 0) = \frac{3}{4\omega} \hat{U} \hat{U}'$$

yields:

$$\frac{(u_f)^2}{2} = \frac{\tau_f}{\mu} \psi + \frac{1}{2} \left(\frac{3}{4\omega} \hat{U} \hat{U}' \right)^2$$

In summary, u_f satisfies the following relations at the junction:

$$\frac{(u_f)^2}{2} \approx \frac{\tau_f}{\mu} \psi + \frac{1}{2} \left(\frac{3}{4\omega} \hat{U} \hat{U}' \right)^2$$

$$(\frac{\partial u_f}{\partial y})_{x,\psi} \approx \frac{\tau_f}{\mu}$$

$$(\frac{\partial^2 u_f}{\partial y^2})_{x,\psi} \approx 0$$

With these approximations, the "outer profile" at the junction becomes:

$$\frac{1}{2}u_{out}^2(x,\psi_j) = \frac{\tau_f}{\mu}\psi_j + \frac{1}{2}(\frac{3}{4\omega}\hat{U}\hat{U}')^2 - \frac{p-p_m}{\rho}$$

$$(\frac{\partial u_{out}}{\partial y})_{x,\psi_j} = \frac{\tau_f}{\mu}$$

$$(\frac{\partial^2 u_{out}}{\partial y^2})_{x,\psi_j} = 0$$

Let us examine the flow in the "inner part" of the boundary layer. Once again, we write $u_{in} = u_{b,in} + h(x)\frac{\partial u_{b,in}}{\partial y}$.

In the "inner layer" the fluid inertial forces in the steady boundary layer equation, which governs the behaviour of u_b, are small and can be neglected. The pressure force is balanced by the gradient of the shear force, and the profile of the "basic flow" has the form:

$$\mu u_{b,in} = \tau_w y + \frac{1}{2}p'y^2 + D(x)y^3$$

which satisfies the boundary condition at the wall,

$$(\frac{\partial^2 u_{b,in}}{\partial y^2})_w = \frac{1}{\mu}\frac{dp}{dx} \tag{4.7}$$

We note at this point, that the term $\frac{dp}{dx} = \overline{UU}'$ does not contain the part of the mean pressure gradient due to flow unsteadiness, $\overline{\tilde{U}\tilde{U}'}$, because the latter appears as the forcing term in the equation for the (second order) steady component of the "Stokes flow". We have already accounted for the presence of this last term by satisfying the boundary condition $\overline{u}_{p,2}(x,0) = -\overline{u}_{s,2}(x,0)$.

Objection may be raised for choosing a third-degree polynomial to represent the "basic velocity" profile in the inner layer since it is known that a steady velocity profile satisfies the condition $\frac{\partial^3 u}{\partial y^3}|_{y=0} = D = 0$. But this is one of the compatibility conditions valid for analytic velocity distributions far from the separation point. Goldstein (1930) showed that these conditions seize to hold near the separation point leading to the appearance of singularity. This justifies our selection. We cite from Rosenhead (1966, p.328): "Stratford's method has the advantage that its assumptions correspond clearly to physical reality, in dividing the boundary layer into an inner flow where viscosity is important and an outer flow where it is not. These solutions correspond in fact to the two series solutions of Goldstein's (1930) method for the continuation of a boundary-layer solution at a singularity." In his original paper, Stratford used polynomials of the form $u = Ay + By^2 + Cy^m$ and considered the cases $m = 4$ and $m = 6$. All these profiles lead to a separation criterion of the type

$$c_p \left(x\frac{dc_p}{dx} \right)^2 = \text{Constant}$$

However, the choice $m = 3$ gives results that agree better with the computations of separated flows (Curle & Skan, 1957).

By adding the second order component $\overline{u}_{p,2}$ to u_b we obtain the full expression for the "inner velocity":

$$\begin{aligned} \mu u_{in} &= \tau_w y + \frac{1}{2}p'y^2 + D(x)y^3 + h(\tau_w + p'y + 3D(x)y^2) \\ &= \underbrace{h\tau_w}_{A} + \underbrace{(\tau_w + h\overline{p}')}_{B} y + \underbrace{(3hD + \frac{\overline{p}'}{2})}_{C} y^2 + Dy^3 \end{aligned}$$

The streamfunction is:

$$\mu\psi = Ay + \frac{B}{2}y^2 + \frac{C}{3}y^3 + \frac{D}{4}y^4$$

The "inner profile" is patched to the "outer profile" at y_j.

The joining conditions stem from the requirement for continuity in ψ, u, $\frac{\partial u}{\partial y}$, $\frac{\partial^2 u}{\partial y^2}$:

$$\mu\psi_j = Ay_j + \frac{B}{2}y_j^2 + \frac{C}{3}y_j^3 + \frac{D}{4}y_j^4 \tag{4.8}$$

$$\mu u_j = A + By_j + Cy_j^2 + Dy_j^3 \tag{4.9}$$

$$\tau_f = B + 2Cy_j + 3Dy_j^2 \tag{4.10}$$

$$0 = 2C + 6Dy_j \tag{4.11}$$

$$\frac{1}{2}u_j^2 = \frac{\tau_f}{\mu}\psi_j + \frac{1}{2}(\frac{3\mu}{4\omega}\hat{U}\hat{U}')^2 - \frac{\overline{p} - \overline{p}_m}{\rho} \tag{4.12}$$

If we eliminate successively a, y_j, ψ_j, and u_j from the above system of equations we get:

$$\begin{aligned}&[\frac{4\tau_f^2(1-\tau)(1-\tau-A)}{\mu\overline{p}'(2-2\tau-A)}]^2\{\frac{1}{2}[C+\frac{2+\tau+A}{3}]^2 - [C+\frac{1+\tau+A}{4}]\}\\ &= -\frac{\overline{p}-\overline{p}_m}{\rho} + \frac{9}{32\omega^2}(\hat{U}\hat{U}')^2\end{aligned} \tag{4.13}$$

where:

$$\begin{aligned}\tau &= \frac{\tau_w}{\tau_f}\\ A &\equiv \frac{h\overline{p}'}{\tau_f}\\ C &\equiv \frac{\tau A(2-\tau-A)}{4(1-\tau)(1-\tau-A)}\end{aligned}$$

This equation describes how the wall shear τ_w, which uniquely determines the "basic" and thus the "Prandtl" velocity profiles, varies with the streamwise location x.

In the next section we put this equation into non-dimensional form and show how it reduces to Stratford's criterion in the limit of vanishing unsteadiness. That equation

combined with the conditions for unsteady separation, (3.6) and (3.7), yields a system of equations that constitute the unsteady separation criterion.

4.2 Nondimensional form of the unsteady separation criterion

We introduce the following nondimesional parameters:

$$x^* = \frac{x}{c},\ y^* = \frac{y}{\delta_p} = y\sqrt{\frac{U_m}{\nu c}},\ t^* = \omega t$$

$$u^* = \frac{u}{U_m},\ \overline{p}^* = \frac{\overline{p}}{\rho U_m^2}$$

U_m being the mean free-stream velocity at the suction peak.

We also use the fact that the Blasius wall shear (which is equal to τ_f in the inner part of the boundary layer, where $u_{Blasius}$ is linear) is:

$$\tau_f = 0.33206\frac{\mu U_m}{x}\sqrt{Re_x}$$

In non-dimensional variables (4.13) reads:

$$16 \cdot 0.33206^4 \left[\frac{(1-\tau)(1-\tau-A)}{x^*(\overline{p}^*)'(2-2\tau-A)} \right]^2 \left\{ \frac{1}{2}\left[C + \frac{2+\tau+A}{3} \right]^2 - \left[C + \frac{1+\tau+A}{4} \right] \right\}$$
$$= -\frac{1-(\overline{U}^*)^2}{2} + \frac{9}{32\lambda^4}[\hat{U}^*(\hat{U}^*)']^2$$

or

$$16 \cdot 0.33206^4 \left[\frac{(1-\tau)(1-\tau-A)}{x^*\frac{c_p'}{2}(2-2\tau-A)} \right]^2 \left\{ \frac{1}{2}\left[C + \frac{2+\tau+A}{3} \right]^2 - \left[C + \frac{1+\tau+A}{4} \right] \right\}$$
$$= -\frac{c_p}{2} + \frac{9}{32\lambda^4}[\hat{U}^*(\hat{U}^*)']^2 \qquad (4.14)$$

where:

$$
\begin{aligned}
c_p &\equiv 1-(\overline{U}^*)^2 \\
\tau &\equiv \frac{\tau_w}{\tau_f} \\
A &\equiv -\frac{3}{4\cdot 0.33206\lambda^2}\frac{\hat{U}^*(\hat{U}^*)'(\overline{p}^*)'x^*}{\tau} \\
C &\equiv \frac{\tau A(2-\tau-A)}{4(1-\tau)(1-\tau-A)}
\end{aligned}
$$

We note that the sum $c_p + \overline{\tilde{U}^*(\tilde{U}^*)'} = c_p + \frac{1}{2}\hat{U}^*(\hat{U}^*)' = \overline{c_p}$ is the mean of the pressure coefficient.

If the flow is steady ($A = 0$, $C = 0$) the above equation reduces to $c_p(x\frac{dc_p}{dx})^2 = 0.0108(1-\frac{\tau_w}{\tau_f})^2(1+2\frac{\tau_w}{\tau_f})$, which is the relation for the variation of skin friction of Curle and Davies (1969, Eq. (6.77)). By letting $\tau_w = 0$ in the last equation we recover Stratford's separation criterion.

In Appendix C we find the non-dimensional form of the three "Prandtl velocity" components:

$$u_b^* = \frac{0.33206\tau}{\sqrt{x^*}}y^* + \frac{(\overline{p}^*)'}{2}(y^*)^2 + D^*(y^*)^3$$

where:

$$D^* = -0.25096\frac{((\overline{p}^*)')^2\sqrt{x^*}}{1-\tau}$$

$$\overline{u}_{p,2}^* = \frac{B^*}{\lambda^2}\left(\frac{0.33206\tau}{\sqrt{x}} + (\overline{p}^*)'y^* + 3D^*(y^*)^2\right)$$

where:

$$B^* = -4.51726\frac{\overline{\tilde{U}^*(\tilde{U}^*)'}\sqrt{x^*}}{\tau}$$

$$\begin{aligned}\tilde{u}^*_{p,2} &= \frac{1}{\lambda^2}\{\,(\tilde{U}^*|_{t-\frac{\tau}{4}}\overline{U}^*)' - 0.33206(\frac{\tau}{\sqrt{x^*}})'\tilde{U}^*|_{t-\frac{\tau}{4}}y^* \\ &\quad +0.5\,[\,(\tilde{U}^*|_{t-\frac{\tau}{4}})'(\overline{p}^*)' - \tilde{U}^*|_{t-\frac{\tau}{4}}(\overline{p}^*)''\,]\,(y^*)^2 \\ &\quad +[\,-2(\tilde{U}^*|_{t-\frac{\tau}{4}})'D^* + \tilde{U}^*|_{t-\frac{\tau}{4}}(D^*)'\,]\,(y^*)^3\}\end{aligned}$$

We note that $\tilde{u}_{p,2}$ lags $\tilde{U}$ by $\frac{\tau}{2}$.

If we substitute the full "Prandtl velocity" $u^*_p = u^*_b + \overline{u}^*_{p,2} + \tilde{u}^*_{p,2}$ into

$$\frac{\partial u^*_p}{\partial y^*} = 0$$

$$u^*_p + \widetilde{U^*} - \lambda^2\frac{dx_0}{dt} = 0$$

we get

$$\begin{aligned}&\frac{0.33206\tau}{\sqrt{x^*}} + \frac{(\overline{p}^*)'B^*}{\lambda^2} + [(\overline{p}^*)' + \frac{6B^*D^*}{\lambda^2}]y^* + 3D^*(y^*)^2 \\ &+\frac{1}{\lambda^2}\{\,-0.33206(\frac{\tau}{\sqrt{x^*}})'\tilde{U}^*|_{t-\frac{\tau}{4}} + \,[\,(\tilde{U}^*|_{t-\frac{\tau}{4}})'(\overline{p}^*)' - \tilde{U}^*|_{t-\frac{\tau}{4}}(\overline{p}^*)''\,]\,(y^*) \\ &+3\,[\,-2(\tilde{U}^*|_{t-\frac{\tau}{4}})'D^* + \tilde{U}^*|_{t-\frac{\tau}{4}}(D^*)'\,]\,(y^*)^2\} = 0\end{aligned} \tag{4.15}$$

$$\begin{aligned}&\frac{0.33206\tau}{\sqrt{x}}(\frac{B^*}{\lambda^2} + y^*) + (\overline{p}^*)'y^*(\frac{B^*}{\lambda^2} + \frac{y^*}{2}) + D^*(\frac{3B^*}{\lambda^2}(y^*)^2 + (y^*)^3] \\ &+\frac{1}{\lambda^2}\{\,(\tilde{U}^*|_{t-\frac{\tau}{4}}\overline{U}^*)' - 0.33206(\frac{\tau}{\sqrt{x^*}})'\tilde{U}^*|_{t-\frac{\tau}{4}}y^* \\ &+0.5\,[\,(\tilde{U}^*|_{t-\frac{\tau}{4}})'(\overline{p}^*)' - \tilde{U}^*|_{t-\frac{\tau}{4}}(\overline{p}^*)''\,]\,(y^*)^2 \\ &+[\,-2(\tilde{U}^*|_{t-\frac{\tau}{4}})'D^* + \tilde{U}^*|_{t-\frac{\tau}{4}}(D^*)'\,]\,(y^*)^3\} + \tilde{U}^*|_t \\ &= \lambda^2\frac{dx^*_0}{dt^*}\end{aligned} \tag{4.16}$$

These relations, combined with (4.14) form a system of two algebraic equations (4.14), (4.15) and one first-order ordinary differential equation (4.16) for the unknowns $x^*_0(t^*)$,

$y_0^*(t^*)$, $\tau(t^*)$ subject to periodic boundary conditions

$$x_0^*(t^*) = x_0^*(t^* + 2\pi)$$

$$y_0^*(t^*) = y_0^*(t^* + 2\pi)$$

$$\tau(t^*) = \tau(t^* + 2\pi)$$

In the absence of unsteadiness (4.16) becomes $u = 0$, with solution $y_0 = 0$ and (C.2) becomes $\frac{\partial u}{\partial y} = 0$, or $\tau_w = 0$, and the separation conditions for steady flow are recovered.

Equation (4.14) yields

$$c_p \left(x \frac{dc_p}{dx} \right)^2 = 0.0108$$

where $c_p = 1 - \frac{U^2}{U_m^2}$. This is the initial form of the Stratford relation (Rosenhead, 1966). However, Curle and Skan (1957) have shown that the value 0.0104 for the constant gives results that agree better with accurate computations (using Görtler's method (1955)) for a large number of cases of steady flow with separation.

The separation criterion can be further simplified by solving equation (4.15) for y^* and sustituting its value into the two other equations. Then the only unknowns are x_0^* and τ. It is this simplified boundary value problem (one first order ODE, and one algebraic equation) that we solve numerically using a collocation method. This method of locating unsteady separation is very efficient computationally. To find a separation trajectory by calculating the location of the separation point at 40 instances throughout a period, we need 50 sec of CPU time on a VAX 3200.

Chapter 5

How the interaction between the airfoil and its wake determines the airfoil circulation and the force and moment acting on the airfoil

As we have mentioned in the introduction, the motion of the separation points on the airfoil determines the net vorticity flux shed into the wake or, equivalently, the rate of change of the circulation around the airfoil. At the same time, the velocity induced by the wake vorticity changes the external flow and thus the location of separation. For this reason, the airfoil circulation must be calculated by an iterative procedure which accounts for the wake-induced effects on separation. In the first section of this chapter, we describe this iterative method for computing the time evolution of the airfoil circulation that simulates the interaction between the airfoil and its wake.

We consider a bluff airfoil in flow that oscillates about a nonvanishing mean. In the examples of chapter 7, we take the farfield velocity to oscillate in magnitude and not in direction. But in this chapter we consider the general case and allow the angle of attack to vary with time. We derive the formulae for lift, drag, and moment for the general case; in the derivations we point out the simplifications arising from the assumption of a constant angle of attack.

5.1 The circulation

In the immediate neighbourhood of separation, the shear layer lifts off the wall, and not far downstream it becomes a free shear layer. The free shear layer leaves the surface of the airfoil tangentially. The argument is given in Batchelor (1967, p. 329) and we repeat it here. Compared to the body dimensions the boundary layer thickness is negligible, and an instantenous streamline near the body surface appears to follow the body contour. If this streamline, leaving the wall at separation, formed an angle with the upstream wall less than 180^0, the situation would resemble flow over a wedge with its vertex located at the separation point. Then the external velocity would be zero at separation, and the decelaration of the stream before reaching the separation location would cause the boundary layer to separate earlier.

The interaction between the two vortex sheets of opposite sign, which originate from the two sides of the airfoil, leads to the formation of alternate large-scale vortices far from the solid boundary (Mezaris et al., 1987). Since discrete vortices can be identified in experiments only aft of the airfoil, in order to model the mechanism of creation of the wake region, we place a point vortex a short distance (typically a small fraction of $W_\infty \, \Delta t$) downstream of the trailing edge. The wake vorticity, which is organised in discrete vortical structures, is modelled by these point vortices in an approximate way: their value represents the net sum of positive and negative vorticity at an x-station downstream of the airfoil. This replicates the vorticity cancellation occurring aft of the airfoil. Changes in the sign of the point vortices mark the boundaries between actual vortices. As we shall discuss later, at some distance downstream of the trailing edge we

merge the vortices of the same sign in order to save computational time (see figure (5.1). Then, the resulting point vortices approximately represent actual vortical sructures that contain vorticity alternating in sign.

At each time step, the circulation of the vortex that is shed is equal and opposite to the change in the airfoil circulation. This change in the airfoil circulation is determined by Helmholtz's relation (Sears, 1976), which states that the rate of change of the airfoil circulation is equal to the net vorticity flux leaving the surface of the host body and being shed into the wake:

$$\begin{aligned} \frac{d\Gamma_{\text{Airfoil}}}{dt} &= -\int_0^{\delta_A} \omega(u_A - u_{\text{sep,A}})dy - \int_{\delta_B}^{0} \omega(u_B - u_{\text{sep,B}})dy \\ &= \frac{1}{2}u_A^2 - u_A u_{\text{sep,A}} - \frac{1}{2}u_B^2 + u_B u_{\text{sep,B}} \end{aligned} \tag{5.1}$$

In this equation $u_{A;B} - u_{\text{sep,A;B}}$ is the speed at which the vorticity is released from the airfoil surface and becomes free vorticity. If $u_{\text{sep,A;B}} = 0$ all the vorticity in the boundary layer at the separation location becomes free vorticity. If $u_{\text{sep,A;B}} = u_{A;B}$ the vorticity contained in the boundary layer at the separation location travels at the same speed as the separation point, which can be considered as "the starting line of the free wake"; then this vorticity remains a part of the body-bound vorticity. In discrete form, this relation can be written in terms of the circulation Γ_j of the vortex that is shed as:

$$-\frac{\Gamma_j}{\Delta t} = \frac{1}{2}u_A^2 - u_A u_{sep,A} - \frac{1}{2}u_B^2 + u_B u_{sep,B} \tag{5.2}$$

Γ_j appears on both sides of this equation (on the right-hand side in the expression for u_A and u_B). This equation is used to determine Γ_j and the new value of the airfoil circulation. To the author's best knowledge this is the first time that Helmholtz's relation is viewed as an equation for the shed circulation. In the literature (see for

example the textbook by Katz, 1991, p. 544), the velocities u_A, and u_B are evaluated by using the system of vortices already shed and then the value of the shed circulation is calculated from equation (5.2) and assigned to the forming vortex.

At every time step, we model the newly created segment of the vortical wake by placing a point vortex, whose strength is the amount of shed circulation, at a short distance downstream of the trailing edge. In reality this segment of the wake consists of two free shear layers containing vorticity of opposite sign, and can be better approximated by two panels of distributed vorticity. In order to compare by how much these two different modelling approaches differ in predicting the rate of change in airfoil circulation $\frac{\Delta\Gamma_{\text{Airfoil}}}{\Delta t}$ we performed the following numerical experiment (see figure 5.2):

- We first calculated the velocity at the locations of separation on the suction and pressure sides due to the free-stream, the already existing wake, and the new point vortex (of strength $-\Delta\Gamma_{\text{Airfoil}}$).

- Then we replaced this new vortex by two panels, the upper having circulation:

$$\Gamma_u = \Delta t(\frac{1}{2}u_A^2 - u_A u_{sep,A})$$

and the lower having circulation:

$$\Gamma_l = \Delta t(-\frac{1}{2}u_B^2 + u_B u_{sep,B})$$

(of course $-\Delta\Gamma_{\text{Airfoil}} = \Gamma_u + \Gamma_l$), and recalculated the velocity at the two separation locations. The lengths of the panels were $d_{u;l} = \Delta t u_{A;B}/2$ (half the distance travelled in the time step by a fluid particle initially located at the separation point). The panels were placed in directions tangent to the surface of the ellipse,

with their upstream edges located at a distance $d_{u;l}/2$ away from the instantaneous position of separation. Note that the velocity due to a vortex panel and its image in the circle plane is:

$$w(\varsigma,t) = \frac{i}{2\pi}\Gamma\{\frac{1}{\varsigma_2 - \varsigma_1}\log(\frac{\varsigma_1 - \varsigma}{\varsigma_2 - \varsigma}) - \frac{1}{\varsigma_2^* - \varsigma_1^*}\log(\frac{\varsigma_1^* - \varsigma}{\varsigma_2^* - \varsigma})\}$$

The difference in velocity was on the order of 1-3% for all the cases that we considered. This means that the differences in shed circulation (and thus in $\frac{\Delta\Gamma_{\text{Airfoil}}}{\Delta t}$) is less than 1/1000 in all cases, since the value of the circulation is proportional to the square of the velocity (see equation (5.2)).

The velocity of the separation point in equation (5.2) must be computed by taking into account the induction of the developing wake. Since we must use the mean as well as the instantaneous value of the external velocity in order to find the separation point trajectory (see chapter 4), we must know the position and strength of the wake elements throughout an oscillation period in order to compute the mean value of the external velocity. For this reason, we use an iterative procedure to determine the time evolution of the circulation. The wake which had been computed in the previous iteration (the iteration typically spans 2 to 5 oscillation periods), is used to calculate the separation velocity, and to create a new wake until, the instantaneous values of the circulation in two succesive iterations agree by a specified amount.

An outline of the computational method is:

- Assume $\Gamma_{\text{Airfoil}}(0)$.
- First iteration: calculate the trajectories of the separation points on the two sides

of the airfoil by using the oncoming flow only as input to the separation criterion of section 4.2.

- Find the strength of the shed vortex from:

$$-\frac{\Gamma_{Shed}}{\Delta t} = \frac{1}{2}u_A^2 - u_A u_{sep,A} - \frac{1}{2}u_B^2 + u_B u_{sep,B}$$

- Shed vorticity for 2 to 5 periods while storing the position and strength of the wake vortices at every time step.

- Set $\Gamma_{\text{Airfoil}}(0)$ equal to the final value of Γ_{Airfoil} and use the stored position and strength of the wake to find the mean and instantaneous external velocity distribution and to recalculate the trajectories of the separation points.

- Iterate until convergence is reached.

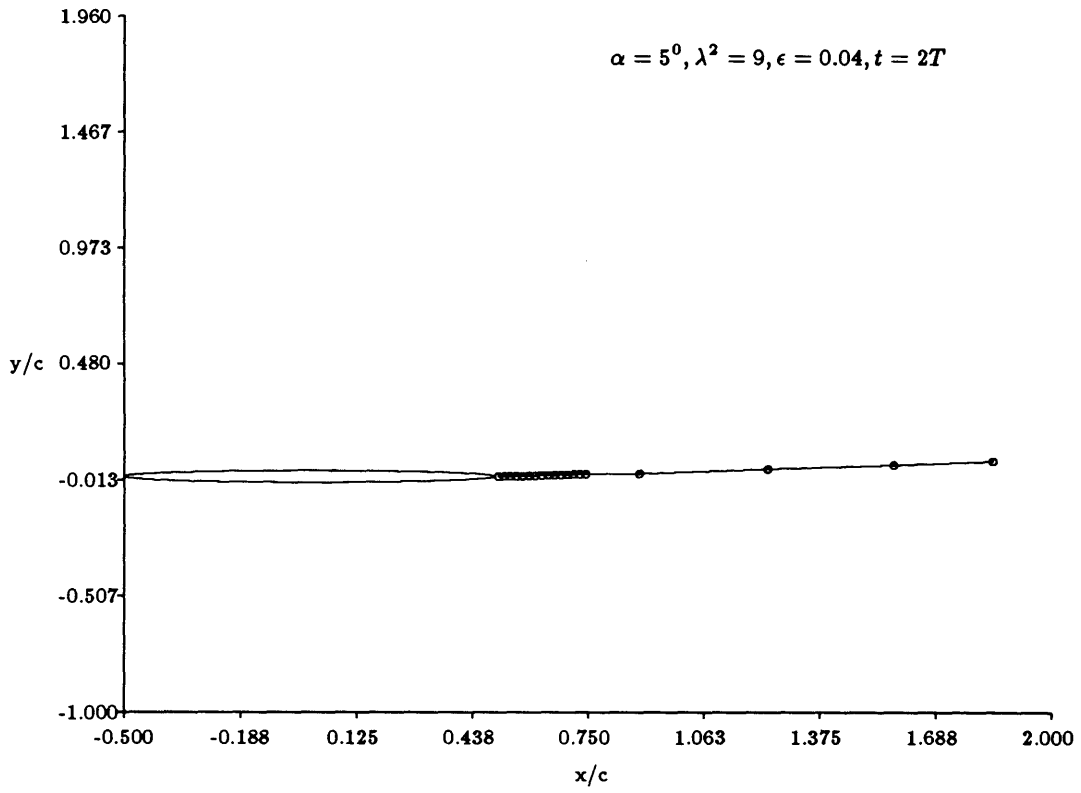

Figure 5.1: The representation of the wake by free point vortices. Note that in order to decrease computational time we merge adjacent vortices of the same sign at distances greater than $0.75c$.

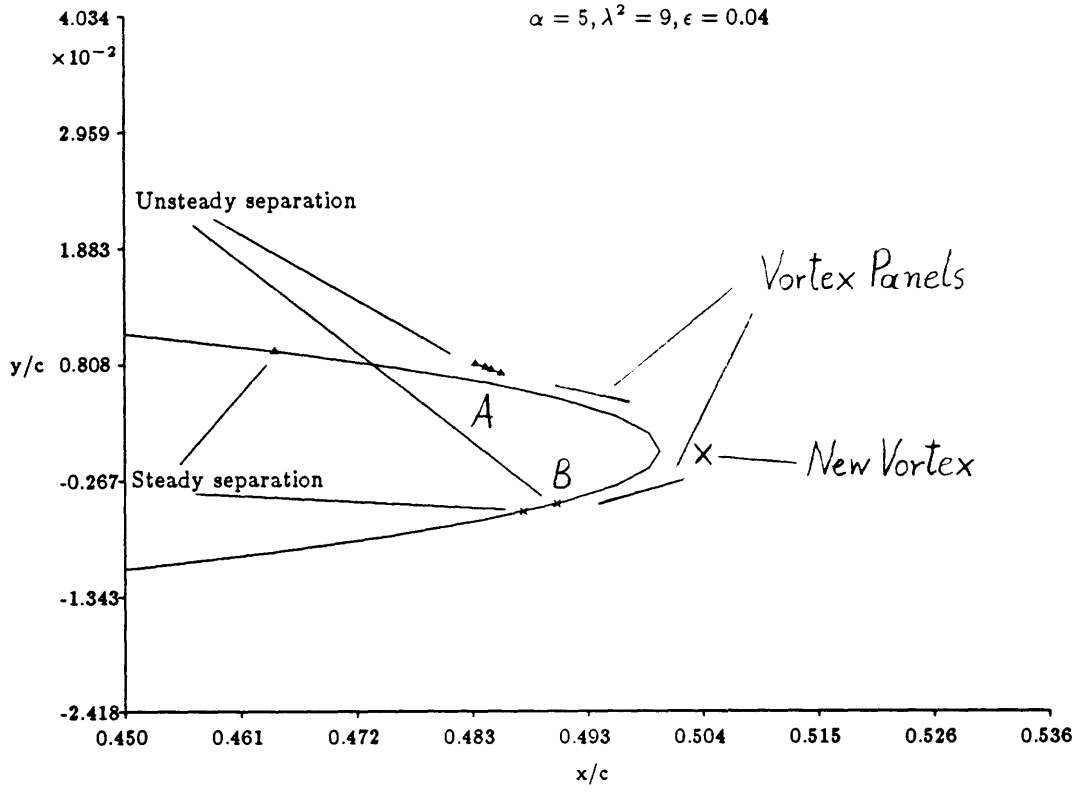

Figure 5.2: A sketch illustrating two types of singularities that model the segment of the wake created in one time step: a point vortex and two vortex panels. The numerical experiment of section 5.2, shows that the two modelling approaches predict essentially the same rate of change in airfoil circulation (difference in the predictions/ predicted value $< 1/1000$).

5.2 Airfoil in oscillating stream vs. oscillating airfoil in steady stream: what is the difference in the aerodynamic force and moment?

The airfoil is held still in an oscillating stream: $W_\infty(t) =< W_\infty > (1 + \epsilon\cos(\omega t))$, where $W_\infty = U_\infty + iV_\infty$ is the complex velocity. In this chapter the symbol $\overline{(\,)}$ denotes the complex conjugate and $< (\,) >$ denotes the time-average. We now discuss how the force and the moment acting on the airfoil in this situation, relate to the force and the moment acting on an airfoil which moves with velocity $-W_\infty(t)$ in still air.

When a body of nonzero cross-section is placed in a stream of accelerating flow, an extra term appears in the expression of the force. What gives rise to this term? In order to answer this question we must first examine how a uniform (in space) and unsteady flow is generated. Suppose that an observer, who is fixed in space (and far away from any solid boundary), sees an unsteady oncoming flow. This observer writes the velocity potential as:

$$\Phi = xU_\infty(t) + yV_\infty(t)$$

By applying Bernoulli's equation between two points in the field:

$$p_1 + \frac{\rho|W_\infty|^2}{2} + \rho x_1\frac{dU_\infty}{dt} + \rho y_1\frac{dV_\infty}{dt} = p_2 + \frac{\rho|W_\infty|^2}{2} + \rho x_2\frac{dU_\infty}{dt} + \rho y_2\frac{dV_\infty}{dt}$$

he finds that there exists a pressure gradient, which is constant throughout the flowfield at a given time instant, but changes in magnitude and in direction with time. This pressure gradient provides the force which accelerates the fluid.

Let us now consider the case when the free-stream velocity changes in magnitude but not in direction (as in the examples of chapter 7). By taking the x axis in the direction of the farfield velocity, we write the unsteady pressure gradient as:

$$\frac{p_1 - p_2}{x_2 - x_1} = \rho \frac{dU_\infty}{dt}$$

Acting on the airfoil, the pressure gradient gives rise to a force which resembles a "buoyancy force", has the constant value $-\rho \frac{dU_\infty}{dt}$ per unit area, and acts in the direction of the free-stream velocity. Therefore, this force appears as a drag force that oscillates about a zero mean value and has the form:

$$D = \rho \frac{dU_\infty}{dt} S_{\text{Airfoil}}$$

We know from Hydrostatics that this force acts on the centre of gravity of the body. Thus, it does not create a moment about the airfoil's centre of symmetry.

In conclusion, we can use an inertial system to find the force and moment acting on the airfoil by applying Bernoulli's equation, and then simply add the additional drag force to get the force in the airfoil system of reference.

5.3 Inertial and airfoil frames of reference

Suppose that the instantaneous position of the airfoil in an inertial frame of reference is $z_0(t) = x_0(t) + iy_0(t)$. Now consider a coordinate system $\check{z}$, the x-axis of which is aligned with the chord of the airfoil. The airfoil reference frame is rotated by an angle α_0 in the clockwise direction with respect to the inertial reference frame. In our problem

the airfoil does not rotate. In the general case, the airfoil rotates by an angle $\tilde{\alpha}(t)$ relative to the airfoil frame of reference.

The inertial and local coordinates are related in the following way:

$$z(\check{z},t) = z_0(t) + \check{z}e^{-i\alpha_0}$$

$$\check{z}(z,t) = (z - z_0(t))e^{i\alpha_0}$$

The time derivative is:

$$\frac{\partial()}{\partial t}|_z = \frac{\partial()}{\partial t}|_{\check{z}} + \frac{\partial()}{\partial \check{z}}|_t \frac{\partial \check{z}}{\partial t}|_z = \frac{\partial()}{\partial t}|_{\check{z}} - \dot{z}_0 e^{i\alpha_0}\frac{\partial()}{\partial \check{z}}|_t \tag{5.3}$$

and the space derivative in the inertial frame is:

$$\frac{\partial()}{\partial z}|_t = \frac{\partial()}{\partial \check{z}}|_t \frac{\partial \check{z}}{\partial z}|_t = e^{i\alpha_0}\frac{\partial()}{\partial \check{z}}|_t \tag{5.4}$$

5.4 Calculation of the force using the unsteady Bernoulli equation

5.4.1 The pressure coefficient

The following discussion follows closely Drela (1990). The conjugate velocity, $\check{u} - i\check{v}$, in the airfoil frame of reference is:

$$\check{u} - i\check{v} = \check{w}(\check{z},t) = \frac{\partial \check{F}}{\partial \check{z}}$$

where $\check{F}(\check{z},t) = \check{\Phi} + i\check{\Psi}$ is the complex potential in the airfoil frame. In the inertial frame of reference, the conjugate velocity, $u - iv$, is:

$$u - iv = \frac{\partial \check{F}}{\partial z}|_t + u_0 - iv_0 = e^{i\alpha_0}\frac{\partial \check{F}}{\partial \check{z}} + u_0 - iv_0$$

In the farfield, the absolute conjugate velocity is zero and thus:

$$\lim_{z\to\infty}\frac{\partial \check{F}}{\partial \check{z}} = \check{W}_\infty = -\overline{\dot{z}_0}e^{-i\alpha_0}$$

The instantenous local angle of attack $\alpha(t)$ is:

$$e^{i\alpha(t)} = \frac{-\dot{z}_0}{|\dot{z}_0|}e^{i\alpha_0}$$

The unsteady Bernoulli equation in the inertial frame yields the pressure:

$$\frac{p}{\rho} = -\frac{\partial \Phi}{\partial t} - \frac{1}{2}|u - iv|^2$$

The absolute potential Φ and streamfunction Ψ are related to the relative complex potential $\check{F}$ by:

$$\Phi + i\Psi = \check{F} + (u_0 - iv_0)z$$

Then:

$$\frac{\partial \Phi}{\partial t} = \Re\{\frac{\partial F}{\partial t}|_z + (\dot{u}_0 - i\dot{v}_0)z\} = \Re\{\frac{\partial F}{\partial t}|_z - \dot{z}_0 e^{i\alpha_0}\frac{\partial F}{\partial \check{z}} + (\dot{u}_0 - i\dot{v}_0)z\}$$

Therefore, the pressure can be expressed as follows:

$$\frac{p}{\rho} = -\Re\{\frac{\partial F}{\partial t} - \dot{z}_0 e^{i\alpha_0}\frac{\partial F}{\partial \check{z}} + (\dot{u}_0 - i\dot{v}_0)z\} - \frac{1}{2}|e^{i\alpha_0}\frac{\partial F}{\partial \check{z}} + u_0 - iv_0|^2$$

Far from the airfoil, $u - iv \to 0$, and $\partial\Phi/\partial t \to 0$. The farfield pressure p_∞ is then given by $\frac{p_\infty}{\rho} = 0$. The pressure coefficient is:

$$\begin{aligned} C_p &= \frac{p - p_\infty}{\frac{\rho|\dot{z}_0|^2}{2}} \\ &= 2\{-\frac{\Re\{\frac{\partial F}{\partial t} - \dot{z}_0 e^{i\alpha_0}\frac{\partial F}{\partial \check{z}} + (\dot{u}_0 - i\dot{v}_0)z\} - \frac{1}{2}|e^{i\alpha_0}\frac{\partial F}{\partial \check{z}} + u_0 - iv_0|^2}{|\dot{z}_0|^2}\} \end{aligned} \tag{5.5}$$

5.4.2 The mapping of the physical to the circle plane

The transformation:

$$z = \varsigma + \frac{k^2}{\varsigma}$$

maps the ellipse:

$$\frac{x^2}{a^2} + \frac{y^2}{b^2} = 1$$

into the circle:

$$\eta^2 + \xi^2 = c^2$$

where $c = \frac{a+b}{2}$, and $k = \frac{\sqrt{a^2-b^2}}{2}$.

The complex potential for the instantaneous velocity field in the circle plane is:

$$F(\varsigma, t) = W_\infty(t)(\varsigma + \frac{c^2 e^{2i\alpha_c}}{\varsigma}) + \frac{i}{2\pi}\Gamma_0 \log(\varsigma) + \frac{i}{2\pi}\sum_{j=1}^{N}\Gamma_j[\log(\varsigma - \varsigma_j) - \log(\varsigma - \varsigma_j^*)]$$

where $\varsigma_j^* = c^2/\overline{\varsigma_j^*}$ is the image of the j-th wake vortex.

The complex potential in the physical plane is given by $F(z(\varsigma), t)$, and the complex velocity by:

$$w = u - iv = \frac{\partial F}{\partial z} = \frac{\partial F}{\partial \varsigma}\frac{\partial \varsigma}{\partial z}$$

Where $\partial F/\partial \varsigma$ is:

$$\frac{\partial F}{\partial \varsigma} = W_\infty(1 - \frac{c^2 e^{2i\alpha_c}}{\varsigma^2}) + \frac{i\Gamma_0}{2\pi\varsigma} + \frac{i}{2\pi}\sum_{j=1}^{N}\Gamma_j(\frac{1}{\varsigma - \varsigma_j} - \frac{1}{\varsigma - \varsigma_j^*}) \qquad (5.6)$$

Since $lim_{\varsigma\to\infty} d\varsigma/dz = 1$, the conjugate freestream velocity in the circle plane is equal to the corresponding velocity in the physical plane. The time derivative of the complex

potential is:

$$\frac{\partial F}{\partial t} = \frac{dW_\infty}{dt}(\varsigma + \frac{c^2 e^{2i\alpha_c}}{\varsigma}) + W_\infty \frac{2c^2 e^{i\alpha_c}}{\varsigma}\frac{de^{i\alpha_c}}{dt} + \frac{i}{2/pi}\sum_{j=1}^{N}\Gamma_j(-\frac{\dot{\varsigma_j}}{\varsigma - \varsigma_j} + \frac{\dot{\varsigma^*}_j}{\varsigma - \varsigma_j^*})$$

where:

$$\frac{de^{i\alpha_c}}{dt} = \dot{\alpha}_c i e^{i\alpha_c} = \frac{u_0\dot{v}_0 - v_0\dot{u}_0}{u_0^2 + v_0^2} i e^{i\alpha_c}$$

5.4.3 The force and moment coefficient

The lift and drag coefficients, defined in the directions of the inertial system axes, are:

$$C_l - iC_d = e^{-i\alpha_0}\oint C_p \frac{dz}{c}$$

$$C_m = -\Re\{\oint C_p \frac{\overline{z}dz}{c^2}\}$$

The integration is performed numerically, using Romberg's method. As we have mentioned in section 5.2, the total drag is given by adding the "buoyancy force" created by the unsteady pressure gradient.

5.5 Calculation of the force using the impulse

The force acting on the airfoil can be calculated either in the circle plane or in the physical plane (Sears, 1957). We chose to work in the circle plane because then the calculation becomes simpler. On the other hand, the moment must be calculated in the physical plane (Sears, 1957).

The force acting on the airfoil is:

$$F = -\frac{\partial I}{\partial t} = -\frac{\partial}{\partial t}(-\oint \rho \Phi \hat{n} ds) \tag{5.7}$$

We shall examine how the various components of the potential Φ, contribute to the force. The complex potential for the instantaneous velocity field in the circle plane is:

$$F(\zeta, t) = W_\infty(t)(\zeta + \frac{c^2 e^{2i\alpha_c}}{\zeta}) + \frac{i}{2\pi}\Gamma_0 \log(\zeta) + \frac{i}{2\pi}\sum_{j=1}^{N}\Gamma_j[\log(\zeta - \zeta_j) - \log(\zeta - \zeta_j^*)]$$

where $W_\infty = |W_\infty|e^{-i\alpha}$ is the farfield conjugate velocity, Γ_j is the circulation of the j-th point vortex, and Γ_0 is the circulation around the computational domain. Since we start our calculation by assuming that the airfoil has the initial circulation Γ_0, the computational domain does not include the starting vortex $-\Gamma_0$. The starting vortex is located very far downstream of the airfoil and its contribution to the complex potential is insignificant. Its image is located at the centre of the circle and gives rise to the second term in the expression for the complex potential.

The Φ component due to the oncoming stream and the doublet is $2|W_\infty|\cos(\theta - \alpha_c)$ and its contribution to the impulse is:

$$\begin{aligned}
&-\rho 2|W_\infty|\int_0^{2\pi}\cos(\theta-\alpha_c)(\cos(\theta) - i\sin(\theta))d\theta \\
&\quad = -\rho 2|W_\infty|\int_0^{2\pi}(\cos^2(\theta)\cos(\alpha_c) + \sin(\theta)\cos(\theta)\sin(\alpha_c) \\
&\quad +i\sin^2(\theta)\sin(\alpha_c) + i\sin(\theta)\cos(\theta)\cos(\alpha_c))d\theta \\
&\quad = -\rho c|W_\infty|(\cos(\alpha_c) + i\sin(\alpha_c)) \\
&\quad = -\rho c|W_\infty|e^{i\alpha_c} = -\rho c\overline{W_\infty}
\end{aligned}$$

Then expression (5.7) yields for the apparent mass component of the force in the airfoil

frame:

$$F_{\text{apparent mass}} = \rho c \frac{d\overline{W_\infty}}{dt}$$

In the general case, when the speed of the airfoil has a component normal to the freestream, the relative angle of attack varies with time:

$$\frac{d\overline{W_\infty}}{dt} = -e^{i\alpha}\left(\frac{d^2 z_0}{dt^2} + i\frac{d\alpha}{dt}\frac{dz_0}{dt}\right)$$

In our problem the angle of attack remains constant:

$$\frac{d\overline{W_\infty}}{dt} = - < W_\infty > \omega\epsilon \sin(\omega t) e^{i\alpha_0}$$

where $< W_\infty >$ is the mean magnitude of the free-stream velocity (we remind the reader that in this chapter the symbol $\overline{(\,)}$ denotes the complex conjugate). Since we define the lift and drag along the coordinate directions of the inertial frame we must rotate this force counterclockwise by α_0:

$$F_{\text{apparent mass}} = \rho c \frac{d\overline{W_\infty}}{dt} e^{-i\alpha_0} = \rho c - < W_\infty > \omega\epsilon \sin(\omega t)$$

In our problem the apparent mass term of the force acts in the direction of the drag (alternating sign every half period).

Next we focus on the component of the force that represents the influence of the wake. Since the wake cannot sustain any loading (the pressure is continuous across the wake), the force acting on the airfoil is equivalent to that acting on the system of vortices which represents the wake and the airfoil. The free wake is modelled by a system of point vortices. Working in the circle plane is more convenient than working in the physical plane because, in the circle plane, the continuous distribution of vorticity

on the surface of the airfoil is replaced by a system of discrete vortices, the images of the wake vortices.

The impulse of a system of vortices, comprised of N vortex pairs, $(\varsigma_{1,j}, \varsigma_{2,j})$, is:

$$I = i\rho \sum_{j=1}^{N} \Gamma_j (\varsigma_{1,j} - \varsigma_{2,j})$$

In the circle plane, a vortex pair consists of a wake vortex and its image:

$$\varsigma_{2,j} = \varsigma_{1,j}^* = \frac{c^2}{\varsigma_{1,j}}, |\varsigma_{2,j}|^2 = |\varsigma_{1,j}^*|^2 = \frac{c^4}{|\varsigma_{1,j}|^2}$$

The force in the inertial coordinate system is:

$$F_{\text{wake \& images}} = -i\rho \frac{\partial}{\partial t} \sum_{i=1}^{N} \Gamma_i (\varsigma_i - \varsigma_i^*) - i\rho \Gamma_0 \dot{\varsigma}_0 \tag{5.8}$$

The last term represents the force acting on the vortex located at the centre of the circle (the image of the starting vortex) as it moves with the airfoil speed and can be interpreted as the quasi-steady part of the force. The starting vortex remains where it has originally been shed and does not contribute to the change in impulse.

When the impulse is evaluated in the airfoil frame of reference, as in our computation, the force is:

$$F_{\text{wake \& images}} = -ie^{-i\alpha_0} \rho \frac{\partial}{\partial t} \sum_{i=1}^{N} \Gamma_i (\check{\zeta}_i - \check{\zeta}_i^*) - i\rho \Gamma_0 \dot{\varsigma}_0 \tag{5.9}$$

This expression is derived in the following way: In the airfoil frame, the starting vortex is moving away from the airfoil with speed $\overline{W_\infty} = -\dot{\varsigma}_0 e^{i\alpha_0}$. (Although the quantity $\Gamma_{\text{start}}\ \varsigma_{\text{start}}$ is undefined, its time rate of change is well defined: $\Gamma_{\text{start}}\ (-\dot{\varsigma}_0 e^{i\alpha_0})$) In the expression (5.8) we replace $\varsigma(t)$ by $\varsigma_0(t) + \check{\varsigma} e^{-i\alpha_0}$, and use the expression (5.3) to

transform the time derivative from the inertial to the airfoil frame:

$$F_{\text{wake \& images}} = -i\rho\frac{\partial}{\partial t}|_{\zeta}\sum_{i=1}^{N}\Gamma_i(\check{\zeta}_i - \check{\zeta}_i^*)e^{-i\alpha_0} - i\rho(-\Gamma_0)\dot{\check{\zeta}}_{\text{start}}e^{-i\alpha_0}$$

$$= -i\rho\frac{\partial}{\partial t}|_{\check{\zeta}}\sum_{i=1}^{N}\Gamma_i(\check{\zeta}_i - \check{\zeta}_i^*)e^{-i\alpha_0} + i\rho\dot{\zeta}_0 e^{i\alpha_0}\frac{\partial}{\partial \check{\zeta}}|_t\sum_{i=1}^{N}\Gamma_i(\check{\zeta}_i - \check{\zeta}_i^*)e^{-i\alpha_0} + i\rho\Gamma_0(-\dot{\zeta}_0 e^{i\alpha_0})e^{-i\alpha_0}$$

$$= -ie^{-i\alpha_0}\rho\frac{\partial}{\partial t}|_{\check{\zeta}}\sum_{i=1}^{N}\Gamma_i(\check{\zeta}_i - \check{\zeta}_i^*) + i\rho\dot{\zeta}_0\underbrace{\sum_{j=1}^{N}(\Gamma_j - \Gamma_j)}_{0} - i\rho\Gamma_0\dot{\zeta}_0$$

Finally, in order to account for the unsteady pressure gradient that exists throughout the flow, we add to the drag the "buoyancy term" as we have explained in section 5.2.

5.6 Calculation of the moment using the moment of impulse

The moment must be calculated in the physical plane.

The moment about the centre of the ellipse is:

$$M = \frac{\partial}{\partial t}\oint \rho\Phi(\vec{r}\times\hat{n})ds$$

Since the wake cannot sustain any loading (the pressure is continuous across the wake), the moment and the force acting on the airfoil are equivalent to those acting on the vortex sheet which represents the wake and the airfoil. The free wake is modelled by a system of point vortices and the airfoil is modelled by a continuous distribution of vorticity on its surface $\gamma(\theta)$. This bound vorticity distribution is equal to the tangential velocity in the physical plane. It is obtained from the value of the tangential velocity

in the circle plane by using the expression:

$$\gamma_z(\theta,t) = -v_{\theta,z}(\theta,t) = -v_{\theta,\zeta}\frac{d\zeta}{dz} = \gamma_\zeta(\theta,t)\frac{d\zeta}{dz} \tag{5.10}$$

Let us assume that at an instant in time the centre of the ellipse coincides with the origin of the inertial coordinate system. Then, in the inertial frame of reference, the moment about the origin is:

$$M_{\text{origin}} = -\frac{\rho}{2}\frac{\partial}{\partial t}\oint_{\text{airfoil}} \gamma_z(z)|z|^2 dz - \frac{\rho}{2}\frac{\partial}{\partial t}\sum_{j=1}^{M}\Gamma_j z_j \overline{z_j} \tag{5.11}$$

When, at a later time, the centre of the ellipse has moved to the location z_0 with respect to the origin, the moment about the centre of the ellipse is:

$$M = M_{\text{origin}} + \vec{z}_0 \times \vec{F}$$

where $\vec{F}$ is the force acting on the ellipse, as it has been calculated in the previous section.

We shall now discuss how the moment about the ellipse centre can be calculated in the airfoil frame of reference. In order to avoid lenghty expressions, we shall manipulate only the second term in the expression (5.11). Recalling that $z(t) = z_0(t) + \check{z}e^{-i\alpha}$, where for simplicity $z_0 = 0$, and using the expression (5.3) to transform the time derivative from the inertial to the airfoil frame, we express the force in terms of variables in the airfoil frame:

$$\begin{aligned} M &= -\frac{\rho}{2}\frac{\partial}{\partial t}|_z \sum_{j=1}^{M}\Gamma_j \check{z}_j e^{-i\alpha}\overline{\check{z}_j}e^{i\alpha_0} \\ &= -\frac{\rho}{2}\frac{\partial}{\partial t}|_z \sum_{j=1}^{M}\Gamma_j \check{z}_j \overline{\check{z}_j} + \frac{1}{2}[\dot{z}_0 e^{i\alpha_0}\frac{\rho}{2}\frac{\partial}{\partial \check{z}}|_t \sum_{j=1}^{M}\Gamma_j \check{z}_j e^{-i\alpha}\overline{\check{z}_j}e^{i\alpha_0} + c.\,c.] \end{aligned}$$

$$= -\frac{\rho}{2}\frac{\partial}{\partial t}|_{\mathbf{z}} \sum_{j=1}^{M} \Gamma_j \check{z}_j \overline{\check{z}_j} + \frac{1}{2}[\dot{z}_0 e^{i\alpha_0} \frac{\rho}{2} \sum_{j=1}^{M} \Gamma_j \overline{\check{z}_j} + c.\ c.]$$

$$= -\frac{\rho}{2}\frac{\partial}{\partial t}|_{\mathbf{z}} \sum_{j=1}^{M} \Gamma_j \check{z}_j \overline{\check{z}_j} + \Im\{\dot{z}_0 e^{i\alpha_0} i\rho \sum_{j=1}^{M} \Gamma_j \check{z}_j\}$$

$$= -\frac{\rho}{2}\frac{\partial}{\partial t}|_{\mathbf{z}} \sum_{j=1}^{M} \Gamma_j \check{z}_j \overline{\check{z}_j} + \Im\{\dot{z}_0 e^{i\alpha_0} \check{I}\}$$

where $c.\ c.$ signifies the complex conjugate of the term in the bracket. We also note that $z_0 e^{i\alpha_0} = -\overline{W_\infty}$.

Thus, the full expression for the moment about the centre of the ellipse in terms of variables in the airfoil frame of reference is:

$$\begin{aligned} M \;=\; & -\frac{\rho}{2}\frac{\partial}{\partial t}\oint_{\text{airfoil}} \gamma_z(\check{z})|\check{z}|^2 d\check{z} + \Im\{\dot{z}_0 e^{i\alpha_0} i\rho \oint_{\text{airfoil}} \gamma_z(\check{z})\check{z} d\check{z} \\ & -\frac{\rho}{2}\frac{\partial}{\partial t}|_{\mathbf{z}} \sum_{j=1}^{M} \Gamma_j \check{z}_j \overline{\check{z}_j} + \Im\{\dot{z}_0 e^{i\alpha_0} i\rho \sum_{j=1}^{M} \Gamma_j \check{z}_j\}\} \end{aligned}$$

The contribution of the starting vortex to the impulse is indeterminate, but this does not affect the end result since the contribution of the starting vortex to the first term of the above expression cancels out its contribution to the second. Indeed:

$$\begin{aligned} & -\frac{\rho}{2}\frac{\partial}{\partial t}\Gamma_s \check{z}_s \overline{\check{z}_s} + \rho \dot{z}_0 \Gamma_s \frac{\check{z}_s e^{i\alpha_0} + \overline{\check{z}_s} e^{-i\alpha}}{2} \\ & \quad = -\frac{\rho}{2}\Gamma_s (\frac{\partial \check{z}_s}{\partial t}\overline{\check{z}_s} + \frac{\partial \overline{\check{z}_s}}{\partial t}\check{z}_s) - \rho \dot{z}_0 \Gamma_s \frac{\check{z}_s e^{i\alpha_0} + \overline{\check{z}_s} + e^{-i\alpha}}{2} \\ & \quad -\frac{\rho}{2}\Gamma_s \dot{z}_0 (\check{z}_s e^{i\alpha_0} + \overline{\check{z}_s e^{-i\alpha}}) + \rho \dot{z}_0 \Gamma_s \frac{\check{z}_s e^{i\alpha_0} + \overline{\check{z}_s} e^{-i\alpha}}{2} \\ & \quad = 0 \end{aligned}$$

In the airfoil frame of reference, the vorticity distribution on the circle is:

$$\gamma_\zeta(\theta, t) = -v_{\theta,\zeta}(\theta, t) = 2|W_\infty| \sin(\theta - \alpha) + \frac{\Gamma_0}{2\pi c} + \frac{1}{2\pi c} \sum_{j=1}^{M} \Gamma_j \Re\{\frac{\check{\zeta}_j + ce^{i\theta}}{\check{\zeta}_j - ce^{i\theta}}\}$$

The vorticity distribution on the surface of the airfoil is found after substituting this value of $\gamma_\zeta(\theta,t)$ into expression (5.10):

$$\gamma_z(\theta,t) = \underbrace{(2|W_\infty|\sin(\theta-\alpha))\frac{d\zeta}{dz}}_{\gamma_{z,0}} + \underbrace{(\frac{\Gamma_0}{2\pi c} + \frac{1}{2\pi c}\sum_{j=1}^{M}\Gamma_j \Re\{\frac{\check{\zeta}_j + ce^{i\theta}}{\check{\zeta}_j - ce^{i\theta}}\})\frac{d\zeta}{dz}}_{\gamma_{z,1}}$$

Now, we can identify the four components of the moment.

- The quasi-steady moment is:

$$M_{\text{q-s}} = \Im\{\dot{z}_0 e^{i\alpha_0} i\rho \oint_{\text{airfoil}} \gamma_{z,0}(\check{z})\check{z}d\check{z}\}$$

  Further manipulation yields:

$$M_{\text{q-s}} = -\pi\rho U_\infty(t)V_\infty(t)(a_{ell}^2 - b_{ell}^2)$$

  Its sense is clockwise, tending to stall the ellipse. Unlike the corresponding lift component, the quasi-steady moment depends only on the body shape and not on circulation.

- The apparent-mass moment is:

$$M_{\text{app-mass}} = -\frac{\rho}{2}\frac{\partial}{\partial t}\oint_{\text{airfoil}} \gamma_{z,0}(\check{z})|\check{z}|^2 d\check{z}$$

- The component of the moment due to the bound vorticity on the airfoil induced by the wake (the effect of the starting vortex being the first term in $\gamma_{z,1}$) is:

$$M_1 = -\frac{\rho}{2}\frac{\partial}{\partial t}\oint_{\text{airfoil}} \gamma_{z,1}(\check{z})|\check{z}|^2 d\check{z} + \Im\{\dot{z}_0 e^{i\alpha_0} i\rho \oint_{\text{airfoil}} \gamma_{z,1}(\check{z})\check{z}d\check{z}\}$$

- The wake contribution to the moment is:

$$M_{\text{w}} = -\frac{\rho}{2}\frac{\partial}{\partial t}|_{\text{z}} \sum_{j=1}^{M}\Gamma_j \check{z}_j\overline{\check{z}_j} + \Im\{\dot{z}_0 e^{i\alpha_0} i\rho \sum_{j=1}^{M}\Gamma_j \check{z}_j\}$$

We have tested the subroutines that perform the calculation of force and moment, by applying them to the case of a very slender ellipse ($b : a = 1 : 1000$, to resemble a flat plate) in translatory oscillation normal to the flight direction. The vertical velocity of the ellipse was $0.01 U_\infty \cos(\omega t)$. This computation, which uses the Kutta condition to determine the circulation, reproduced the results obtained by McCune et al. (1990).

5.7 The free wake convection

We calculate how the row of free vortices, which represent the body wake, deforms in the airfoil frame. Each point vortex is convected by the velocity induced to its location by the others. We use a four-stage Runge-Kutta method to find how the vortex position z changes from time $t^{(n)}$ to time $t^{(n+1)} = t^{(n)} + \Delta t$.

$$\Delta z^{(1)} = \Delta t \frac{dz}{dt}|_{z=z^{(n)}} \quad \rightsquigarrow \quad z^{(1)} = z^{(n)} + \frac{1}{(2)}\Delta z^{(1)}$$

$$\Delta z^{(2)} = \Delta t \frac{dz}{dt}|_{z=z^{(1)}} \quad \rightsquigarrow \quad z^{(2)} = z^{(n)} + \frac{1}{2}\Delta z^{(2)}$$

$$\Delta z^{(3)} = \Delta t \frac{dz}{dt}|_{z=z^{(2)}} \quad \rightsquigarrow \quad z^{(3)} = z^{(n)} + \Delta z^{(3)}$$

$$\Delta z^{(4)} = \Delta t \frac{dz}{dt}|_{z=z^{(3)}}$$

$$z^{(n+1)} = z^{(n)} + \frac{1}{6}(\Delta z^{(1)} + 2\Delta z^{(2)} + 2\Delta z^{(3)} + \Delta z^{(4)})$$

The instantaneous velocity $\frac{dz}{dt}$ of each vortex is obtained from equation (5.6).

Because the computational effort at every time-step scales with N^2, where N is the number of point vortices in the flowfield, we reduce N by merging adjacent vortices. This is done, if the vortices are far enough from the trailing edge (typically one chord length), and if they have the same sign (if two vortices of opposite signs are replaced

by a single vortex, the latter will lie outside the segment joining the centres of the two vortices). The single vortex that replaces the two adjacent vortices has circulation $\Gamma_c = \Gamma_j + \Gamma_{j+1}$ and is placed at the centroid:

$$z_c = \frac{\Gamma_j z_j + \Gamma_{j+1} z_{j+1}}{z_j + z_{j+1}}$$

Chapter 6

The influence of reduced frequency, strength of flow unsteadiness, and ellipse slenderness on unsteady separation

6.1 Comparison between theoretical predictions and experiment

Mathioulakis and Telionis (1989) studied experimentally the phenomenon of unsteady separation. They considered the laminar, pulsating flow over an ellipse of slenderness 1 : 2.96 at an angle of attack 14^0. The farfield velocity was oscillating in magnitude but not in direction about a nonvanishing mean:

$$U_\infty = \overline{U}_\infty(1 + 0.05\cos(\omega t)) \tag{6.1}$$

They obtained two-component LDV measurements in the two separation regions, the two free shear layers, and the stagnation region. They presented both time-averaged and ensemble-averaged velocity measurements. The amplitude of the free-stream oscillation wass 5% of the mean value ($\epsilon = 0.05$), and the Reynolds number was 14300. In laminar flow, the location of the separation point, expressed in ***nondimensional variables***, does

not depend on the Reynolds number, because the Reynolds number does not appear in the corresponding boundary layer equations. But since the y-variable is scaled by the inverse square root of the Reynolds number, the latter determines how far from the wall the separation point is situated.

This situation presents us with an opportunity to test our separation criterion. The reduced frequency was 0.91. This value is out of the range of reduced frequency values for which our theory (based on the assumption $\lambda^2 \gg 1$) is valid. On the other hand, this value of reduced frequency lies in the intermediate range (usually taken as $0.05 < \lambda^2 < 5$), where high frequency and quasi-steady approximations may overlap. We applied our theory to this example for two reasons: (a) to the author's best knowledge it is the only set of experimental data available in the literature that are relevant the problem under consideration, and (b) we wanted to investigate whether our theory, developed for high-frequency unsteady flows, could be used to predict separation in a flow that has a dual character: unsteady and quasi-steady.

Our theory predicts that the pressure-side flow separates very close to the steady separation location. On the pressure-side of the ellipse, the amplitude of the separation point oscillation and the displacement of the mean separation location downstream of the steady separation location are so small that, for all practical purposes, the separation point can be considered fixed at the steady separation location. This is exactly what Mathioulakis and Telionis (1989) saw in their experiment. They noted that "the periodic character of the separation phenomenon on the pressure-side can barely be detected. For all practical purposes the flow is almost steady, only a little affected by the periodic pulsations of the free stream or the flapping of the free shear layer on the suction-side

of the body. The average unsteady profiles also differ marginally from their steady-flow counterparts." Our calculation locates pressure-side separation at $x/c = 0.467$. The mean velocity profiles in figure 16 of the above reference, show that indeed the boundary layer thickness increases sharply between the measuring stations located at $x/c = 0.450$ and $x/c = 0.475$ (in terms of the coordinates that the experimentalists use, these measuring stations are $x/a = 1.90$ and $x/a = 1.95$ ($a = c/2$ and their ellipse was placed between $x/a = 0$ and $x/a = 2$).

Two factors combine to yield this almost steady character of pressure-side separation:

- The sharp increase in the mean pressure gradient near the trailing edge causes the flow to separate at a short distance downstream of the pressure minimum for both steady and unsteady flows. Figure 6.2 shows the mean pressure coefficient distribution on the pressure-side of the ellipse, as calculated by our method.

- The difference in phase between the two components of the unsteady velocity at the pressure-side separation location: the one due to the oncoming stream, and the one induced by the wake, causes their sum to oscllate with an amplitude which is smaller than the amplitude of each component (see figure 6.3).

Since the pressure-side separation point hardly moves, the amplitude and the phase of the unsteady part of the circulation is controlled by the motion of the suction-side separation point. In figure 6.4 we plot the trajectory of the suction-side separation point during an oscillation cycle as predicted by the unsteady separation criterion of section 4.2. The chord of the ellipse is the unit length for both x and y axes. The ellipse lies

between $x = -0.5$ and $x = 0.5$. We indicate the location of the separation point at four instances (t= T/4, T/2, 3T/4, T). We also plot the steady separation point on the surface of the ellipse.

In figure 6.5 we have rescaled the y axis by using the "Prandtl layer thickness" $\delta_p = \frac{c}{\sqrt{Re}}$ (see also sections 2.1 and 2.2) as the unit length of the normal axis. Of course, δ_p does not represent the actual thickness of the boundary layer, but only the length scale over which y-variations in the boundary layer velocity are of the the same order as the velocity itself. In that figure, the surface of the ellipse is at $y = 0$.

The main conclusions that Mathioulakis and Telionis drew, are the following:

- The mean position of separation in unsteady flow is located downstream of that for steady flow. Our theory predicts that the mean position of separation is about $x/c = -0.20$, downstream of the steady separation location at $x/c = -0.265$. To explain this behaviour, we refer the reader to the analysis of section 2.6, where we show that by adding the time-mean second order component of the "Prandtl velocity" to the "basic flow", we effectively clip a portion of height $h(x)/\lambda^2$ from the "basic flow" profile. In other words, the steady streaming decreases the displacement thickness of the "basic flow" and makes the mean "Prandtl flow" more energetic than the "basic flow". This causes the zero-skin-friction point to appear downstream of the steady separation point and the mean location of the unsteady separation point to appear even further downstream. The mean location of the suction-side separation together with the mean position of the pressure-side separation determine the mean value of the ellipse circulation $\overline{\Gamma}$.

- Decelaration of the free-stream results in a thickening of the reversed-flow region and in a small upstream excursion of the separation point. Indeed, as figure 6.5 indicates, the separation point between t=0 and t=T/2 moves upstream. The opposite happens when the flow accelerates. The direction of the motion of the suction-side separation point controls the phase of the oscillating part of the ellipse circulation $\tilde{\Gamma}(t)$ (the time-mean value, the amplitude, and the phase of the circulation will be given later in this section).

- The experiments show that the amplitude of the excursion of the zero-skin-friction point is approximately 5% of the chord. The experimentalists note: "A more pronounced periodic disturbance can be observed in the deviations of the separation line. This can be more clearly seen by observing the thickness of the reverse-flow region in the most downstream (measuring) stations (in the suction-side separation region)." Our calculation shows that the amplitude of the excursion of the separation point is approximately 7% of the chord. In our calculation we find that the skin friction $\tau = \tau_{p,w}/\tau_f$ (see section 4.1), measured at the instantaneous location of separation, ranges from -0.06 to -0.03. τ is the skin friction of the lowest order component of the "Prandtl" velocity (the "basic flow") and does not exhibit the large oscillations of the "Stokes" skin friction (see section 3.1). It is approximately the mean skin friction to accuracy $O(\frac{1}{\lambda})$ (in $\overline{\tau_w}$ the term next in order is $\overline{\tau}_{s,2,w}$ (see the opening paragraphs of section 3.1)). Therefore, the point of zero skin friction follows closely the motion of the separation point, is situated upstream from it, and oscillates with a smaller amplitude than the latter (if the wall stress at the instantaneous separation location were approximately constant,

we would have expected the amplitudes of the two motions to be approximately equal, but in the calclulation it varies between $-0.06 < r < -0.03$).

The experiment locates the steady stagnation point at $x/c = -0.480$, our calculation at $x/c = -0.480$ (the circulation that renders the trailing edge a stagnation point yields a forward stagnation point at $x/c = -0.441$). The steady value of the non-dimensional circulation is $\frac{\Gamma_{\text{Howarth}}}{cU_\infty} = 0.15$. In unsteady flow, our calculation shows that the stagnation point shifts in the mean to $x/c = -0.4795$ (figure 6.7). Figure (6.6) is taken from Mathioulakis and Telionis; it shows the instantaneous velocity vectors at $t = T$ (vectors with tips $\times$), and at $t = T/2$ (vectors with tips $\triangle$), in the stagnation region. The boundary layer thickness in this region is very small, and for that reason, no measurements inside the boundary layer were possible. As the normal velocity decelerates approaching the wall, the velocity parallel to the wall varies linearly with distance from the stagnation point, as the theory of potential flow near a stagnation point predicts (for analysis of the steady flow toward a stagnation point at a rigid boundary, including the vorticity layer on the wall, see Batchelor, p.p. 285-289). By inspecting the velocity vectors (their differences are very small) we conclude that the intantaneous position of the separation point at $t = T$ and $t = T/2$ is approximately $x/c = -0.48$ (note the difference in the scale of the x-axis, explained in the caption). According to figure 6.7 the calculated stagnation location at these two instances is $x/c = -0.4783$ and $x/c = -0.4790$. That figure also indicates that if measurements were taken at the instances $t = T/4$ and $t = 3T/4$ the difference in the velocity vectors would have been more substantial.

The position of the stagnation point controls the circulation about the ellipse. Our calculations show that when the suction-side separation point moves upstream, the stagnation point moves upstream (see figure 6.7). To explain this trend, let us recall equation (5.2) (A and B are the suction- and pressure-side separation points, respectively):

$$\frac{d\Gamma}{dt} = \frac{1}{2}u_A^2 - u_A u_{\text{sep,A}} - \frac{1}{2}u_B^2 + u_B u_{\text{sep,B}}$$

Since the pressure-side separation point for all practical purposes remains still, $u_{\text{sep,B}} \approx 0$. Now consider the two instances $t_1 \approx T/8$ and $t_1 \approx T/8 + T/2$, when the suction-side separation point is stationary. At these instances, the circulation is stationary, $\frac{d\Gamma}{dt} = 0$ (see figure 6.8). Then the above equation yields:

$$\begin{aligned} u_A(t_1) &= u_B(t_1) \\ u_A(t_2) &= u_B(t_2) \end{aligned} \tag{6.2}$$

Since A has moved upstream in the time $t_2 - t_1$, $u_A(t_2) > u_A(t_1)$. The system 6.2 can be satisfied only if the circulation decreases in the interval $t_2 - t_1$ so that $u_B(t_2) > u_B(t_1)$ (since B does not move, changes in u_B are caused by changes in circulation only). Because of periodicity, the opposite must happen in the other half of the period. Therefore, at $t_1 = T/8$ the circulation has a maximum. At times $T/8 < t < T/8 + T/2$ the circulation decreases and the stagnation point moves upstream.

The non-dimensional circulation predicted by our interactive calculation as described in section 6.1 is (see also figure 6.8):

$$\frac{\Gamma}{c\overline{U}_\infty} = 0.19 + 0.06\cos(\omega t - 40\frac{2\pi}{360})$$

Although the experimentalists note that "during deceleration and acceleration of the oncoming stream, the stagnation point is displaced downstream and upstream, respec-

tively", as our calculation predicts (see figure 6.7), they do not present any data to support this conclusion. To measure the instantaneous stagnation location, and thus infer how the circulation varies with time, one needs much greater accuracy than the accuracy of their experiment. Two consecutive measurement locations were a distance $\Delta x/c = 0.04$ apart, whereas the calculated excursion of the stagnation point was $\Delta x/c \approx 0.03$.

Very small changes in the location of the stagnation point correspond to large changes in the circulation. If we ignore the wake and perform a calculation in which the stagnation location is determined only from the oncoming flow and the circulation, we find that when the non-dimensional circulation changes from $\frac{\Gamma}{cU_\infty} = 0.13$ to 0.19 to 0.25, the stagnation point moves from $x/c = -0.481$ to -0.479 to -0.477. A way of inreasing accuracy would be to take measurements along lines that are not normal to the surface of the ellipse. Then, by finding one point where the velocity parallel to the wall is zero we could find the stagnation point on the ellipse: it would be the trace of the normal to the surface of the ellipse drawn from the above measuring point (because in two-dimensional flow toward a stagnation point, $u = kx$ and $v = -ky$ outside the vortical layer, thus $u = 0$ yields the abscissa of the stagnation point, see Batchelor, p.p. 285-289).

In conclusion, our results compare well with the experimental observations. This suggests that we may be able to effectively predict unsteady separation in the intermediate range of the reduced frequency, although the assumption of high reduced frequency, which is required to justify the model of quasi-independent "Stokes" and "Prandtl" components of the boundary layer velocity field, is violated. We believe that this is

because the key physical features brought out in the analysis of chapter 2 probably hold up relatively well even when the two velocity distributions are not distinct in the formal sence.

In order to test the accuracy of the separation criterion in the range of high reduced frequencies, we need experimental results at high reduced frequencies. In the following sections we test the criterion against established results in the limits of:

- vanishing unsteadiness
- very high reduced frequency
- very thin ellipse

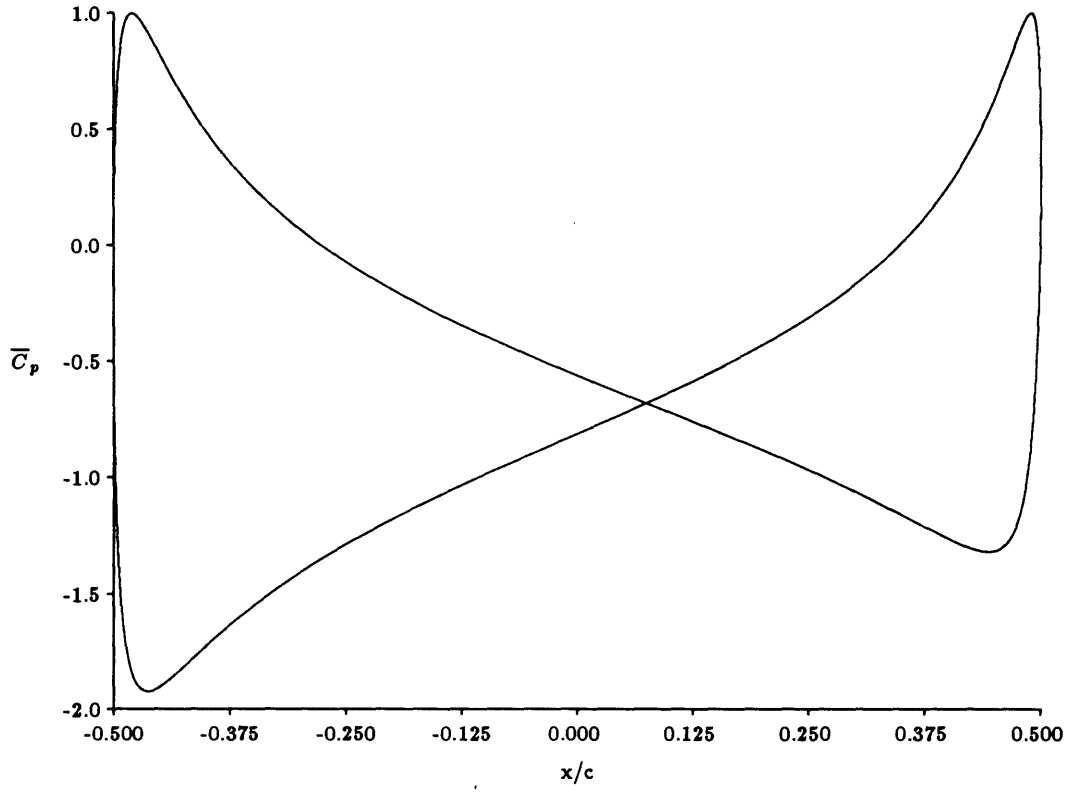

Figure 6.1: Calculated distribution of the mean pressure coefficient on the ellipse used by Mathioulakis and Telionis (1989) in their experiment.

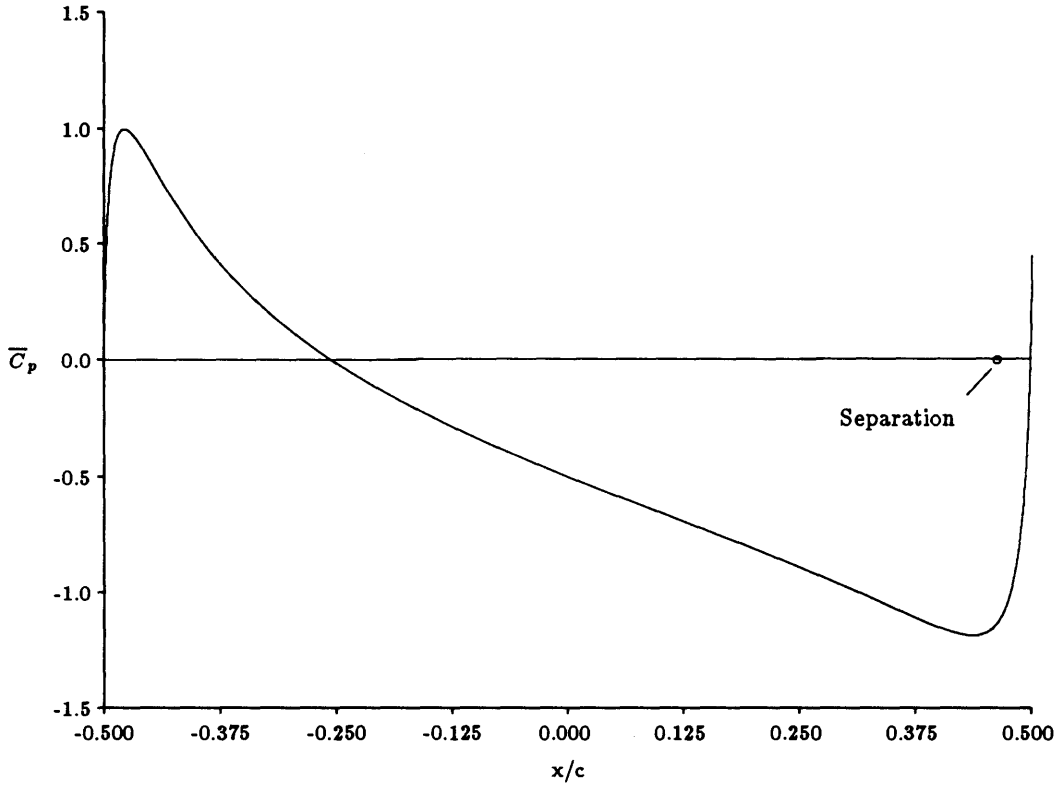

Figure 6.2: Unsteady separation on the pressure side of the ellipse occurs as the pressure begins to rise sharply near the trailing edge. The calculation indicates that for all practical purposes, the separation point can be considered fixed at the steady separation location, indicated on this plot of the mean pressure coefficient on the pressure side of the ellipse.

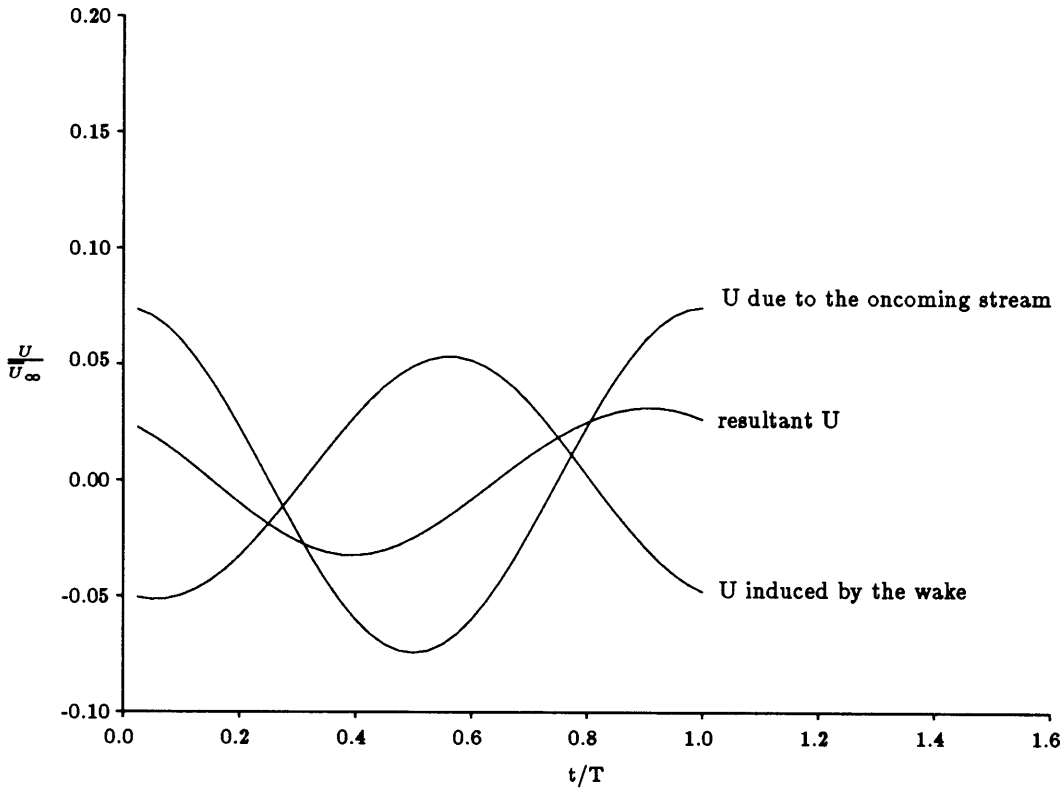

Figure 6.3: At the location of pressure-side separation the phase difference between the component of the external velocity due to the oncoming stream and that induced by the wake decreases the amplitude of the external velocity (calculated values).

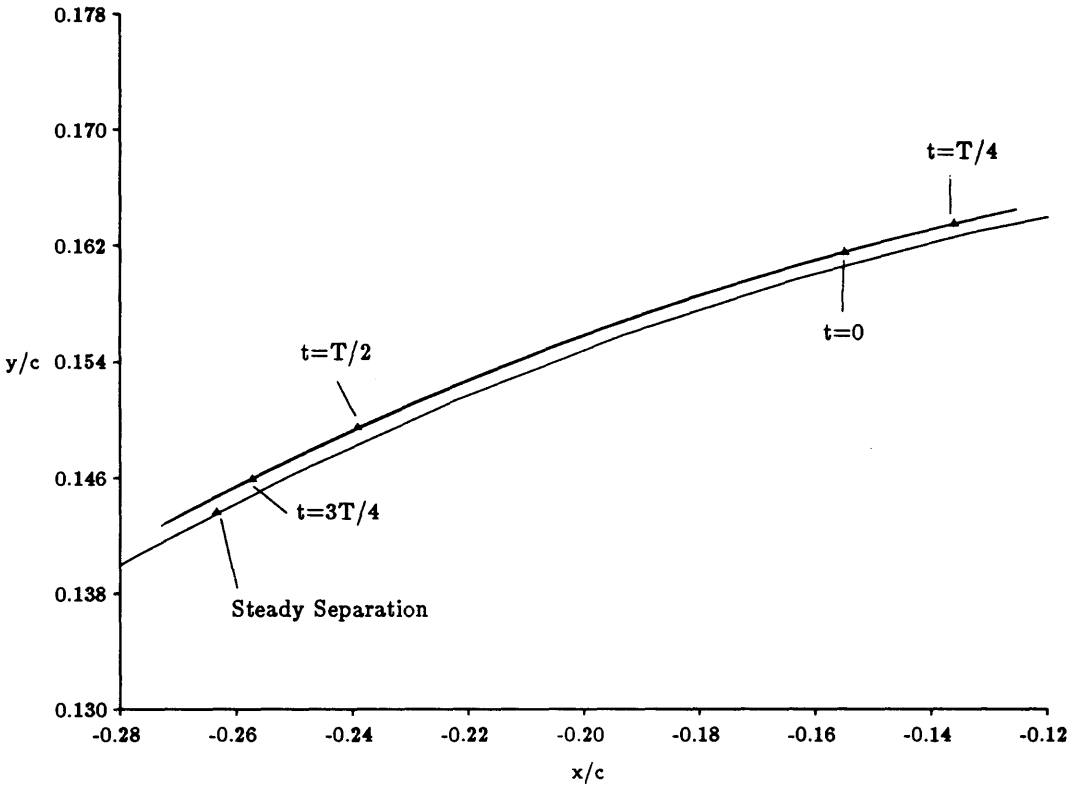

Figure 6.4: Computed trajectory of the suction-side separation point during an oscillation cycle in the ellipse coordinate system. The leading edge of the ellipse is located $x/c = -0.5$, the trailing edge at $x/c = 0.5$.

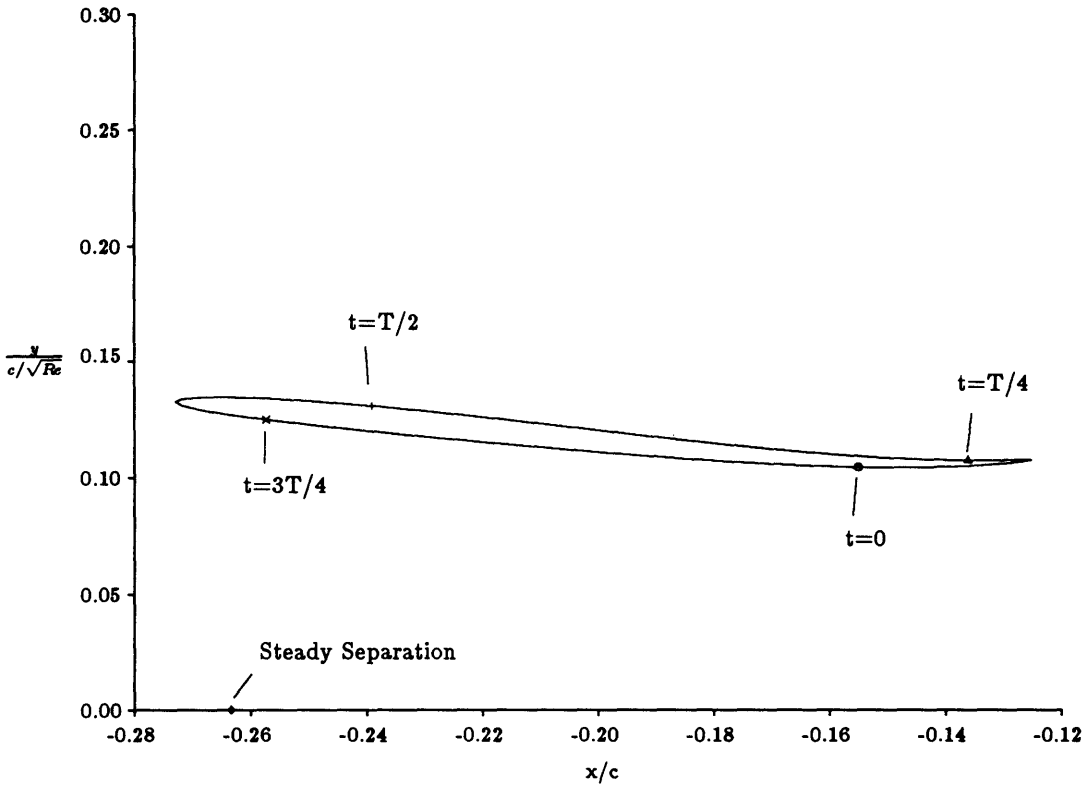

Figure 6.5: Computed trajectory of the suction-side separation point during an oscillation cycle. The leading edge of the ellipse is located $x/c = -0.5$, the trailing edge at $x/c = 0.5$. Note that the y coordinate is scaled by δ_p and thus greatly exaggerated.

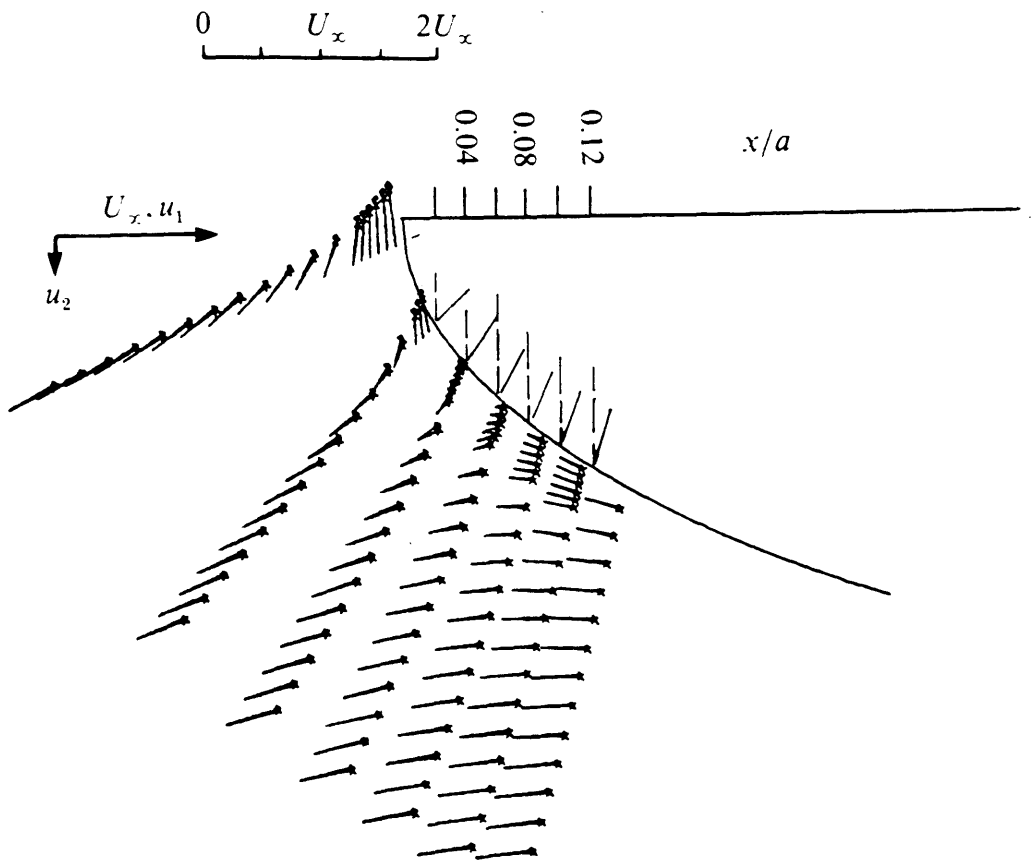

Figure 6.6: Measured unsteady velocity vectors near the stagnation point ($\times, t = T; \Delta, t = T/2$) (from Mathioulakis and Telionis, 1989). Note that $a = c/2$, and their ellipse is placed between $0 < x/a < 2$; therefore the locations $x/a = 0.04, 0.08$ correspond to $x/c = -0.48, -0.46$ in our coordinate system.

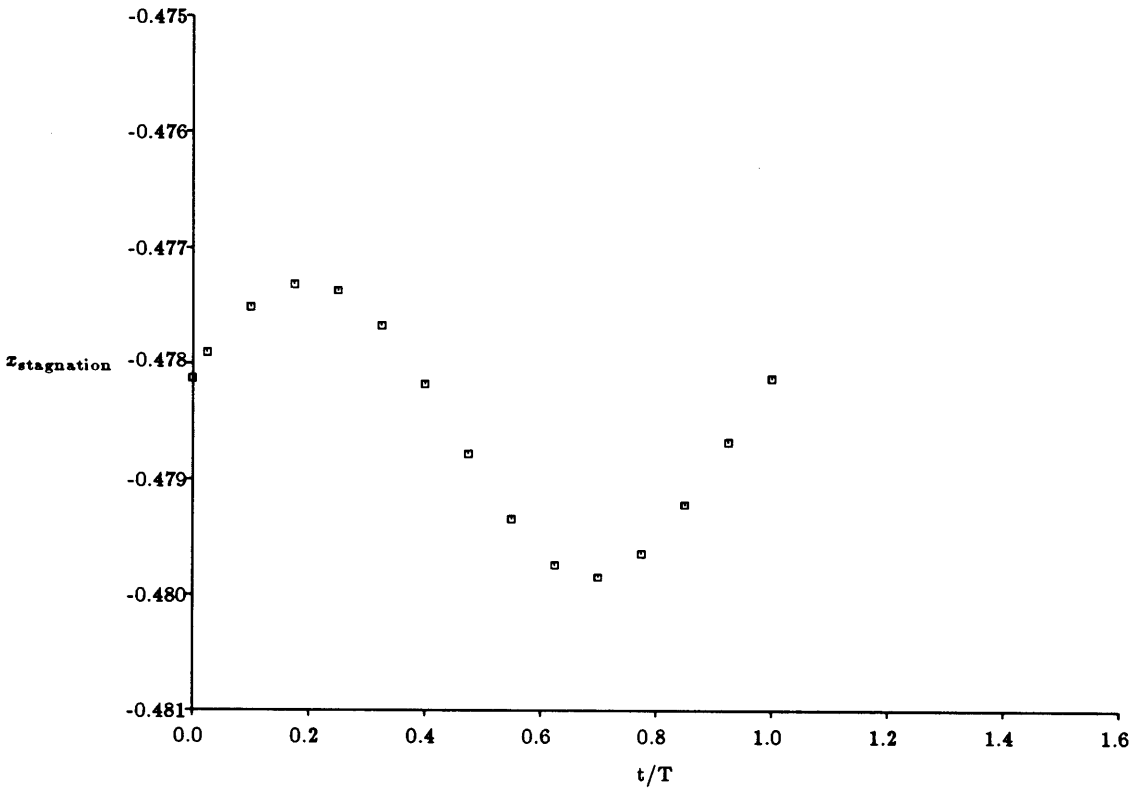

Figure 6.7: Calculated location of the stagnation point within one period.

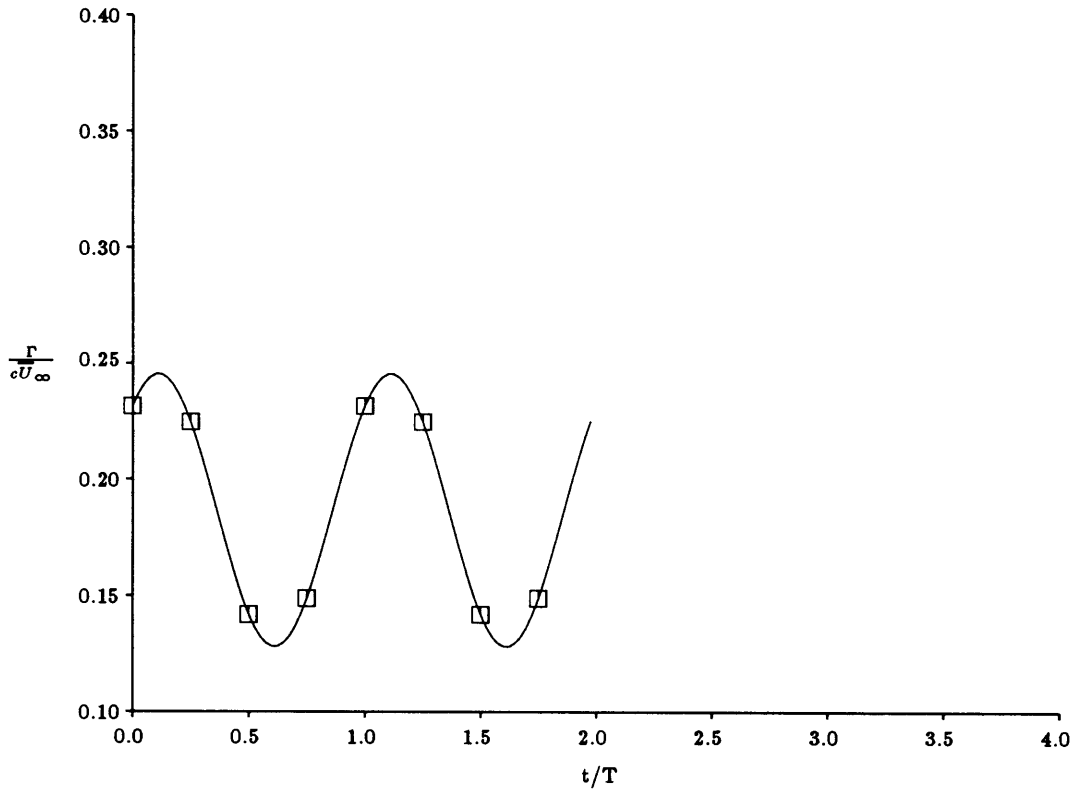

Figure 6.8: Calculated ellipse circulation.

6.2 The influence of the strength of the unsteadiness on unsteady separation

We now apply our theory to the oscillating flow past an ellipse of slenderness 1:20 at zero angle of attack. In the following examples, we keep the reduced frequency constant, $\lambda^2 = 9$, and vary the strength of unsteadiness (the ratio of the amplitude of the oscillating far-field velocity to its time-mean value $\epsilon = \frac{\widehat{U}_\infty}{U_\infty}$, as in equation (6.1)).

The results presented in the present as well as in the following sections, include one common test case, that with $\lambda^2 = 9, \epsilon = 0.04$. We chose this value of the reduced frequency, because it is close to the frequency of rotor-stator interactions in turbomachinery (see section 1.1). The strength of the unsteadiness was chosen to be close to that selected by Mathioulakis and Telionis. It represents a value easily attainable in an experiment (as we have noted in section 2.1, our analysis is nonlinear and not restricted to small amplitudes of oscillation). In figure 6.9 we plot the trajectory which the separation point describes during a period, for this test case. The position of the separation point at four instances (t=0, T/4, T/2, 3T/4) is marked on this plot. The separation location is plotted in nondimensional coordinates x^* and y^* (defined in section 2.3) as it is obtained from the application of the unsteady separation criterion; x^* measures the distance along the contour of the ellipse, whereas $y^* = \frac{y}{c/\sqrt{R\,e}}$ normal to it.

In figure 6.10 we plot the separation trajectory using a coordinate system in which the unit length on both the x and the y axes is the chord of the ellipse.

In figure 6.11 we plot the trajectories of the separation point during an oscillation

cycle for $\epsilon = 0.001, 0.005$, and 0.01. The x and y axes are scaled by the chord of the ellipse, c. We have zoomed in the neighbourhood of the steady separation point in order to distinguish between the three trajectories (notice that the ordinate y spans a distance $0.0018c$). The trailing edge of the ellipse is at $x/c = 0.5$. As the strength of the unsteadiness diminishes, the separation trajectory shrinks and moves toward the location of steady separation. For $\epsilon = 0$ the calculation yields $x = x_{\text{steady separation}}, y = 0, \tau = 0$, as it should.

In figure 6.12 we plot the separation trajectories for $\epsilon = 0.01, 0.02, 0.04$. The amplitude of the excursion of the separation point scales with the strength of the unsteadiness. In the following section we present an explanation for this behaviour as the reduced frequency becomes very large.

We note that the entire separation trajectory lies downstream of the steady separation location. As the strength of the unsteadiness increases, the scaled skin friction τ, decreases from $\tau = -0.001$ to $\tau = -0.05$.

The computation requires an initial guess for the time evolution of the two unknowns: $x(t), \tau(t)$. If the initial guess is far from the solution, the algorithm fails to converge. When we want to calculate the separation trajectory for a relatively large value of ϵ (or, as we will see in the next section, for a value of λ^2 that is not very large), we obtain an educated guess by starting from a small value of the strength of the unsteadiness (or a very large value of the reduced frequency, respectively) and moving towards the desired value.

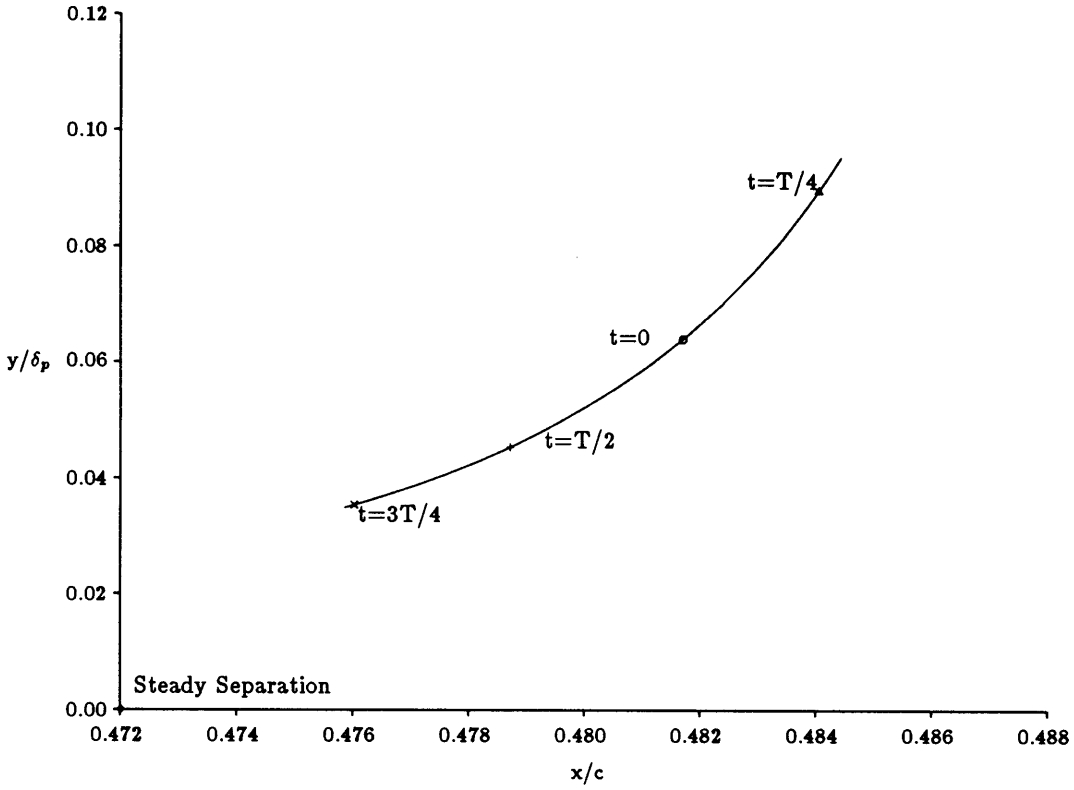

Figure 6.9: Separation trajectory and the position of the separation point at four instances within one period in nondimensional coordinates ($\alpha = 0^0, \lambda^2 = 9, \epsilon = 0.04$). The trailing edge of the ellipse is at $x/c = 0.5$. The steady separation position is $x/c = 0.472$.

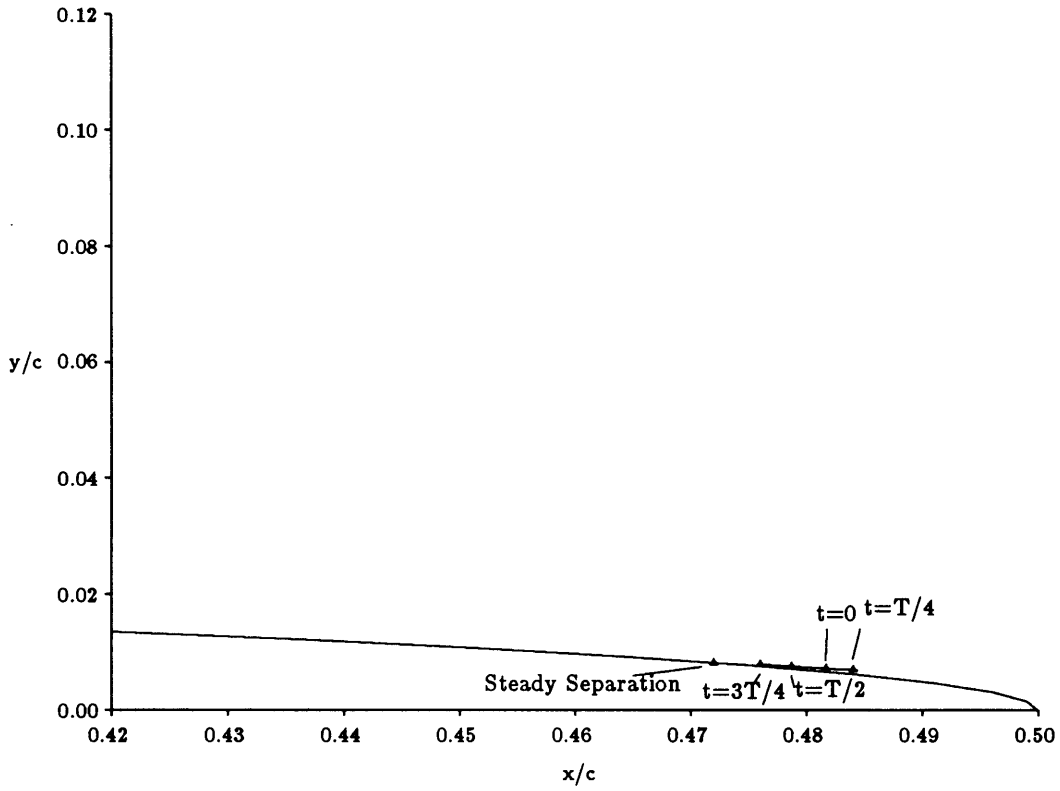

Figure 6.10: The separation trajectory in the ellipse coordinate system.

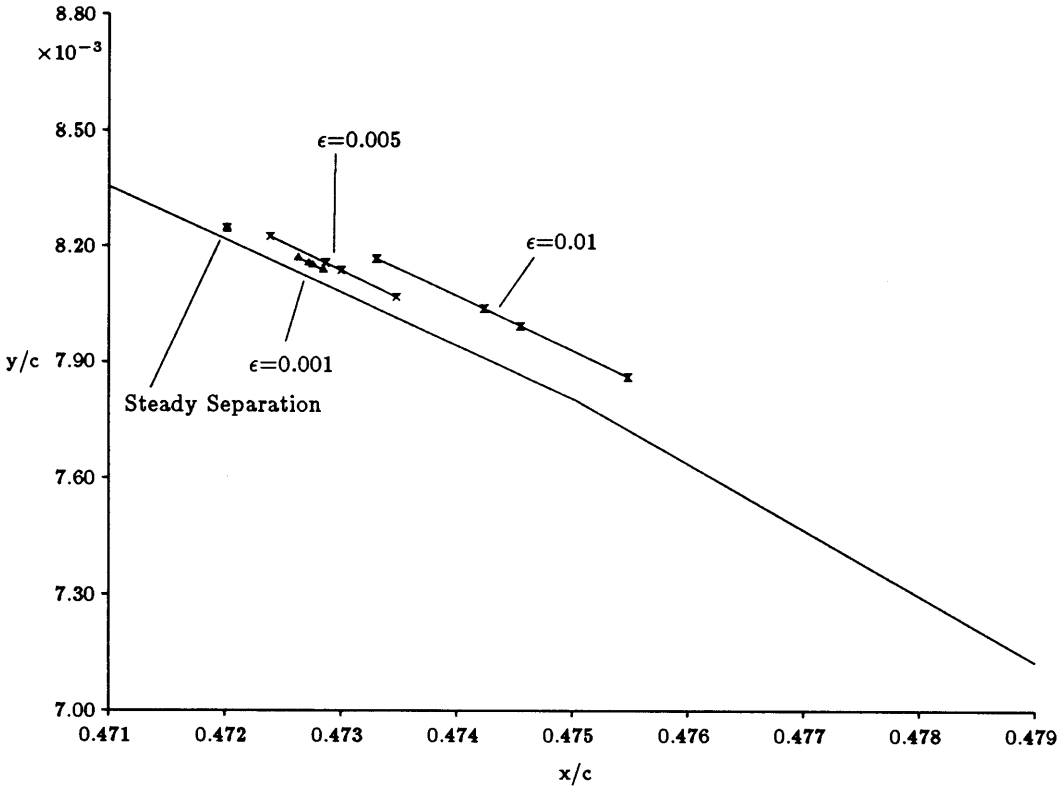

Figure 6.11: The separation trajectory for varying strength of flow unsteadiness, $\epsilon = 0.001, 0.005, 0.01$, and constant reduced frequency, $\lambda^2 = 9$. The separation trajectory shrinks and approaches the location of steady separation as ϵ approaches zero.

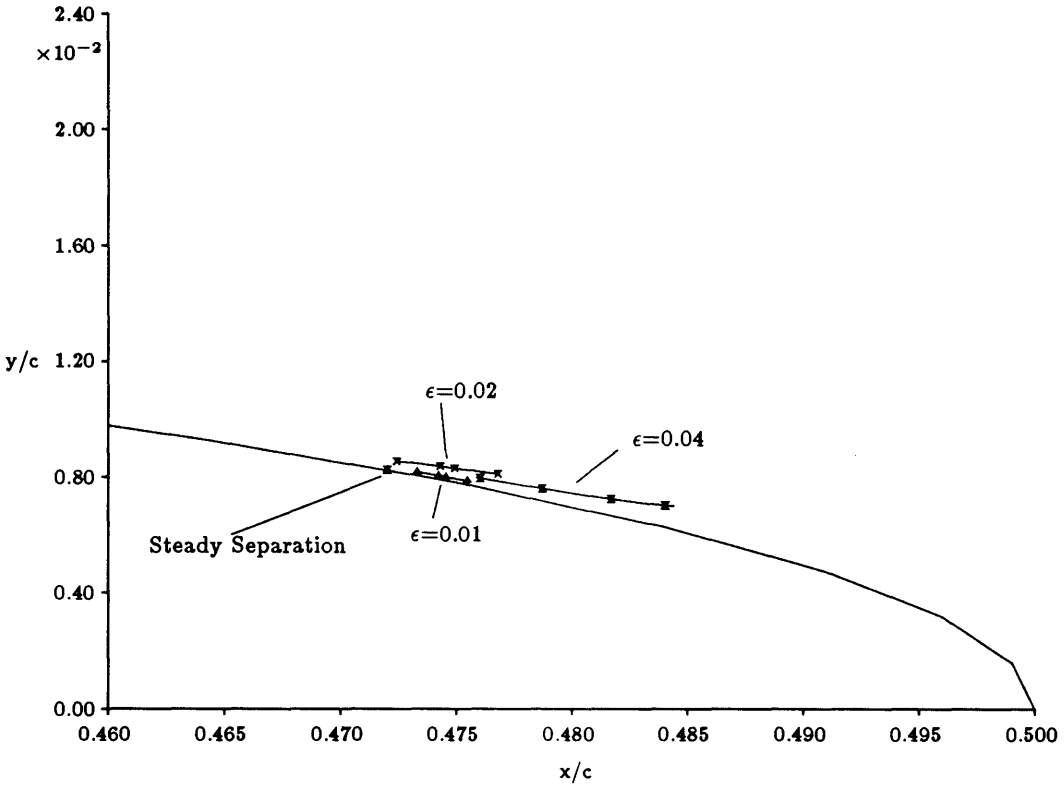

Figure 6.12: The separation trajectory for varying strength of flow unsteadiness, $\epsilon = 0.01, 0.02, 0.04$, and constant reduced frequency, $\lambda^2 = 9$. The amplitude of the separation point excursion scales with ϵ.

6.3 The influence of the reduced frequency on unsteady separation

In the unsteady flow past the ellipse of the previous section, we keep the strength of the unsteadiness constant, $\epsilon = 0.04$ and vary the reduced frequency in the range, $\lambda^2 = 9, 18, 36$.

In figure (6.13) we plot the trajectories of the separation point during an oscillation cycle. As the reduced frequency increases, the separation trajectory shrinks and moves toward the location of steady separation. (A case with $\lambda^2 = 500$ showed that the separation trajectory degenerated to the steady separation point.) The "Stokes flow" affects the "Prandtl flow", as we saw in Chapter 2, (a) by displacing the "basic flow" by h/λ^2 (effect of the wall boundary condition), and (b) by transferring momentum within the "Prandtl flow" and thus generating a "Reynolds stress". Both effects are on the order of $1/\lambda^2$ and as the reduced frequency increases, they become weaker. At very high values of the reduced frequency the two flows become decoupled. Then, the "Prandtl flow" is steady and separates as such.

When the reduced frequency is high, y_{sep} becomes approximately zero, and since $u_p^*(x, y = 0, t) \sim 1/\lambda^2$ is very small, the second condition for unsteady separation (in non-dimensional variables):

$$u_p^*(x_{\text{sep}}^*, y_{\text{sep}}^*, t^*) + \widetilde{U^*} - \lambda^2 \frac{dx_{\text{sep}}^*}{dt^*} = 0$$

yields:

$$\frac{dx_{\text{sep}}^*}{dt^*} \approx \frac{\widetilde{U^*}}{\lambda^2} \approx \frac{\epsilon \overline{U^*} \cos(t^*)}{\lambda^2}$$

This explains why the amplitude of the separation point excursion scales with the strength of the unsteadiness and the inverse of the reduced frequency.

Since in the limit of quasi-steady flow, $\lambda^2 \to 0$, the separation point trajectory also shrinks towards the steady separation point, the distance between the mean position of the separation point and the steady separation location attains a maximum at some reduced frequency (presumably $\lambda^2 \leq 1$). This is the reduced frequency at which the mean circulation is also maximized (see section 7.1; for implications regarding aerodynamic design see section 8.2).

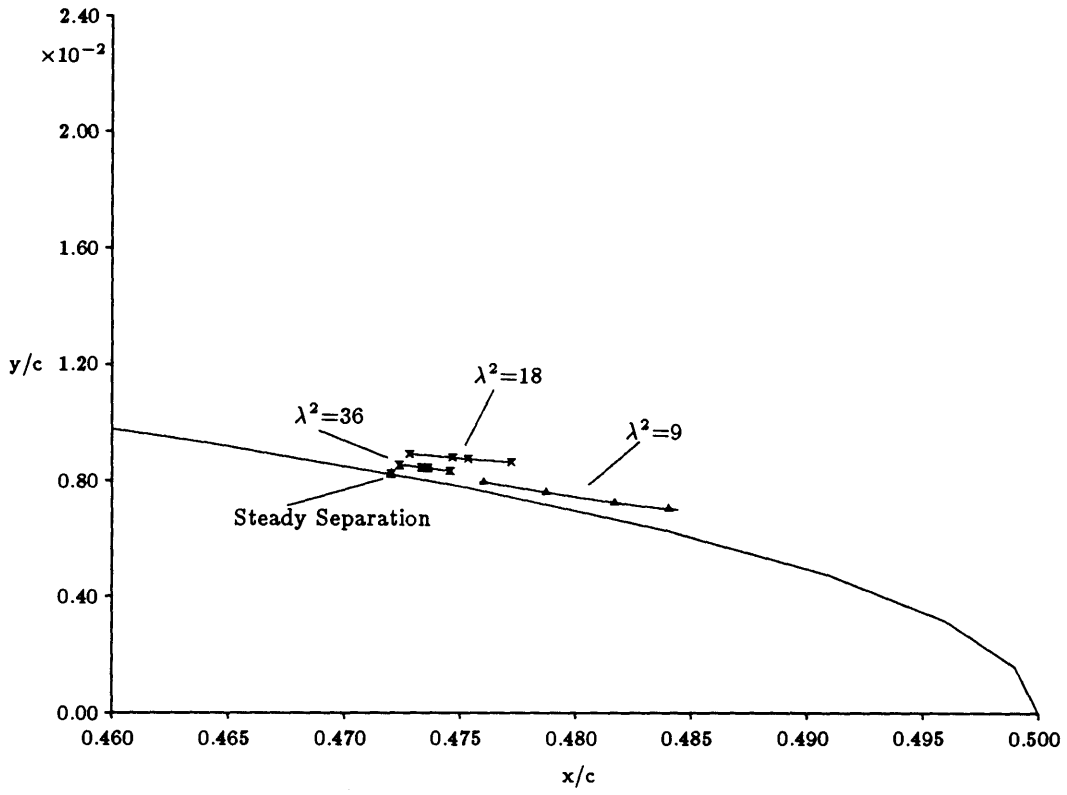

Figure 6.13: The separation trajectory for varying reduced frequency, $\lambda^2 = 9, 18, 36$, and constant strength of flow unsteadiness, $\epsilon = 0.04$. The amplitude of the separation point excursion scales with $1/\lambda^2$.

6.4 The influence of ellipse slenderness on unsteady separation

As the ellipse becomes slimmer the separation trajectory moves towards the trailing edge. In figure 6.14 we plot the separation trajectories for three ellipses with slenderness $b/a = 1:20, 1:30, 1:40$. The strength of the unsteadiness is $\epsilon = 0.04$ and the reduced frequency is $\lambda^2 = 9$ in all cases shown in the figure.

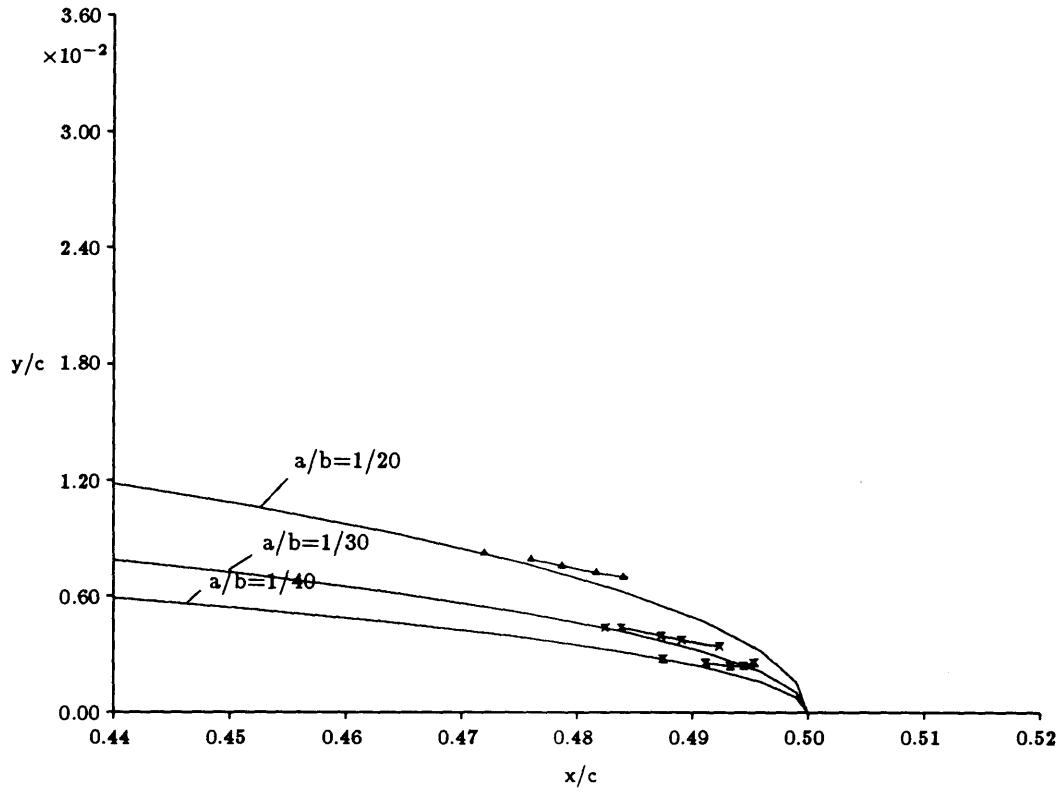

Figure 6.14: The separation trajectory for varying slenderness ratio, $b/a = 1 : 20$, $1 : 30$, $1 : 40$. The reduced frequncy is $\lambda^2 = 9$, and the strength of flow unsteadiness is $\epsilon = 0.04$. The separation trajectory moves towards the trailing edge as the ellipse becomes slimmer.

Chapter 7

A parametric study of the circulation and of the aerodynamic forces acting on an airfoil in unsteady separated flow

In this chapter we study in detail how the circulation, the aerodynamic forces, and the moment respond to changes in parameters that determine:

- the flow geometry i.e. the angle of attack and the slenderness of the ellipse
- the unsteady character of the flow i.e. the reduced frequency and the strength of the unsteadiness

In the calculations that we present, we use the method described in section 5.1, to calculate the interaction between the airfoil and its wake.

First, we examine how the response of the separation point trajectories to changes in the above parameters (as established in the last chapter), determines the properties of the circulation.

7.1 How the separation trajectories influence circulation

Our results indicate that, even at small angles of attack, the pressure-side boundary layer faces a sharply increasing pressure gradient near the trailing edge. In addition, the induction of the wake is out of phase with the oscillatory part of the oncoming stream and reduces the amplitude of the local velocity. These two effects combined, cause the pressure-side boundary layer to separate a short distance downstream of the steady separation location (which lies a short distance downstream of the minimum pressure location). This separation point oscillates with a very small amplitude and can be considered to be fixed with time. Then, it is the motion of the separation point on the suction-side of the ellipse that controls the circulation. In particular:

- The mean location of the suction-side separation point controls the mean value of the circulation $\overline{\Gamma}$. In chapter 6 we have explained why the flow unsteadiness causes the mean position of unsteady separation to lie downstream of the steady separation location. This observation reveals that the mean value of the circulation lies within two bounds:
  - the upper bound is the value of the Kutta circulation Γ_{Kutta}; this is the value of the circulation that causes the trailing edge of the airfoil to be a stagnation point.
  - the lower bound is the value of the circulation, that in steady flow, yields zero net vorticity flux into the wake. As we have mentioned in the introduction, it is found by requiring that the external flow velocities at the locations of steady separation be equal (separation can be located by applying, for

example, Stratford's criterion). In the limit of steady flow, letting in equation (5.2) $\frac{d\Gamma}{dt} = 0$, $u_{\text{sep,A}} = u_{\text{sep,B}} = 0$, we obtain, $u_A = u_B$. Since this method for determining circulation in steady separated flow was first proposed by Howarth (1935), we call this value Γ_{Howarth}.

As the separation point moves in the mean towards the steady separation location or towards the trailing edge, the mean value of circulation approaches Γ_{Howarth} or Γ_{Kutta} respectively.

- The amplitude of the excursion of the suction-side separation point controls the amplitude of the oscillating part of the circulation $\hat{\Gamma}$.

- The direction of the motion of the suction-side separation point controls the phase of the oscillating part of the circulation. As we see in figure 7.1, the time instant $t = T/4$ at which the suction-side separation point turns upstream, corresponds roughly to the maximum value of the circulation Γ. The time instant $t = 3T/4$ at which the suction-side separation point turns downstream corresponds roughly to the minimum value of the circulation Γ.

In the last chapter we found how the separation trajectories respond to changes in the geometry of the airfoil and in the properties of the unsteady flow. Having established the connection between the behaviour of $\Gamma(t)$ and the form of the separation trajectories, we can now predict the behaviour of the circulation in the following cases:

- When the strength of the flow usteadiness ϵ increases, the suction-side separation trajectory is swept towards the trailing edge and its amplitude increases propor-

tionally to ϵ. Then both the mean and the amplitude of the circulation increase (the latter increases proportionally to ϵ).

- When the reduced frequency λ^2 increases, the suction-side separation trajectory moves towards the steady separation point and its amplitude diminishes proportionally to $1/\lambda^2$; therefore, both the mean and the amplitude of the circulation decrease (the latter decreases proportionally to $1/\lambda^2$).

- When the thickness of the ellipse decreases, the suction-side separation trajectory moves towards the trailing edge and its amplitude decreases; thus the mean circulation increases, whereas its amplitude decreases, and both tend to the values predicted by the Kutta condition.

The results that follow verify these predictions.

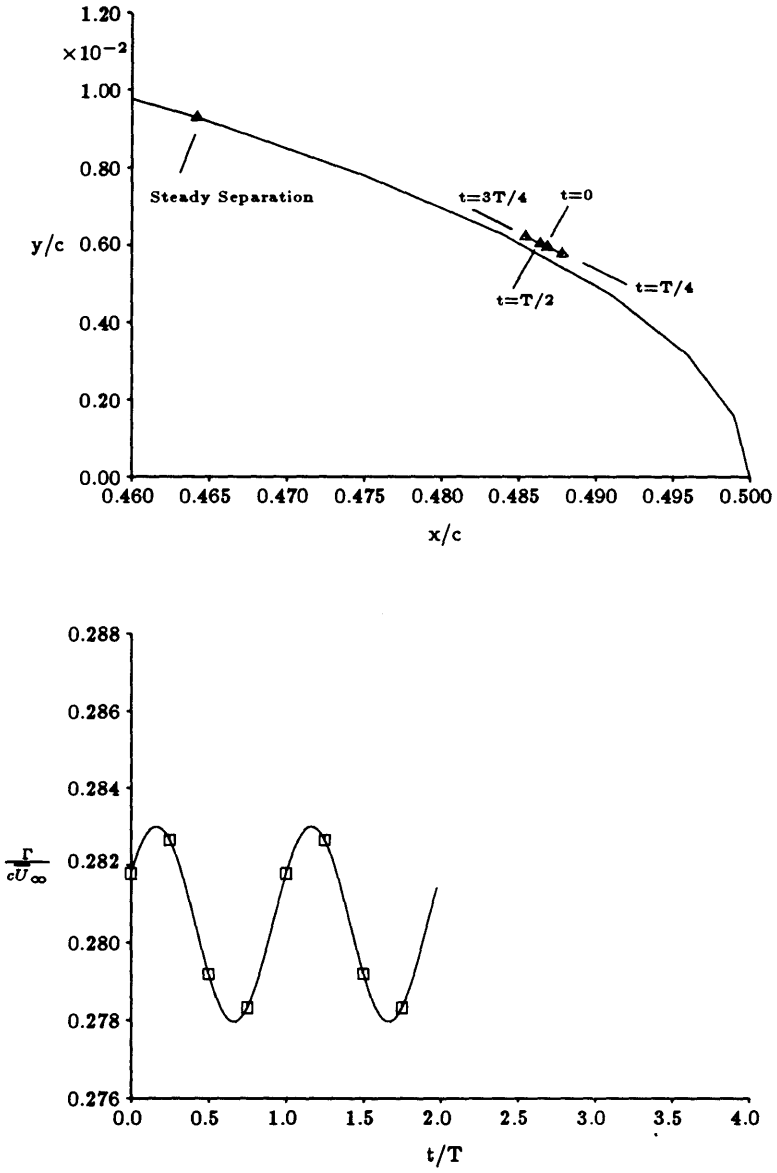

Figure 7.1: The stationary points $t = T/4, /; t = 3T/4$ of the suction-side separation trajectory roughly correspond to the stationary points in $\Gamma^*(t)$. The ellipse $(b/a = 1 : 20)$ is placed at an angle of attack $\alpha = 5^0$ in a stream oscillating with strength $\epsilon = 0.04$ at reduced frequency $\lambda^2 = 9$.

7.2 The time evolution of the aerodynamic forces with varying angle of attack

In this section we describe how the lift and drag change if we place the ellipse of slenderness ratio 1 : 20 in a stream with velocity

$$U_\infty = \overline{U}_\infty(1 + 0.04\cos(\omega t)),$$

and vary the angle of attack in the range $\alpha = 1^0, 3^0, 5^0$.

The separation point on the pressure side of the ellipse oscillates with a very small amplitude, even at the smallest angle of attack considered, and for all practical purposes it can be taken to be fixed at a location which lies downstream of the steady separation position. At the angles of incidence $\alpha = 3^0$ and 5^0 the pressure-side boundary layer faces a very steep adverse pressure gradient and separates a short distance downstream of the location of minimum pressure. At $\alpha = 1^0$ the pressure does not rise as abruptly; in that case, the calculation indicates that the above behaviour is caused by the influence of the wake. At the first iteration, when we use only the oncoming stream to obtain the separation trajectories, we find that the amplitude of the separation point excursion is considerable. When the feedback of the wake is included in the calculation, the separation trajectory shrinks to practically a point. As we have mentioned in section 6.1 the steady character of the flow at the pressure side region is observed in experiment.

In figure (7.2) we present plots of the non-dimensional circulation for three different angles of incidence. From these plots one can determine the instantaneous value of the non-dimensional circulation. The oval encircling the mean value of the non-dimensional

circulation has coordinates $(x, y) = (\text{constant} + \cos(\omega t), \Gamma^*(t))$ and the value of the constant for $\alpha = 1^0, 3^0, 5^0$ is $1, 3, 5$ respectively. We think that this is a convenient way for displaying information on both the angle of attack and the time evolution of the circulation. We observe that $\overline{\Gamma^*}$ is bracketed by the Kutta and the Howarth values of the circulation.

In figures (7.4), (7.4), and (7.5) we plot the lift coefficient, the drag coefficient, and the moment coefficient on the ellipse at different angles of incidence.

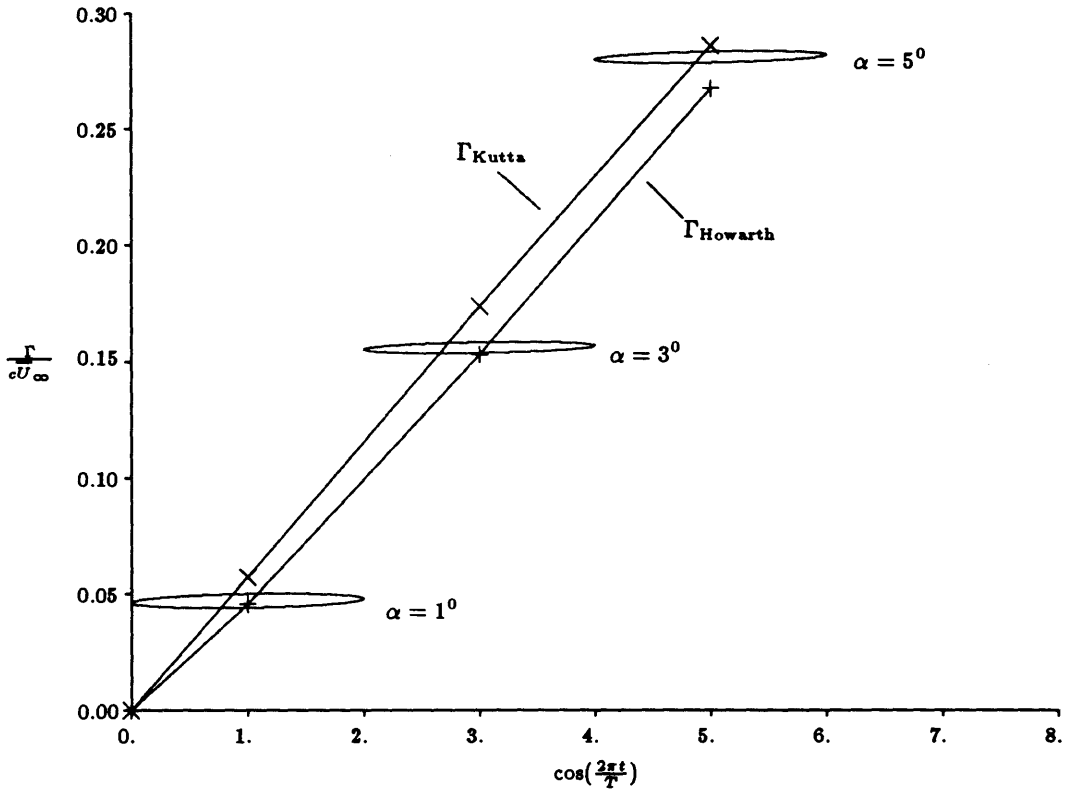

Figure 7.2: Time evolution of the nondimensional circulation around an ellipse $(b/a = 1:20)$ at different angles of attack plotted against $x_0+\cos(\frac{2\pi t}{T})$. For $\alpha = 1^0, 3^0, 5^0$ the centre of the oval is placed at $x_0 = 1,3,5$ respectively. For example, in the case $\alpha = 3^0$, and at the instances $t = 0, T/4, T/2, 3T/4$, the ordinate is $x = 4,3,2,3$ The reduced frequency is $\lambda^2 = 9$, and the strength of the flow unsteadiness is $\epsilon = 0.04$.

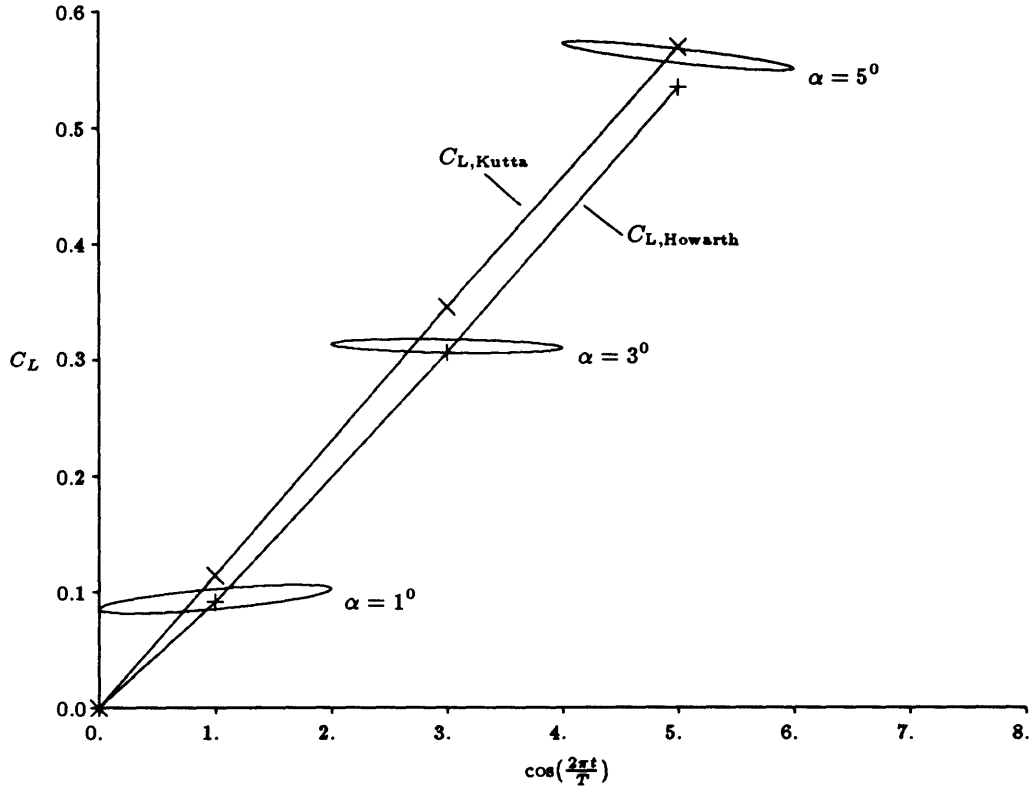

Figure 7.3: Time evolution of the lift coefficient on an ellipse ($b/a = 1 : 20$) at different angles of attack. The reduced frequency is $\lambda^2 = 9$, and the strength of the flow unsteadiness is $\epsilon = 0.04$.

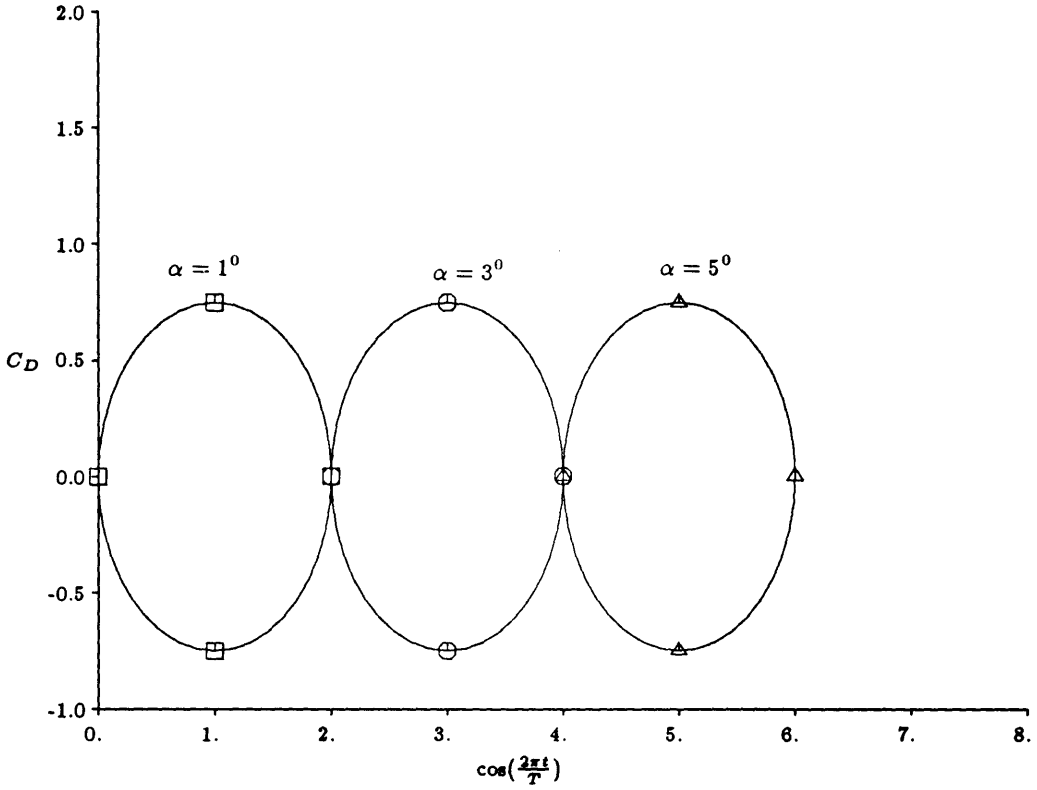

Figure 7.4: Time evolution of the drag coefficient on an ellipse ($b/a = 1 : 20$) at different angles of attack. The reduced frequency is $\lambda^2 = 9$, and the strength of the flow unsteadiness is $\epsilon = 0.04$.

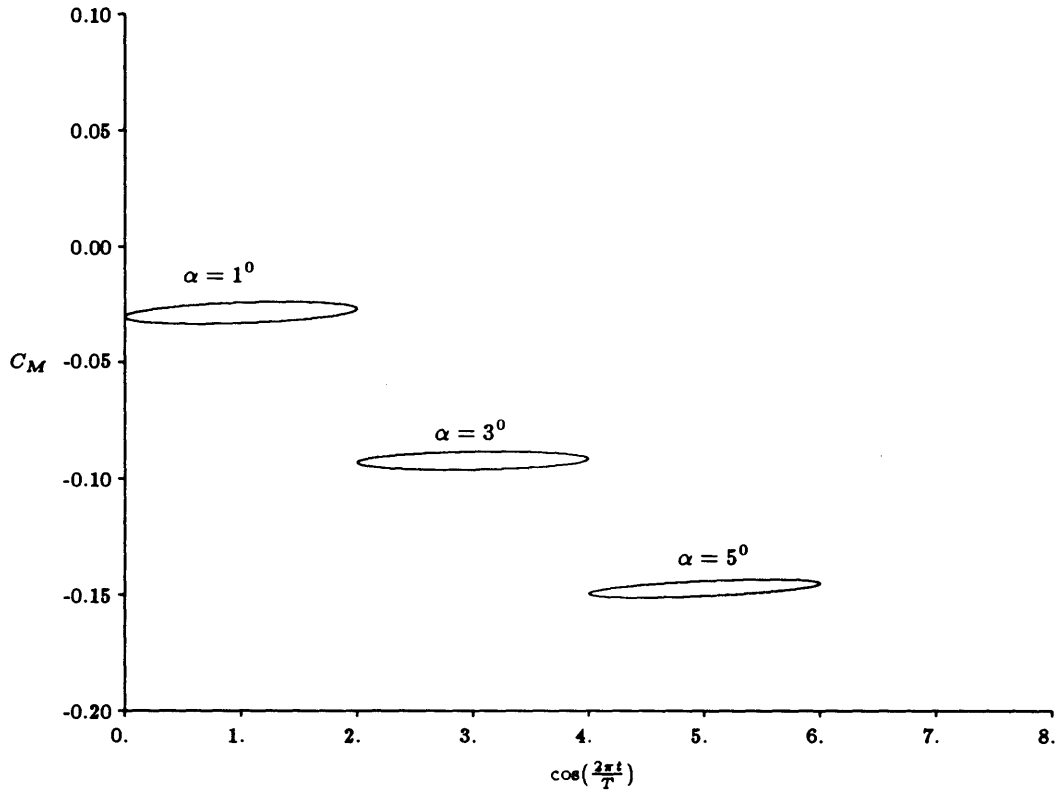

Figure 7.5: Time evolution of the moment coefficient on an ellipse ($b/a = 1 : 20$) at different angles of attack. The reduced frequency is $\lambda^2 = 9$, and the strength of the flow unsteadiness is $\epsilon = 0.04$.

7.3 The influence of the reduced frequency on the aerodynamic forces

In the following we place the ellipse at an angle of attack $\alpha = 5^0$. We keep the strength of the flow unsteadiness constant, $\epsilon = 0.04$, and vary the reduced frequency.

In figure (7.6) we plot the time evolution of the nondimensional circulation for three values of the reduced frequency, $\lambda^2 = 9, 18, 36$. As the reduced frequency increases, the mean value of the circulation decreases because the mean separation location shifts upstream for reasons explained in section 6.3. The circulation amplitude also decreases, because the separation trajectories shrink.

In table 7.1 we compare the amplitude and phase of the circulation predicted (a) by our method and (b) by classical unsteady wing theory, which assumes the Kutta condition. We find that the two methods predict similar trends in the amplitude and phase of circulation, but different actual values. Furthermore, whereas application of the Kutta condition yields constant $\overline{\Gamma}$, the new method predicts that $\overline{\Gamma}$ decreases tending to $\Gamma_{\text{Howarth}} = 0.267$.

Table 7.2 shows that the Kutta condition results are approached systematically by the present method as the ellipse becomes slimmer.

	(a) Kutta Condition			(b) Separation		
λ^2	$\overline{\Gamma}$	$\hat{\Gamma}$	θ_Γ	$\overline{\Gamma}$	$\hat{\Gamma}$	θ_Γ
9	0.288	0.0015	-50^0	0.279	0.003	-46^0
18	0.288	0.001	-52^0	0.272	0.002	-59^0
36	0.288	0.0005	-54^0	0.271	0.001	-65^0

Table 7.1: The circulation $\Gamma(t) = \overline{\Gamma} + \hat{\Gamma}\cos(\omega t + \theta_\Gamma)$ around an ellipse calculated by: (a) assuming smooth flow at the trailing edge and (b) using the new separation criterion, as the reduced frequency increases ($b : a = 1 : 20, \alpha = 5^0, \epsilon = 0.04$). Note that $\overline{\Gamma} \rightarrow \Gamma_{\text{Howarth}} = 0.267$ as the reduced frequency increases.

Slenderness	(a) Kutta Condition			(b) Separation		
Ratio	$\overline{\Gamma}$	$\hat{\Gamma}$	θ_Γ	$\overline{\Gamma}$	$\hat{\Gamma}$	θ_Γ
1:20	0.288	0.0015	-50^0	0.279	0.003	-46^0
1:50	0.279	0.002	-46^0	0.279	0.002	-46^0

Table 7.2: The circulation $\Gamma(t) = \overline{\Gamma} + \hat{\Gamma}\cos(\omega t + \theta_\Gamma)$ around an ellipse calculated by: (a) assuming smooth flow at the trailing edge and (b) using the new separation criterion, as the ellipse becomes slimmer ($\alpha = 5^0, \lambda^2 = 9, \epsilon = 0.04$).

In figure 7.7 we plot the time evolution of the lift coefficient as the reduced frequency increases.

If we compare the change of the circulation amplitude with reduced frequency to the corresponding change of the lift amplitude, we notice a striking difference in the form of response. This is because the lift, apart from a term proportional to Γ, contains a term proportional to $\frac{d\Gamma}{dt}$ which increases, and even dominates (compare the curves corresponding to $\lambda^2 = 18$ and 36), as the reduced frequency increases.

In figure 7.8 we show how the drag coefficient changes as the reduced frequency changes. As we have shown in chapter 5, the drag is the sum of the "buoyancy-like" force, created by the pressure gradient that accelerates the flow, and the "apparent mass" force which acts in the direction of the vector change of the free stream velocity (in our problem the free stream velocity does not change direction and the "apparent mass" force is purely drag, see chapter 5). As expected, the average value of the drag is zero, and its amplitude scales with the reduced frequency.

Finally, in figure 7.9 we plot the time evolution of the moment coefficient for the above values of the reduced frequency. The moment coefficient is negative, tending to stall the ellipse.

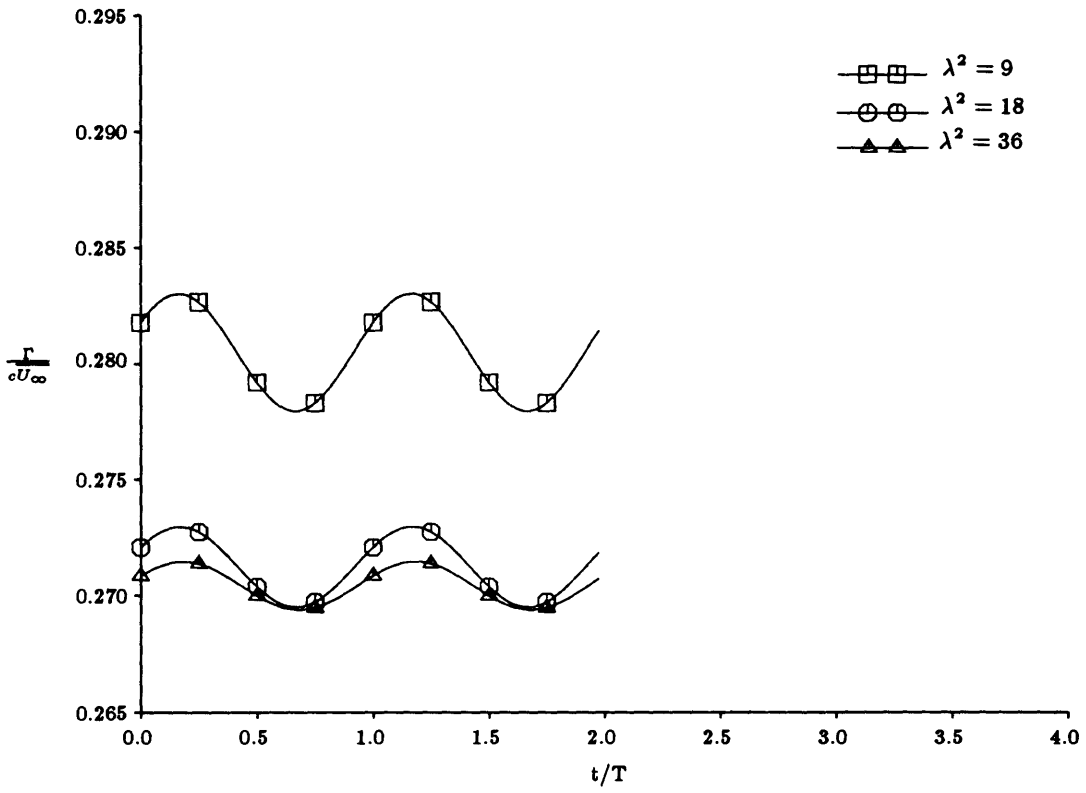

Figure 7.6: Time evolution of the nondimensional circulation for varying reduced frequency ($\lambda^2 = 9, 18, 36$) and constant strength of flow unsteadiness($\epsilon = 0.04$). The circulation is bracketed by $\Gamma_{\text{Kutta}} = 0.283$ and $\Gamma_{\text{Howarth}} = 0.267$. The ellipse ($b/a = 1 : 20$) is at an angle of attack $\alpha = 5^0$.

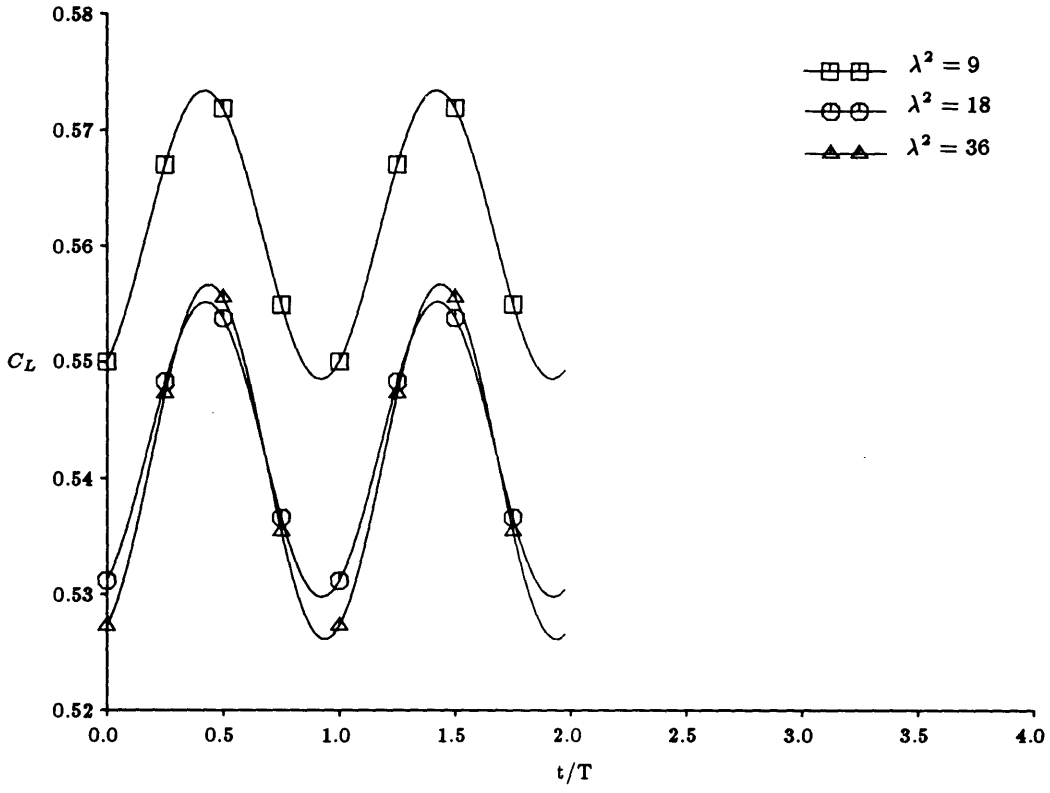

Figure 7.7: Time evolution of the lift coefficient for varying reduced frequency ($\lambda^2 = 9, 18, 36$) and constant strength of flow unsteadiness($\epsilon = 0.04$). The ellipse ($b/a = 1:20$) is at an angle of attack $\alpha = 5^0$.

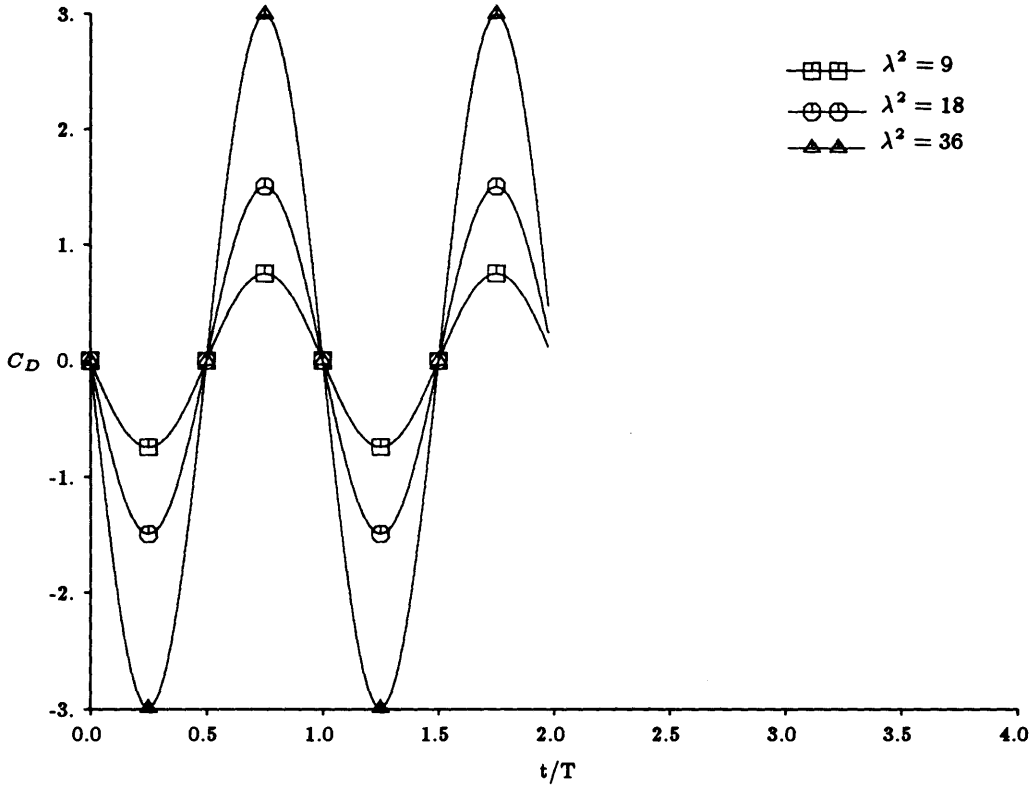

Figure 7.8: Time evolution of the drag coefficient for varying reduced frequency ($\lambda^2 = 9, 18, 36$) and constant strength of flow unsteadiness($\epsilon = 0.04$). The ellipse ($b/a = 1:20$) is at an angle of attack $\alpha = 5^0$.

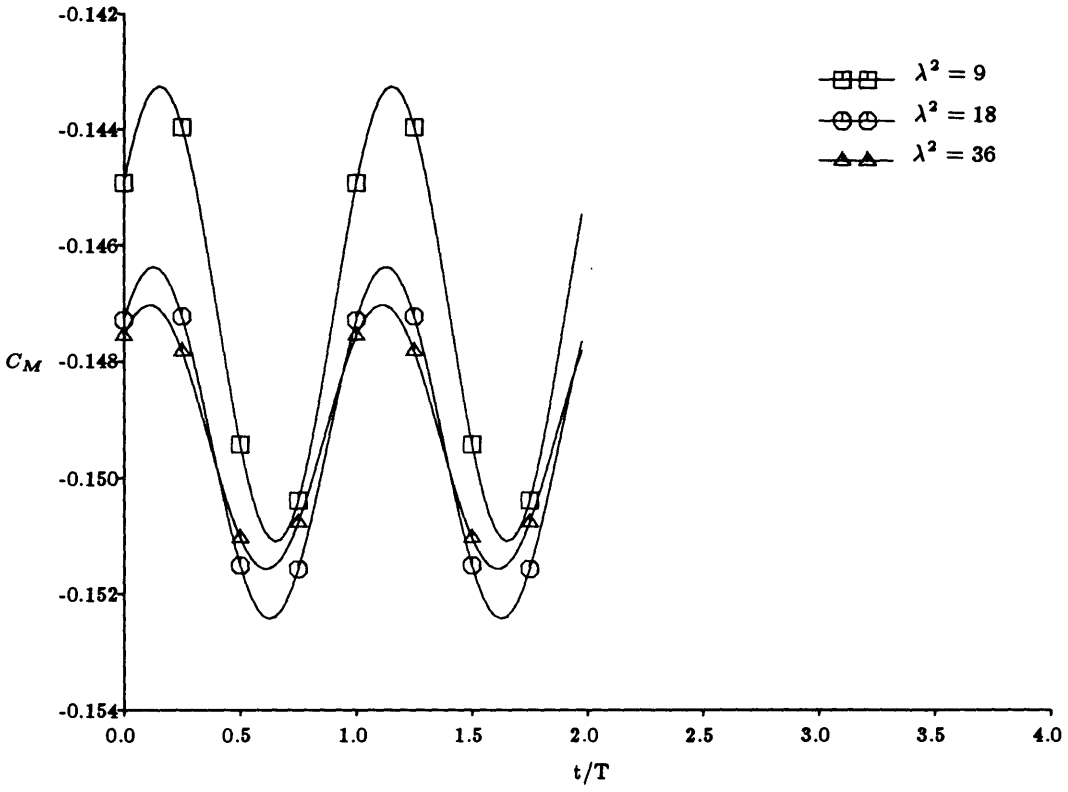

Figure 7.9: Time evolution of the moment coefficient for varying reduced frequency ($\lambda^2 = 9, 18, 36$) and constant strength of flow unsteadiness($\epsilon = 0.04$). The ellipse ($b/a = 1:20$) is at an angle of attack $\alpha = 5^0$.

7.4 The influence of the strength of the flow unsteadiness on the aerodynamic forces

In figure 7.10 we plot the non-dimensional circulation about an ellipse of slenderness 1:20, at angle of attack $\alpha = 5^0$ and reduced frequency $\lambda^2 = 9$ against non-dimensional time, for three different values of stength of unsteadiness $\epsilon = 0.04, 0.02, 0.01$.

The amplitude of oscillation in Γ scales with the strength of the unsteadiness. It is noted, however, that the mean value of the circulation differs in the three cases. This is explained on examination of the corresponding "separation trajectories", which reveals that the time-mean location of the separation point is different (figure 7.11). As ϵ increases, the mean location of the separation point is displaced downstream. The situation resembles more the idealized situation where the Kutta condition holds and the mean value of the circulation is higher. The amplitude of the excursion of the separation point, which is proportional to the strength of the unsteadiness, determines the amplitude of the circulation.

The lift coefficient (see figure 7.12) follows the same trends as the circulation.

In figure 7.13 we show how the drag coefficient changes as the strength of the unsteadiness changes. As expected, its amplitude scales with ϵ.

Finally, in figure 7.14 we plot the time evolution of the moment coefficient for the above values of ϵ.

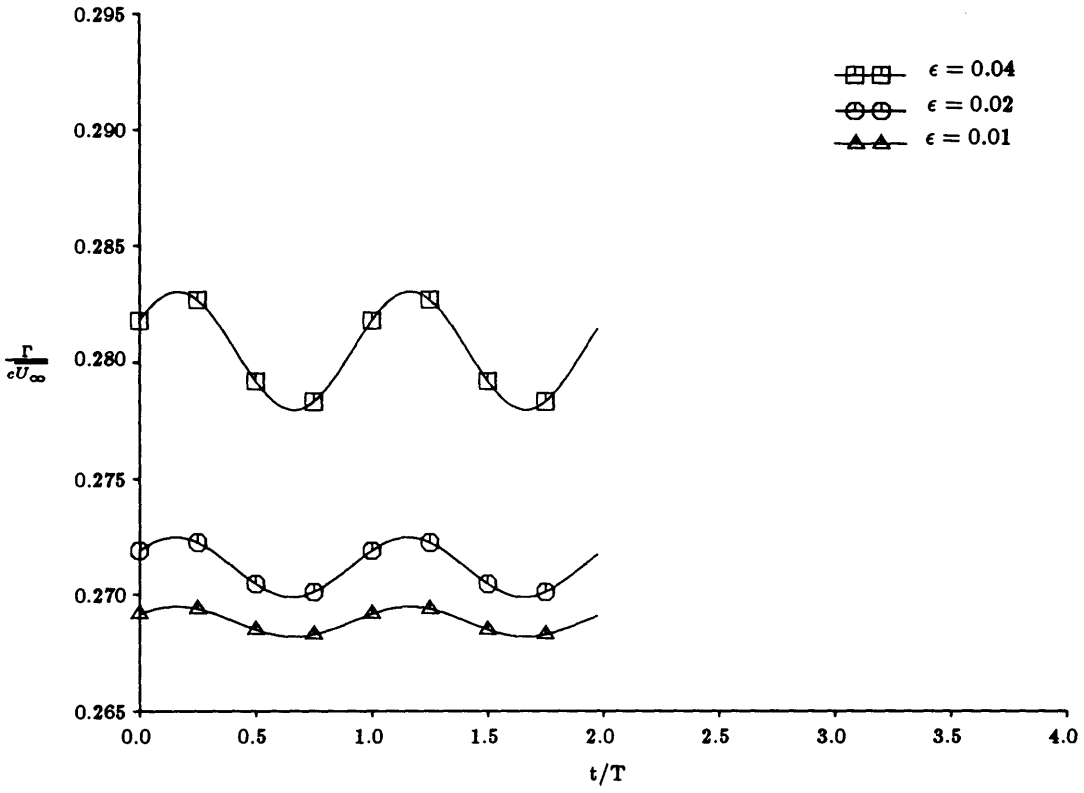

Figure 7.10: Time evolution of the nondimensional circulation for varying strength of flow unsteadiness($\epsilon = 0.04, 0.02, 0.01$) and constant reduced frequency ($\lambda^2 = 9$). The circulation is bracketed by $\Gamma_{\text{Kutta}} = 0.283$ and $\Gamma_{\text{Howarth}} = 0.267$. The ellipse ($b/a = 1:20$) is at an angle of attack $\alpha = 5^0$.

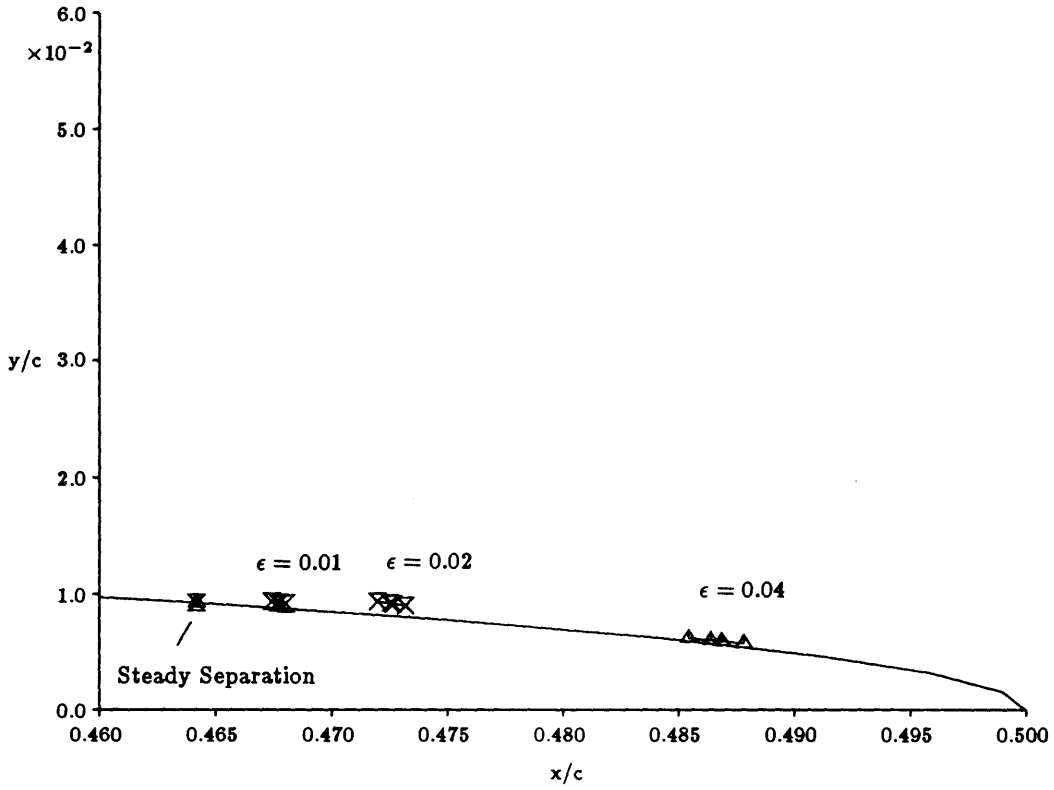

Figure 7.11: Trajectories of the separation point on the suction side of the ellipse during an oscillation cycle for varying strength of flow unsteadiness($\epsilon = 0.04, 0.02, 0.01$) and constant reduced frequency ($\lambda^2 = 9$). The ellipse ($b/a = 1:20$) is at an angle of attack $\alpha = 5^0$.

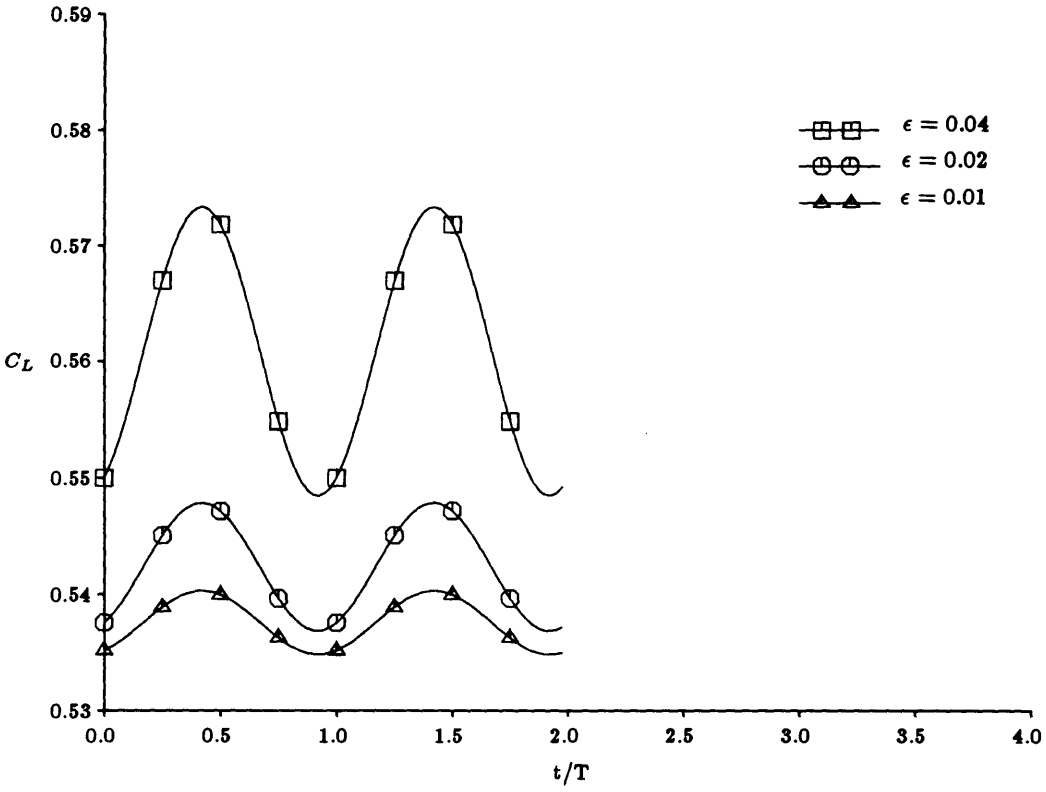

Figure 7.12: Time evolution of the lift coefficient for varying strength of flow unsteadiness($\epsilon = 0.04, 0.02, 0.01$) and constant reduced frequency ($\lambda^2 = 9$). The ellipse ($b/a = 1 : 20$) is at an angle of attack $\alpha = 5^0$.

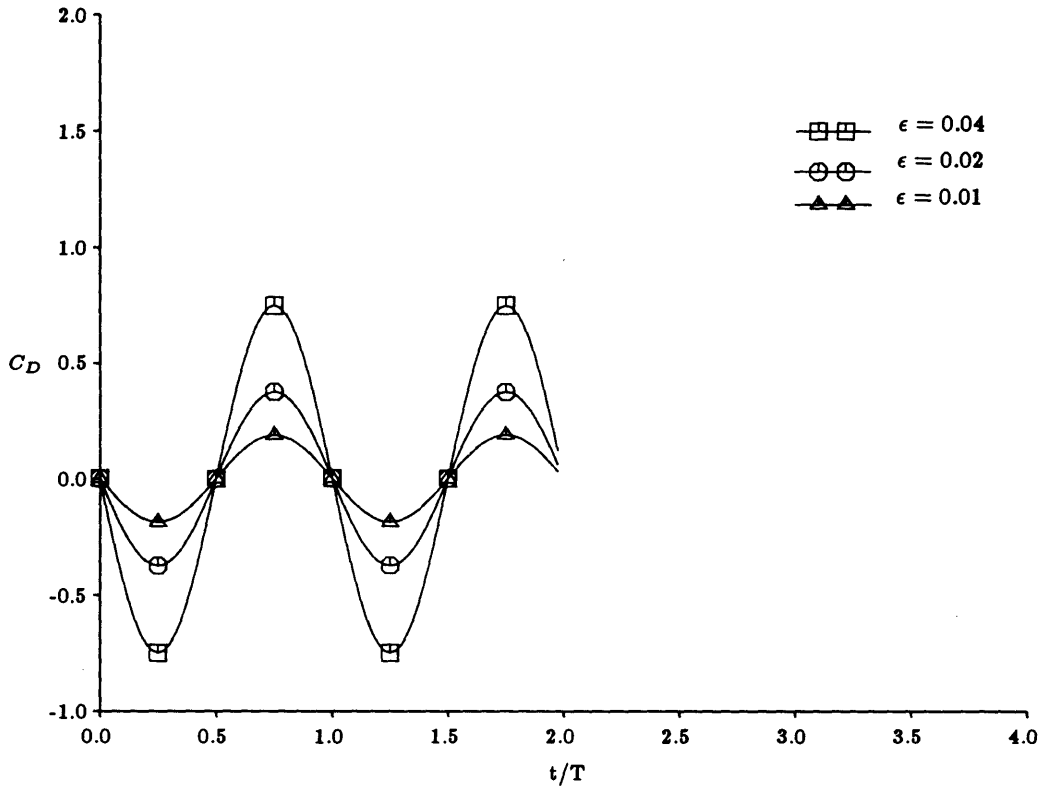

Figure 7.13: Time evolution of the drag coefficient for varying strength of flow unsteadiness($\epsilon = 0.04, 0.02, 0.01$) and constant reduced frequency ($\lambda^2 = 9$). The ellipse ($b/a = 1:20$) is at an angle of attack $\alpha = 5^0$.

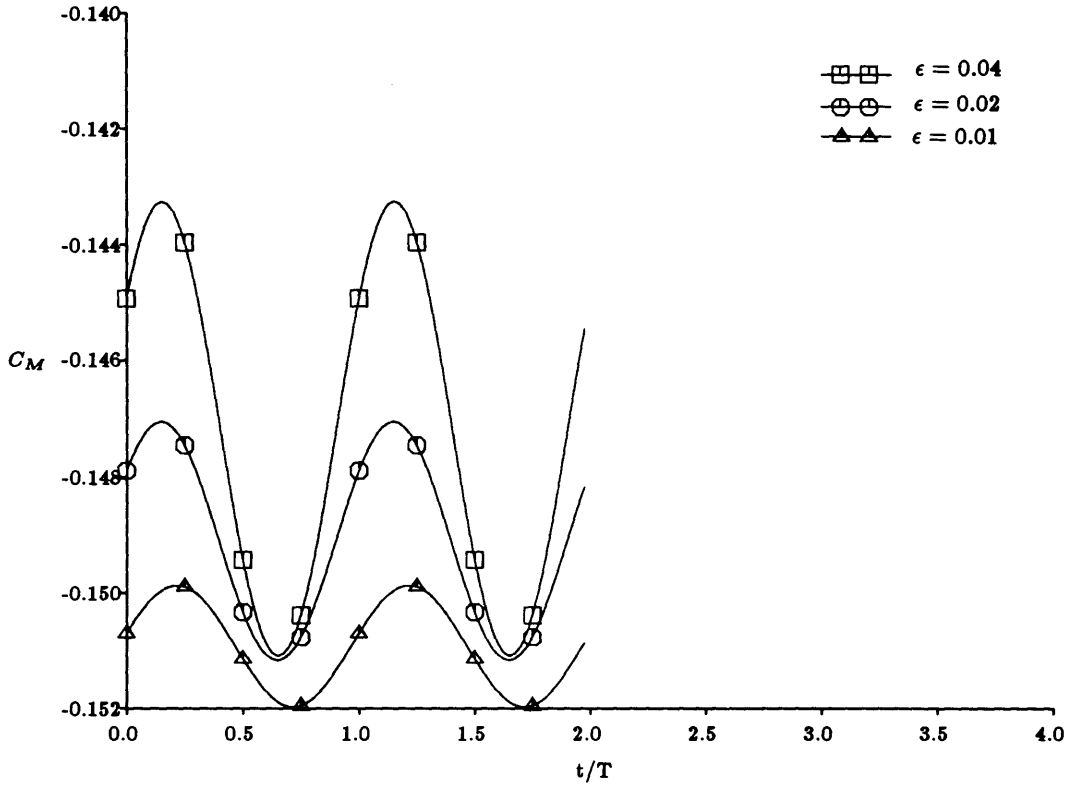

Figure 7.14: Time evolution of the moment coefficient for varying strength of flow unsteadiness ($\epsilon = 0.04, 0.02, 0.01$). and constant reduced frequency ($\lambda^2 = 9$). The ellipse ($b/a = 1:20$) is at an angle of attack $\alpha = 5^0$.

Chapter 8

Conclusions and recommendations for future research

8.1 Conclusions

A new unsteady separation criterion for high frequency flows has been developed. This criterion is simple to use (because its only inputs are parameters of the external flow) and requires small computational effort (see section 4.2). Based on this criterion, we have calculated how the interaction between the airfoil and its wake determines the time evolution of the airfoil circulation. The new separation criterion plays for high frequency, separated flows the role that the Kutta condition plays for flows around thin airfoils.

It reveals that the mean circulation lies in an interval with upper bound the value of the Kutta circulation, Γ_{Kutta}, and lower bound the value of the circulation that in steady flow yields zero net vorticity flux Γ_{Howarth}. This is because the mean location of the separation point on the suction-side of the ellipse, which controls the mean value of the circulation (see chapters 6 and 7), always lies downstream of the steady separation location for reasons explained in chapter 6. As the mean location of separation moves

towards the steady separation location or towards the trailing edge, the mean value of circulation approaches Γ_{Howarth} or Γ_{Kutta} respectively. The amplitude of the circulation is controlled by the the amplitude of the excursion of the suction-side separation point (see section 7.1).

For a given reduced frequency and as the strength of the flow unsteadiness increases, the separation trajectory shifts in the mean towards the trailing edge, and thus the mean value of the circulation tends towards Γ_{Kutta}. The breadth of the separation trajectory increases, and as a consequence the amplitude of the circulation increases.

When the reduced frequency increases, while the strength of flow unsteadiness remains constant, the separation trajectory shrinks and its mean position shifts towards the location of steady separation. This result at first sight seems paradoxical, but can be easily explained by considering how the boundary layer responds to unsteadiness as the reduced frequency increases. The contribution of the "Stokes component" of the boundary layer velocity to the displacement thickness, which is proportional to $\frac{1}{\sqrt{\text{reduced frequency}}}$ (see section 3.1), becomes unimportant relative to that of the "Prandtl component" at high reduced frequencies. Thus separation (identified by a dramatic increase in the displacement thickness) occurs when the "Prandtl flow" separates. The coupling between the two velocity distributions, which generates unsteadiness in the "Prandtl velocity", becomes weaker as the reduced frequency increases. The steady character of the "Prandtl flow" becomes even more pronounced, and it separates like a steady boundary layer. The steady streaming, which makes the "Prandtl flow" more energetic compared to a steady boundary layer and thus delays separation, scales with the inverse of the reduced frequency and in the limit of very high reduced frequency be-

comes negligible. Then, the "Prandtl flow" separates at the steady separation location, and the mean circulation tends to Γ_{Howarth}.

The theory and its implementation on the computer were tested against:

- experimental observations (see section 6.1). The reduced frequency of the experiment, $\lambda^2 \approx 1$, indicates that the flow has a dual character: quasi-steady and unsteady. The success of our criterion in predicting separation for this case, suggests that mainly the unsteady effects control the flow behaviour at separation.
- established theoretical predictions in the limits of:
  - steady flow. The unsteady separation criterion reduces to the Stratford criterion in the limit of vanishing unsteadiness (see chapter 4). In section 6.2 we showed that the computation reproduces the steady results as $\epsilon \rightarrow 0$.
  - very thin ellipse. As the slenderness ratio of the ellipse tends to zero, the results approach systematically those obtained by using the Kutta condition (see sections 7.2, and 6.4).
  - very high reduced frequency (see section 6.3).

8.2 Suggestions for future research

An immediate extension of the present theory would be the calculation of the separated flow past an airfoil performing rotational oscillations. Let us consider the situation arising when the airfoil itself moves in an unsteady fashion in the fluctuating oncoming

stream. We then refer the flow to a coordinate system which is fixed to the airfoil and has its origin at the centre of rotation. The free-stream velocity is determined by the relative motion of the oncoming stream with respect to the moving frame of reference.

The momentum equation in the inertial frame of reference is:

$$\vec{a}_a + \nu \nabla \times \vec{\omega}_a = -\frac{1}{\rho} \nabla p$$

where $\vec{a}_a$ and $\vec{\omega}_a$ denote the acceleration and the vorticity of a fluid particle at a point P.

Suppose now that the airfoil is rotating with angular velocity $\vec{\Omega}$ about the point O which is moving with velocity $\vec{u}_O$ and acceleration $\vec{a}_O$. The velocity and acceleration of the fluid particle in the frame of reference fixed to the airfoil are:

$$\vec{u}_r = \vec{u}_a - \vec{u}_O - (\vec{\Omega} \times \vec{OP}); \; \vec{a}_r = \vec{a}_a - \vec{a}_O - 2(\vec{\Omega} \times \vec{v}_r)$$

The vorticity is:

$$\vec{\omega}_r = \vec{\omega}_a - 2\vec{\Omega}$$

and the momentum equation becomes:

$$\vec{a}_r + 2(\vec{\Omega} \times \vec{u}_r) + \nu \nabla \times \vec{\omega}_r = -(\vec{a}_O + \frac{1}{\rho} \nabla p)$$

The Coriolis force contributes a term $2v\Omega$ in the streamwise momentum balance. Should this term be included in the boundary layer equations?

The transverse velocity, v, in the boundary layer approximation is on the order of $v \sim \frac{U\delta_p}{c}$, where U, δ_p, and c are a velocity scale, the boundary layer thickness, and the

chord of the airfoil respectively. If ω is a typical frequency of the airfoil rotation, the magnitude of the Coriolis term is approximately:

$$2v\Omega \sim \frac{U\delta_p\Omega}{c}$$

Compared with the convection terms, which are on the order of $\frac{U^2}{c}$, the Coriolis force is $\frac{U^2}{c} \,/\, \frac{U\delta_p\omega}{c} = \frac{1}{\lambda^2}\sqrt{Re}$ times smaller. In the applications of interest (see introduction), $\lambda^2 = \frac{\omega c}{U} = 9$ whereas the Reynolds number is $2 \cdot 10^6$. Thus, the Coriolis force is about 160 times smaller than the convective terms and can be neglected. In the case of an F-15 in maneuver: $\frac{\omega c}{U} = \frac{\frac{2\pi}{5}6}{60} = 0.12$ and $Re = 4 \cdot 10^6$; then, the Coriolis terms are 16,000 times smaller than the convection terms. Since the contribution of the Coriolis force to the streamwise momentum equation can be neglected, nothing would change in the modelling of the boundary layer. The unsteady separation criterion has been derived without any restrictive assumptions for the external velocity and thus could be used to determine the airfoil circulation. The potential flow about the rotating airfoil, which is the input to the separation criterion, would be easy to calculate (see for example Drela, 1990, pp. 11-12). Some extra work would be needed to account for the motion of the stagnation point when calculating the length of the "equivalent constant pressure region."

In order to apply the present theory to an airfoil with arbitrary geometry, one could use the mapping function employed by Drela (1990, pp. 5-7) to conformally map any airfoil geometry in the physical plane z to the unit circle in the ς plane. Drela uses a time-depended mapping $z(\varsigma, t)$ to allow rotation of the airfoil in time. The derivative

$\partial z/\partial \varsigma$ of this function is:

$$\frac{dz}{d\varsigma}(\varsigma) = (1 - \frac{1}{\varsigma})^{1-\epsilon} \exp(\sum_{n=0}^{\infty} C_n \varsigma^{-n}) e^{-i\tilde{\alpha}}$$

where $\tilde{\alpha}$ is the instantaneous angle of attack in the airfoil frame (see section 5.2), and $\pi\epsilon$ is the trailing edge angle. The complex coefficients C_n can be specified from any airfoil shape z. Of course for practical applications a finite number of these coefficients needs to be calculated, and a method for their calculation is given in the above reference. Then the potential flow about the airfoil is known and the unsteady separation criterion yields the circulation.

The present theory has been applied to cases where separation occurs near the trailing edge of the airfoil. This has been dictated by the model that we have chosen to represent the wake: a single row of vortices. In section 5.6 we have proven that the two shear layers emanating from the two separation points (modelled by vortex panels) can be replaced by a point vortex located downstream of the trailing edge. Furthermore, the comparison with experimental results in chapter 6 shows that leading edge separation is predicted well by our separation criterion. Mathioulakis and Telionis point out that "with vortex shedding activities displaced far downstream, (suction-side) separation is very little affected by periodicity in the wake." The present theory predicts not only separation, but the circulation of the ellipse as well, as indicated by the good agreement between the measured and predicted location of the stagnation point at the two instances in time for which data are available. It would be particularly interesting to find what improvement the modelling of the free shear layer (using the vortex panels of section 5.6) adds to the present model in the case of leading edge separation.

The present theory could be extended to the calculation of unsteady separated flow past a cascade of airfoils. The unsteady separation criterion uses as only inputs parameters of the potential flow. The potential flow past the airfoil in the cascade could be calculated by one of the standard methods, (for reviews of the subject see Traupel, 1942, section 6.4, and Horlock section 2.5). The circulation then could be determined as in the present work by finding the separation point trajectories.

Then a simplification proposed by Sears (1975) could be used. He suggested a dual model according to which the circulation is determined by a boundary layer calculation requiring a complete picture of the airfoil's contour and its stagnation point (it is this part of the calculation that our theory simplifies), but the lift and moment are calculated as in thin airfoil theory.

He based his proposition on the following argument: If the angle of attack, amplitude of oscillations, and thickness ratio are on the order $O(\epsilon)$, the model must predict fluctuations in the aerodynamic quantities to that order. Indeed, the equation that yields the rate of change of the airfoil circulation (5.2) involves quantities like the external flow velocity, and the speed of the separation points, which fluctuate with amplitude $O(\epsilon)$. On the other hand, the streamwise and normal displacement of the two vortical layers emanating from the upper and lower surface, as well as the displacement of the wake from the streamwise plane, and the departure of the speed of the free vortices from U_∞ are effects of order higher than $O(\epsilon)$. McCune et al. (1990) have performed calculations with a nonlinear wake (assuming the Kutta condition) and proved that the last two effects are indeed of order higher than $O(\epsilon)$.

Thus the problem of the unsteady flow past a cascade of airfoils with trailing edge separation, reduces to the problem of unsteady flow past a cascade of flat plates whose circulation as a function of time is known. The interaction between the blades and their wakes is a much harder problem that must be attacked in the spirit of the work of von Kármán and Sears (1938).

An extension of the present work to turbulent flows would be particularly interesting. If we denote by u' the turbulent fluctuations (whose ensemble average is zero, $< u' >= 0$, and should not be confused with the average over a period of oscillation, $< \tilde{u} >= \tilde{u}$), we could quite confidently assume that the turbulent fluctuations and the periodic oscillations are uncorrelated, so that $< u'\tilde{u} >= 0$, $\frac{\partial}{\partial t} < u'^2 >= 0$. Then, if we represent the boundary layer velocity by $u(x,y,t)+u'$, we find the following momentum equation for the non-turbulent velocity component:

$$\frac{\partial u}{\partial t} + (u\frac{\partial}{\partial x} + v\frac{\partial}{\partial y})u - \nu\frac{\partial^2 u}{\partial y^2} = \frac{\partial U}{\partial t} + U\frac{\partial U}{\partial x} + R(x,y)$$

The greatest difficulty is the correct modelling of the Reynolds stress of the turbulent fluctuations, $R(x,y)$. If this is achieved, then we can analyze the above equation as in chapter 2, with the only difference that the "basic flow" is driven by $\overline{U}\frac{\partial \overline{U}}{\partial x} + R(x,y)$.

In deriving the turbulent separation criterion, the outer part of the "basic flow" would be treated as in the laminar case. The inner part must be modified along the following lines. Equation (4.7) reads:

$$\frac{\partial \tau}{\partial y} = \frac{dp}{dx};\ y \approx 0$$

and for small y yields:

$$\tau = \tau_w + y\frac{dp}{dx}$$

According to the "Prandtl mixing length hypothesis" the turbulent stress in the near wall region is:

$$\tau = \rho(\nu + K^2 y^2 |\frac{\partial u}{\partial y}|)\frac{\partial u}{\partial y}$$

where Ky is the mixing length, and K is the von Kármán constant (approximately equal to 0.41). Elimination of τ between the above two equations yields the form of the "basic velocity" profile near the wall. Then, the inner and outer velocities are patched together, and the "basic velocity" is used to build the second order components (steady and unsteady) of the "Prandtl velocity". The major difference between laminar and turbulent separation is that the latter occurs at a streamwise location which depends on the Reynolds number.

More experimental investigations of the phenomenon of unsteady separation are needed. For the range of high reduced frequency, which is of particular interest for turbomachinery applications, there are no experimental data available. There is an inherent difficulty in locating unsteady separation. In order to identify the exact location of separation, an observer must be moving with the speed of the separation point. In the present work we have established that, at high reduced frequencies, the sign reversal of the wall stress does not indicate that the flow has separated. On the other hand flow breakaway and abrupt increase of the boundary layer thickness are clear indications of separation. Experiments on high frequency separation would test the accuracy of the criterion that we propose.

It has been known from experimental observations that unsteadiness delays separation, and the present work explains this phenomenon by showing how the steady streaming decreases the momentum thickness. But the rest of the predicted trends in

the response of the mean separation location to changes in λ^2 and ϵ need experimental verification. An experiment where the reduced frequency increases from zero, while the strength of unsteadiness remains constant, would show that initially, at low reduced frequency, the mean separation location moves downstream of the steady separation position and later, as the reduced frequency reaches very high values, it moves upstream and eventually asymptotes the location of steady separation. This suggests that there is a maximum in circulation for some reduced frequency. That value should be chosen in the design, say of cascades, where the spacing of the blades of the upstream row determines the reduced frequency of the blade-wake interaction.

Appendix A

Why the boundary layer cannot be divided when the reduced frequency is low

In this appendix we explain why the method of dividing the flowfield into two components, driven by the mean and the oscillatory part of the pressure gradient respectively, fails when the reduced frequency of the external oscillation is low (Gibson, 1957, p. 224).

In this case, the Prandtl thickness is smaller than the Stokes thickness ($\lambda = \frac{\delta_p}{\delta_s} < 1$). In the part of the "Stokes layer" that lies above the edge of the "Prandtl layer" the "Prandtl velocity" has attained its free-stream value $(u_p, v_p) = (\overline{U}, -y_p \frac{d\overline{U}}{dx} + W_p(x,t))$.

Using the dimensionless parameters defined in section 2.2, we write the momentum equation for the "Stokes flow" as follows:

$$[\,(u_s + \overline{U})\frac{\partial}{\partial x} + (v_s - y_s \frac{d\overline{U}}{dx})\frac{\partial}{\partial y_s}\,]\,(u_s + \overline{U}) - U\frac{\partial U}{\partial x}$$
$$+\lambda W_p \frac{\partial u_s}{\partial y_s} + \lambda^2\,(\,\frac{\partial u_s}{\partial t} - \frac{\partial^2 u_s}{\partial y_s^2} - \frac{\partial \widetilde{U}}{\partial t}\,) = 0$$
$$\frac{\partial u_s}{\partial x} + \frac{\partial v_s}{\partial y_s} = 0 \qquad \text{(A.1)}$$
$$y_s = \infty : u_s = \widetilde{U}(x,t);\;\; y_s = 0 : u_s = -u_p(0), v_s = 0 \qquad \text{(A.2)}$$

The first order system is:

$$[\,(u_{s,0}+\overline{U})\frac{\partial}{\partial x}+(v_{s,0}-y_s\frac{d\overline{U}}{dx})\frac{\partial}{\partial y_s}\,]\,(u_{s,0}+\overline{U})=U\frac{\partial U}{\partial x}$$

$$\frac{\partial(u_{s,0}+\overline{U})}{\partial x}+\frac{\partial(v_{s,0}-y_s\frac{d\overline{U}}{dx})}{\partial y_s}=0$$

$$y_s=\infty: u_{s,0}+\overline{U}=U;\;\; y_s=0: u_{s,0}=-u_p(0),\; v_{s,0}-y_s\frac{d\overline{U}}{dx}=0$$

Let us introduce the stream function ψ:

$$u_{s,0}+\overline{U}=\frac{\partial\psi}{\partial y_s},\; v_{s,0}-y_s\frac{d\overline{U}}{dx}=-\frac{\partial\psi}{\partial x}$$

Then, if we differentiate the last momentum equation with respect to y_s we obtain:

$$\frac{\partial\,[\,\frac{\partial^2\psi}{\partial y_s^2},\psi\,]}{\partial\,[\,y_s,x\,]}=0$$

The latter has two possible solutions:

$\frac{\partial^2\psi}{\partial y_s^2}=$ constant, or $\psi=f(\frac{\partial^2\psi}{\partial y_s^2})$

According to the boundary condition at infinity $\psi\sim y_s\overline{U}$, and $\frac{\partial^2\psi}{\partial y_s^2}=0$. Then the last solution yields $\psi=$ constant, leading to a contradiction, and thus it is unacceptable.

Therefore, $\psi=a(t)y_s^2+b(x,t)y_s+c(x,t)$.

Because of the boundary condition at infinity: $a=0, b=U(x,t)$.

The boundary condition at the wall yields: $v_{s,0}=-\frac{\partial c}{\partial x}=0$, thus $c=c(t)$ only.

Therefore $(u_{s,0},v_{s,0})$ is the potential solution:

$$u_{s,0}=\tilde{U},\; v_{s,0}=-y_s\frac{\partial\tilde{U}}{\partial x}$$

Since it satisfies (A.2) identically, all the higher order "Stokes components" are identically zero. Then the "Prandtl system" is the general unsteady boundary layer equation with the corresponding boundary conditions. The method of partial solutions has not succeeded.

Appendix B

A simplification in the "Stokes equations"

In this appendix we show how the system (2.4) can be simplified by replacing u_p and v_p by their Taylor series expansions about the point $(x, y_p = 0)$. The rationale for this substitution is that the "Stokes thickness" is small compared to the "Prandtl thickness" ($\frac{\delta_s}{\delta_p} = \sqrt{\frac{U}{\omega c}} = \frac{1}{\lambda} \ll 1$). Then,

$$u_p = \sum_{n=0}^{\infty} \frac{y_p^n}{n!} \frac{\partial^n u_p}{\partial y_p^n}(x,0) = \sum_{n=0}^{\infty} \frac{1}{\lambda^n} \frac{y_s^n}{n!} \frac{\partial^n u_p}{\partial y_p^n}(x,0)$$

$$v_p = \sum_{n=0}^{\infty} \frac{y_p^n}{n!} \frac{\partial^n v_p}{\partial y_p^n}(x,0) = \sum_{n=0}^{\infty} \frac{1}{\lambda^n} \frac{y_s^n}{n!} \frac{\partial^n v_p}{\partial y_p^n}(x,0)$$

The boundary condition at the wall requires that $v_p(x,0) = 0$, while $u_p(x,0) \neq 0$ is allowed by the coupling condition.

The system (2.4) becomes:

$$\frac{\partial u_s}{\partial t} - \frac{\partial \tilde{U}}{\partial t} - \frac{\partial^2 u_s}{\partial y_s^2} + \frac{1}{\lambda^2} \{ [(u_s + u_p) \frac{\partial}{\partial x} + (v_s + \lambda v_p) \frac{\partial}{\partial y_s}] (u_s + u_p)$$
$$-(\tilde{U} + u_p) \frac{\partial}{\partial x} (\tilde{U} + u_p) - (\lambda v_p + V_s) \frac{\partial u_p}{\partial y_s} \} = 0$$

By substituting in this equation the above expressions for (u_p, v_p) written as:

$$u_p = \sum_{n=0}^{\infty} \frac{1}{\lambda^n} \frac{y_s^n}{n!} \frac{\partial^n u_p}{\partial y_p^n}(x,0) \equiv u_p(x,0) + S_1$$

$$v_p = \sum_{n=0}^{\infty} \frac{1}{\lambda^n} \frac{y_s^n}{n!} \frac{\partial^n v_p}{\partial y_p^n}(x,0) \equiv \frac{y_s}{\lambda} \frac{\partial v_p}{\partial y_p}(x,0) + S_2$$

we get:

$$\frac{\partial u_s}{\partial t} - \frac{\partial \tilde{U}}{\partial t} - \frac{\partial^2 u_s}{\partial y_s^2} +$$
$$+\frac{1}{\lambda^2}\{[(u_s+u_p(x,0))\frac{\partial}{\partial x}+(v_s+\lambda\frac{y_s}{\lambda}\frac{\partial v_p}{\partial y_p}(x,0))\frac{\partial}{\partial y_s}](u_s+u_p(x,0))-$$
$$-(\tilde{U}+u_p(x,0))\frac{\partial}{\partial x}(\tilde{U}+u_p(x,0))+(S_1\frac{\partial}{\partial x}+\lambda S_2\frac{\partial}{\partial y_s})(u_s+u_p(x,0))+$$
$$+[(u_s+u_p(x,0))\frac{\partial}{\partial x}+v_s\frac{\partial}{\partial y_s}]S_1+(S_1\frac{\partial}{\partial x}+\lambda S_2\frac{\partial}{\partial y_s})S_1-S_1\frac{\partial}{\partial x}(\tilde{U}+u_p(x,0))-$$
$$-(\tilde{U}+u_p(x,0))\frac{\partial S_1}{\partial x}-S_1\frac{\partial S_1}{\partial x}-(\lambda S_2+V_s)\frac{\partial S_1}{\partial y_s}\}=0\Rightarrow$$

$$\frac{\partial u_s}{\partial t} - \frac{\partial \tilde{U}}{\partial t} - \frac{\partial^2 u_s}{\partial y_s^2} +$$
$$+\frac{1}{\lambda^2}\{[(u_s+u_p(x,0))\frac{\partial}{\partial x}+(v_s+\lambda\frac{y_s}{\lambda}\frac{\partial v_p}{\partial y_p}(x,0))\frac{\partial}{\partial y_s}](u_s+u_p(x,0))-$$
$$-(\tilde{U}+u_p(x,0))\frac{\partial}{\partial x}(\tilde{U}+u_p(x,0))+(S_1\frac{\partial}{\partial x}+\lambda S_2\frac{\partial}{\partial y_s})u_s+S_1\frac{\partial u_p(x,0)}{\partial x}+$$
$$+[(u_s+u_p(x,0))\frac{\partial}{\partial x}+v_s\frac{\partial}{\partial y_s}]S_1+(S_1\frac{\partial}{\partial x}+\lambda S_2\frac{\partial}{\partial y_s})S_1-S_1\frac{\partial}{\partial x}(\tilde{U}+u_p(x,0))-$$
$$-(\tilde{U}+u_p(x,0))\frac{\partial S_1}{\partial x}-S_1\frac{\partial S_1}{\partial x}-(\lambda S_2+V_s)\frac{\partial S_2}{\partial y_s}\}=0\Rightarrow$$

$$\frac{\partial u_s}{\partial t} - \frac{\partial \tilde{U}}{\partial t} - \frac{\partial^2 u_s}{\partial y_s^2} +$$
$$+\frac{1}{\lambda^2}\{[(u_s+u_p(x,0))\frac{\partial}{\partial x}+(v_s+\lambda\frac{y_s}{\lambda}\frac{\partial v_p}{\partial y_p}(0))\frac{\partial}{\partial y_s}](u_s+u_p(x,0))-$$
$$-(\tilde{U}+u_p(x,0))\frac{\partial}{\partial x}(\tilde{U}+u_p(x,0))+(S_1\frac{\partial}{\partial x}+\lambda S_2\frac{\partial}{\partial y_s})(u_s-\tilde{U})+$$
$$+[(u_s-\tilde{U})\frac{\partial}{\partial x}+(v_s-V_s)\frac{\partial}{\partial y_s}]S_1\}=0\Rightarrow$$

$$\frac{\partial u_s}{\partial t} - \frac{\partial \tilde{U}}{\partial t} - \frac{\partial^2 u_s}{\partial y_s^2} + \frac{1}{\lambda^2}\{-(\tilde{U}+u_p(x,0))\frac{\partial(\tilde{U}+u_p(x,0))}{\partial x}+$$
$$+[(u_s+u_p(x,0))\frac{\partial}{\partial x}+(v_s+y_s\frac{\partial v_p}{\partial y_p}(x,0)\frac{\partial}{\partial y_s}](u_s+u_p(x,0))\}+$$
$$+\sum_{n=1}^{\infty}\frac{1}{\lambda^{n+2}}\{[(\frac{y_s^n}{n!}\frac{\partial^n u_p}{\partial y_p^n})(x,0)\frac{\partial}{\partial x}+\frac{y_s^{n+1}}{(n+1)!}\frac{\partial^{n+1}v_p}{\partial y_p^{n+1}}(x,0)\frac{\partial}{\partial y_s}](u_s-\tilde{U})+$$
$$+[[(u_s-\tilde{U})\frac{\partial}{\partial x}+(v_s-V_s)\frac{\partial}{\partial y_s}]\frac{y_s^n}{n!}\frac{\partial^n u_p}{\partial y_p^n}(x,0)\}=0$$

Appendix C

The nondimensional form of the "Prandtl velocity" distribution

In this appendix we cast the "Prandtl velocity" (in the inner part of the boundary layer) in nondimensional form. We start by nondimensionalizing the "basic velocity", which is the building block for constructing the "Prandtl velocity":

$$u_b = \frac{\tau_w}{\mu} y + \frac{\overline{p}'}{2\mu} y^2 - \frac{(\overline{p}')^2}{12\mu(\tau_f - \tau_w)} y^3$$

Dividing by the reference velocity U_m:

$$\frac{u_b}{U_m} = \frac{\tau_w}{\mu U_m} y + \frac{\overline{p}'}{2\mu U_m} y^2 - \frac{(\overline{p}')^2}{12\mu U_m(\tau_f - \tau_w)} y^3$$

and rewriting the terms in the latter as

$$\begin{aligned} \frac{\tau_w}{\mu U_m} y &= \frac{\tau_w}{\tau_f} \frac{\tau_f}{\mu U_m} y = \frac{\tau_w}{\tau_f} \frac{0.33206 \mu U_m \sqrt{\frac{U_m}{\nu x}}}{U_m \mu} y^* \sqrt{\frac{\nu c}{U_m}} = \qquad \text{(C.1)} \\ &= 0.33206 \tau \sqrt{\frac{c}{x}} y^* = 0.33206 \tau \frac{y^*}{\sqrt{x^*}} \end{aligned}$$

$$\frac{\overline{p}'}{2\mu U_m} y^2 = \frac{(\overline{p}^*)' \frac{\rho U_m^2}{c}}{2\mu U_m} (y^*)^2 \frac{\nu c}{U_m} = \frac{(\overline{p}^*)'(y^*)^2}{2} \qquad \text{(C.2)}$$

$$\begin{aligned} -\frac{(\overline{p}')^2}{12\mu U_m(\tau_f - \tau_w)} y^3 &= -\frac{((\overline{p}^*)')^2 \frac{\rho^2 U_m^4}{c^2}}{12(1 - \frac{\tau_w}{\tau_f}) 0.33206 \mu U_m \sqrt{\frac{U_m}{\nu x}}} \frac{(y^*)^3 (\frac{\nu c}{U_m})^{\frac{3}{2}}}{\mu U_m} \qquad \text{(C.3)} \\ &= -0.25096 \frac{(\overline{p}^*)^2 (y^*)^3 \sqrt{x^*}}{1 - \tau} \end{aligned}$$

we get

$$u_b^* = \frac{0.33206\tau}{\sqrt{x^*}} y^* + \frac{(\overline{p}^*)'}{2}(y^*)^2 + D^*(y^*)^3$$

where:

$$D^* = -0.25096\frac{((\overline{p}^*)')^2\sqrt{x^*}}{1-\tau}$$

Now, we write for the second order component of the mean "Prandtl velocity":

$$\overline{u}_{p,2}^* = \frac{h\frac{\partial u_b}{\partial y}}{U_m} = \frac{h\tau_w}{\mu U_m} + \frac{h\overline{p}'}{\mu U_m} y + \frac{3hD}{\mu U_m} y^2$$

Using the relations

$$\begin{aligned}
h &= -\frac{3\mu}{2\omega}\frac{\overline{\tilde{U}\tilde{U}'}}{\tau_w} = -\frac{3\mu}{2\omega}\frac{\overline{\tilde{U}^*(\tilde{U}^*)'}\frac{U_m^2}{c}}{\tau\,\tau_f} \\
&= -\frac{3\mu}{2\omega}\frac{\overline{\tilde{U}^*(\tilde{U}^*)'}}{\tau}\frac{\frac{U_m^2}{c}}{0.33206\sqrt{\frac{\mu\rho U_m^3}{x}}} \\
&= -4.51726\frac{\overline{\tilde{U}^*(\tilde{U}^*)'}}{\tau}\frac{U_m}{\omega c}\sqrt{\frac{\nu c}{U_m}}\sqrt{\frac{x}{c}} \\
&= -4.51726\frac{\overline{\tilde{U}^*(\tilde{U}^*)'}\sqrt{x^*}}{\tau}\frac{\delta_p}{\lambda^2} \\
&= B^*\frac{\delta_p}{\lambda^2}
\end{aligned}$$

and

$$\delta_p = \frac{y}{y^*}$$

the three right-hand-side terms of $\overline{u}_{p,2}^*$ can be written as:

$$\frac{h\tau_w}{\mu U_m} = \frac{B^*\frac{\delta_p}{\lambda^2}\tau_w}{\mu U_m} = \frac{B^*}{\lambda^2}\frac{\tau_w y}{\mu U_m}\frac{1}{y^*} = (\text{using (C.2)})\frac{B^*}{\lambda^2}\frac{0.33206\tau}{\sqrt{x^*}}$$

$$\frac{h\overline{p}'}{\mu U_m} y = \frac{B^*\frac{\delta_p}{\lambda^2}\overline{p}'}{\mu U_m} y = \frac{B^*}{\lambda^2}\frac{\overline{p}' y^2}{\mu U_m}\frac{1}{y^*} = (\text{using (C.2)})\frac{B^*}{\lambda^2}(\overline{p}^*)'(y^*)^2\frac{1}{y^*} = \frac{B^*}{\lambda^2}(\overline{p}^*)' y^*$$

$$\frac{3hD^2}{\mu U_m} y^2 = 3\frac{B^*\frac{\delta_p}{\lambda^2}D}{\mu U_m} y = \frac{3B^*}{\lambda^2}\frac{D y^3}{\mu U_m}\frac{1}{y^*} = (\text{using (C.4)})\frac{3B^*}{\lambda^2}D^*(y^*)^3\frac{1}{y^*} = \frac{3B^*}{\lambda^2}D^*(y^*)^2$$

Thus,

$$\overline{u}^*_{p,2} = \frac{B^*}{\lambda^2}\left(\frac{0.33206\tau}{\sqrt{x^*}} + (\overline{p}^*)'y^* + 3D^*(y^*)^2\right)$$

where:

$$B^* = -4.51726\frac{\overline{\tilde{U}^*(\tilde{U}^*)'}\sqrt{x^*}}{\tau}$$

and by adding the latter to the "basic flow" we get:

$$\overline{u^*_p} = \frac{0.33206\tau}{\sqrt{x}}\left(\frac{B^*}{\lambda^2} + y^*\right) + (\overline{p}^*)'y^*\left(\frac{B^*}{\lambda^2} + \frac{y^*}{2}\right) + D^*(y^*)^2\left(\frac{3B^*}{\lambda^2} + y^*\right)$$

The unsteady component of the "Prandtl velocity" is:

$$\begin{aligned}\tilde{u}_{p,2} &= \frac{1}{i\omega}\left\{\frac{\partial}{\partial x}[\tilde{U}(\overline{U} - u_b)] + y_p\frac{\partial u_b}{\partial y_p}\frac{\partial \tilde{U}}{\partial x}\right\} \\ &= \frac{1}{\omega}\left[\,(\tilde{U}|_{t-\frac{T}{4}}\overline{U})' + \tilde{U}|'_{t-\frac{T}{4}}\left(-u_b + y\frac{\partial u_b}{\partial y}\right) - \tilde{U}|_{t-\frac{T}{4}}u'_b\,\right]\end{aligned}$$

Expressed in dimensionless variables:

$$\begin{aligned}\frac{\tilde{u}_{p,2}}{U_m} &= \frac{1}{\omega U_m}\frac{U_m^2}{c}\left\{(\tilde{U}^*|_{t-\frac{T}{4}}\overline{U}^*)' + (\tilde{U}^*|_{t-\frac{T}{4}})'\left[-0.33206\frac{\tau}{\sqrt{x^*}}y^*\right.\right. \\ &\quad -0.5(\overline{p}^*)'(y^*)^2 - D^*(y^*)^3 + 0.33206\frac{\tau}{\sqrt{x^*}}y^* + 0.5(\overline{p}^*)'(y^*)^2 + 3D^*(y^*)^3 \\ &\quad \left.\left. -\tilde{U}^*|_{t-\frac{T}{4}}\left[\,0.33206y^*\left(\frac{\tau}{\sqrt{x^*}}\right)' + 0.5(\overline{p}^*)''(y^*)^2 + D^*(y^*)^3\,\right]\right\}\end{aligned}$$

The end result is:

$$\begin{aligned}\tilde{u}^*_{p,2} &= \frac{1}{\lambda^2}\left\{(\tilde{U}^*|_{t-\frac{T}{4}}\overline{U}^*)' - 0.33206\left(\frac{\tau}{\sqrt{x^*}}\right)'\tilde{U}^*|_{t-\frac{T}{4}}y^*\right. \\ &\quad +0.5\left[\,(\tilde{U}^*|_{t-\frac{T}{4}})'(\overline{p}^*)' - \tilde{U}^*|_{t-\frac{T}{4}}(\overline{p}^*)''\,\right](y^*)^2 \\ &\quad \left. +\left[\,-2(\tilde{U}^*|_{t-\frac{T}{4}})'D^* + \tilde{U}^*|_{t-\frac{T}{4}}(D^*)'\,\right](y^*)^3\right\}\end{aligned}$$

Bibliography

[1] Curle, N. and Davies, H. J., 1969, *Modern Fluid Mechanics*, Van Nostrand, 217-222.

[2] Curle, N. and Skan, S. W., 1957, Approximate methods for predicting separation properties of laminar boundary layers, *Aeronaut. Quart.*, vol. 8, 278-289.

[3] Drela, M., 1990, Unsteady Airfoil Flow Prediction Method, *CFDL TR-90-1*, MIT.

[4] Gibson, W. E., 1957, Unsteady laminar boundary layers, *Ph. D. Thesis*, MIT, Department of Mathematics.

[5] Görtler, H., 1957, A new series for the calculation of steady laminar boundary layer flows, *J. Math. Mech.*, 1-66.

[6] Greitzer, E. M., 1984, Unsteady flows in Turbomachines, *VKI Lecture Series*, 1984-02, 1-61.

[7] Howarth, L., 1935, The theoretical prediction of the lift coefficient for a thin elliptic cylinder, *Proc. Royal Society*, ser. A, vol. 149, 558-586.

[8] Katz, J., and Plotkin, A., 1991, *Low Speed Aerodynamics*, McGraw-Hill.

[9] Koromilas, C. A., and Telionis, D. P., 1980, Unsteady laminar separation : an experimental study, *J. Fluid Mech.*, vol. 97, part 2, 347-384.

[10] Landau, L. D., and Lifshitz, E. M., 1959, *Fluid Mechanics*, 2nd edition, Pergamon Press, 163-167.

[11] Lam C.-M. G., 1989, Non-linear unsteady vortex wake evolution behind Joukowski airfoils including explicit free panel method, *S. M.Thesis*, MIT, Department of Aeronautics and Astronautics.

[12] Lighthill, M. J., 1953, The response of laminar skin friction and heat transfer to fluctuations in the stream velocity, *Proc. Roy. Soc.*, ser. A, vol. 224, 1-23.

[13] Lin, C. C., 1956, Motion in the boundary layer with a rapidly oscillating external flow, *9th International Congress of Applied Mechanics*, University of Brussels, 155-167.

[14] Mathioulakis, D. S. and Telionis, D. P., 1987, Velocity and vorticity distributions in periodic separating laminar flow, *J. Fluid Mech.*, vol. 184, 303-333.

[15] Mathioulakis, D. S. and Telionis, D. P., 1989, Pulsating flow over an ellipse at an angle of attack, *J. Fluid Mech.*, vol. 201, 99-121.

[16] McCune, J. E., Lam, C-M. G. and , Scott, M. T., 1990, Nonlinear aerodynamics of two-dimensional airfoils in severe maneuver, *AIAA J.*, vol. 28, no. 3, 385-393.

[17] Messiter, A. F., 1983, Boundary-layer interaction theory, *J. Appl. Mech.*, 50, 1104-1113.

[18] Mezaris, T. B., Barbi, C., Jones, G. S. and Telionis, D. P., 1987, Separation and wake of pulsating laminar flow, *Phil. Trans. R. Soc. Lond.*, A 322, 493-523.

[19] Moore, F. K., 1955, Lift hysteresis at stall as an unsteady boudary layer phenomenon, *NACA TN-3571.*

[20] Moore, F. K., 1958, On the separation of the unsteady boundary layer, *Boundary Layer Research*, (ed. H. Görtler), Springer, 296-311.

[21] Rosenhead, L.,(ed.) 1963, *Laminar Boundary Layers*, Oxford University Press.

[22] Rott, N., 1964, *Theory of Laminar Flows*, (ed. Moore, F. K.), Princeton University Press, 395-397.

[23] Sears, W. R., 1976, Unsteady motion of airfoils with boundary layer separation, *AIAA J.*, vol. 14, no. 2, 210- 220.

[24] Sears, W. R. and Telionis, D. P., 1975, Boundary layer separation in unsteady flow, *SIAM J. Appl. Math.* , 28, 215-235.

[25] Shen, S.-F., 1968, Unsteady separation according to the boundary layer equation, *Adv. in Appl. Mech.*, vol. 18, 117-220.

[26] Smith, A. M. O. , 1975, High-Lift Aerodynamics, *J. of A.*, volv 12, no. 6, 1975, 501-531.

[27] Stratford, B. S., 1954, Flow in the laminar boundary layer near separation, *Rep. and Mem. Aero. Res. Cou. Lond.*, No. 3002.

[28] Stratford, B. S., 1957, The prediction of separation of the turbulent boundary layer, *J. Fluid Mech.*, vol.15, 1-17.

[29] Sychev, V. V., 1972, Laminar separation, Translation from the Russian original: 1974, *Fluid Dyn.*, 407-417.

[30] Sychev, V. V., 1978, Asymptotic theory of nonstationary separation, Translation from the Russian original: 1980, *Fluid Dyn.*, 829-838.

[31] Telionis, D. P., 1981, *Unsteady Viscous Flows* , Springer, Chs 5 and 7.

[32] Traupel, W., 1942, *Neue algemeine Theorie der mehrstufigen axialen Turbomaschine*, Leeman and Co., Zürich.

[33] Van Dommelen, L. L., 1981, Unsteady boundary-layer separation, *Ph.D. Thesis*, Cornell University.

[34] Van Dommelen, L. L., and Shen, S.-F., 1977, The laminar boundary layer in Lagrangian description, *XIII Biennial Fluid Mechanics Symposium*, Olsztyn-Kortowo, Poland.

[35] von Kármán, T., and Sears, W. R., 1938, Airfoil theory for non-uniform motion, *J. Aeron. Sci.*, vol. 5, 10, 379-390.